12-2006

Direct Integration of Surface Enhanced Raman Spectroscopy as a Detection Mode for Microfluidic Separations and Fluid Handling: μfluidic-SERS

Raynella Magdalene Connatser
University of Tennessee - Knoxville

To the Graduate Council:

I am submitting herewith a dissertation written by Raynella Magdalene Connatser entitled "Direct Integration of Surface Enhanced Raman Spectroscopy as a Detection Mode for Microfluidic Separations and Fluid Handling: µfluidic-SERS." I have examined the final electronic copy of this dissertation for form and content and recommend that it be accepted in partial fulfillment of the requirements for the degree of Doctor of Philosophy, with a major in Chemistry.

Michael J. Sepaniak, Major Professor

We have read this dissertation and recommend its acceptance:

Georges A. Guiochon, Mark D. Dadmun, Gary S. Sayler

Accepted for the Council:

Carolyn R. Hodges

Vice Provost and Dean of the Graduate School

(Original signatures are on file with official student records.)

To the Graduate Council:

I am submitting herewith a dissertation written by Raynella Magdalene Connatser entitled "Direct Integration of Surface Enhanced Raman Spectroscopy as a Detection Mode for Microfluidic Separations and Fluid Handling: μfluidic-SERS." I have examined the final electronic copy of this dissertation for form and content and recommend that it be accepted in partial fulfillment of the requirements for the degree of Doctor of Philosophy, with a major in Chemistry.

Michael J. Sepaniak
Major Professor

We have read this dissertation
and recommend its acceptance:

Georges A. Guiochon

Mark D. Dadmun

Gary S. Sayler

Acceptance for the Council:

Anne Mayhew

Vice Chancellor and
Dean of Graduate Studies

(Original signature are on file with official student records.)

Direct Integration of Surface Enhanced Raman Spectroscopy as a Detection Mode for Microfluidic Separations and Fluid Handling: μfluidic-SERS

A Dissertation
Presented for the
Doctor of Philosophy Degree
University of Tennessee, Knoxville

Raynella Magdalene Connatser
December, 2006

Dedication

To my husband, Scott…the light at the end of all my tunnels

And to

Mama…the eternal spark of hope in the bottom of my heart

Katie…the constant word of assurance in the back of my mind

And Nathan, who, in combination with the other four of us, represents a future that grows better with each passing year

In Memory of Daddy, Eddie, and Grannie…

Thanks for the grit, the curiosity, and the spunk, respectively.

Acknowledgements

Thanks to God for comfort through pain, guidance in upheaval and a life to do something with in the first place. I hope that some part of what I do is for the greater good. Thanks to Scott for being my calm in the storm and loving me through some serious tsunamis, not the least of which was grad school; I love you boundlessly. Thanks to my parents for an unspoken requirement to live up to your complete potential in every facet of your life, and thanks to my sister for being just as diligent about adhering to this silent credo as I am; it's nice not to be alone. Thanks also to Mama and Katie for the afternoon visits and being excited about my small positives. Thanks to Nathan for his "mad skills, yo" on the tractor and with cows, for the boat rides and the plowed gardens, and for being willing to explain some biochem to me. Thanks to Lisa for sharing grad school woes alongside hurts deeper than any paper or test; and thanks to newer friends, without whom my time here and my life in general would've been much lower quality: Amber, Kasey, Jenny…without you guys, I think grad school might have killed the "girl" in me forever. Thanks for saving her. Thanks to the good senior grad students who showed me what to do (and not to do): Chris, Shannon, Jeremy. Thanks to Marco and Kathleen for having hearts of gold and heads of stone; we honed each other like steel sharpening steel. Thanks to Nate, Pete, and Matt for the laughs and the help when I've needed it, and thanks to Nahla and Lance for being around to count on when I was bumbling through TA-ing analytical. Thanks to my professors and committee members, as well as John Sanseverino, Mel Eldridge, Pampa Dutta and Dr. Feigerle for teaching and helping me, and Linda and Sam Lewis for opening my eyes to what it means to be 100% self-employed. Mostly, thanks to Dr. Sepaniak. I have no idea how he did it, but he managed to mentor a talky history major whose life was totally littered with non-science distractions, both good and terrible, into a passable scientist who someday might actually be able to contribute to the body of analytical knowledge. He has been an excellent example of a skilled, organized, focused professional, able to manage many different types of students and always tempering his professionalism with genuine concern when appropriate. I can never thank him enough for believing I was capable of more than I myself could ever have fathomed.

Abstract

The arena of microfluidics (μfluidics) has grown over the past decade to encompass myriad separation techniques and exploit copious detection modes. The direct integration of a vibrational spectroscopic detection technique, rich with structural information, onto a platform that is portable and potentially highly controllable such as μfluidics, could offer redress for some of the problems inherent in many of the electrophoretically driven separations carried out on said devices. Herein, this direct integration is explored, and methods of device fabrication, spectroscopic data collection conditions, analytical figures of merit of the detection technique, and separations method development results are discussed. The creation of surface enhanced Raman scattering/spectroscopy (SERS) substrates within the architecture of miniaturized separation devices made of glass, polymer, silicon, and combinations thereof represents not only a novel and useful detection tool for μfluidics but also a facile means of interrogating new, optimized SERS substrates for increased enhancement activity with low-volume fluidic delivery. Finally, the contemporary, "real-world" relevance of the development of μfluidic-SERS comes to light with preliminary studies of aflatoxins, a fungal byproduct contaminating foodstuffs and a threat from both an agribusiness and a Homeland Security standpoint, and, even more important, endocrine disrupting chemicals, a wide class of ubiquitous pollutants that act both as acute teratogens and, in the long term, as potent carcinogens.

Table of Contents

List of Tables

List of Figures

CHAPTER 1

Introduction

In an increasingly "wireless" world, the capability to take conventional analysis tools, such as efficient separations with detection of components in a sample, to the field has become desirable. The advent of a "better, smaller, faster" era in chemistry has seen countless innovations in such miniaturization along with advantages concurrent with portability such as improved physicochemical control of fluidic, thermal, and optical processes as well as more focused observation of biological events on-chip.[1-4]

The analytical chemical communities have embraced the benefits of moving separations and detection to miniaturized systems comprised of fluidic pathways and architecture ranging from simple cross- and x-patterns to three dimensional cavernous networks.[5,6] Aforementioned benefits include portability, faster analysis, reduced solvent and sample requirements, and integration of multiple processes onto a single, self-contained platform.[7] However, μfluidic electrophoretic separations suffer some of the same limitations as CE, e.g., irreproducibility in analyte migration times due to changing channel wall characteristics and low detection sensitivity due to short optical detection path lengths, except in the case of laser induced fluorescence (LIF). Surface enhanced Raman spectroscopy / scattering (SERS) detection of electrophoretic analyte bands nullifies migration time irreproducibility by providing a vibrational fingerprint of the band, whereas the conventional UV-visible or fluorescence spectroscopies generally offer only broad spectral features. In fluorescence, this results from the vibrational band

broadening: fluorescent emission is a measure of the energy difference between two molecular energy levels, and Boltzmann population statistics imply that some molecules will be leaving from vibrationally excited levels, and in the excited state will undergo variable energetic vibrational interconversions before relaxing via a fluorescent emission event. In UV-visible absorbance detection, the measurement of light lost from incident to transmitted beam reduces sensitivity as well as suffers the same vibrational and even rotational broadening of the spectroscopic output as many different energies from the various molecular states absorb slightly differently and blur what would be sharp spectroscopic bands in such techniques as atomic absorption (no vibrations). Raman bands remain sharp due the fact that a simple vibrational energy difference due to an inelastic scattering event, with no true molecular absorption, takes place.

While only certain molecules offer the fluorescent yield required for detection of analytes in CE at 10^{-8}M and lower concentrations, the chemical and electromagnetic enhancement mechanisms at work in SERS allow the more ubiquitous Raman-active molecules to be detected at nanomolar levels.[8] Hence, μfluidic separations-SERS offers the potential for a portable, controlled separation platform with label-free, structurally descriptive detection at limits of detection (LODs) lower than UV-vis detection. Despite these marked advantages of coupling capillary-type electrophoretic separations in general, and μfluidics particularly, with SERS, little has been reported on this hyphenation. Michael Morris has demonstrated that Raman spectroscopy can be used for on-line detection in capillary electrophoresis and on μfluidic chips with a Raman microprobe, using preconcentrating separation methods with specific strong Raman scatterers.[9,10,11] Christine Keating employed off-column SERS detection of analyte

bands in CE eluent transferred onto SERS substrates on glass slides.[12] W. Ewen Smith used μfluidics as a platform for reduced volume in-situ synthesis of a resonance-enhanced TNT derivative with surface enhanced resonance Raman (SERRS) sensing, although no separations were achieved nor were any chromatographic efficiencies quoted.[13] Research in our own group has also sought to address the shortcomings of CE with SERS. On-capillary SERS detection via in-buffer, sheathing flow, and counter-current flow of silver colloid for enhancement have been explored and have resulted in reasonably descriptive spectra but suffer from altered analyte migration behaviors, compromised efficiencies, and significant analyte band dilution, respectively.[14] To mitigate such disadvantages of buffer-borne SERS substrate, off-column SERS detection of electrofilament-transferred CE eluent was employed.[15,16] Other groups have also carried out SERS detection of immobilized CE bands transferred by various means of droplet contact transfer and electrospray.[12,17,18] Although useful, none of these hyphenations offers the control afforded by the μfluidic platform, nor do they fully utilize all the inherent combined advantages of the techniques. By having the SERS active substrate contained within the architecture of a microchannel, tight fluidic control of solution and analyte movement by voltage alone is possible and combines with the convenience SERS detection either on-the-fly or post-separation within the nanocomposite Raman-active regions of the μfluidics.

The most novel aspect about this technique is that the SERS-active substrate is directly integrated into the architecture of the devices. The process of physically vapor depositing (PVD) silver onto the polydimethylsiloxane (PDMS) creates partially embedded, three-dimensional clusters of silver in the polymer that form a

nanocomposite SERS substrate. Compared with other SERS substrates, these materials have shown advantages in both enhancement factor and robustness due to the dielectric properties of the PDMS and its capacity to partially protect the silver from oxidation.[19] Extensive characterization and assays for a range of analytes with said nanocomposites demonstrate their utility as stand-alone substrates.[20,21] They have also been employed for post column structural detection of eluting analytes for HPLC.[22] This pliable, moldable nanocomposite SERS substrate material covers the open channel structure created from positive molding, thus completing the enclosed μfluidic channel with one of its four walls an inherent sensing material. This work marks the first coupling of SERS detection of an electrophoretic separation integrated directly onto a μfluidic.

Microfluidics / Separations Background

Capillary Electrophoresis

Microfluidics (μfluidics), whether in glass or polymers, offers the aforementioned portability, control, and has been developed for myriad separation and detection modes. The foundations of μfluidics grow largely out of the more mature suite of techniques within the field of capillary electrophoresis (CE) and its related chromatographies. Capillary electrophoresis has origins in the technical advancements within other analytical techniques of the 1980s: small-bore, polyimide-coated fused silica columns from the field of gas chromatography (GC); general optical and electrochemical detection methods from high performance/pressure liquid chromatography (HPLC); and mechanisms of pumping and chemical separations from electrochemistry, and for techniques involving pseudo-stationary phases such as cyclodextrins (CDs) and micelles (MEKC), theory from HPLC as well.[23] The move

from long (30-100cm), free-standing, circular cross section fused silica capillaries to rectangular (or trapezoidal) cross-sectioned μfluidic channels embedded on small footprint (usually 1”x3” or less) slabs of glass, polymer, or a combination, was a more natural move than may seem obvious due to the fact that all these materials have significant surface silanol content which imparts their walls with a zeta potential, which is the charge gradient across a solid-liquid interface, and thereby facilitates solution zone electrophoresis. When silanol groups in the channel or column wall are deprotonated via treatment with basic solutions, cations in the subsequent buffer solutions filling the channel or capillary arrange in a charge double layer, clinging tightly at the wall (described by Helmholtz at the inner layer) and less tightly out into the bulk solution (outer Helmholtz layer). In conventional solution zone electrophoresis, when an electrical potential is applied between the two ends of the column filled with electrolyte and buffering salts, the cations move toward the negatively charged electrode normally placed at the outlet end of the capillary or μfluidic channel. The plug-like flow profile that results theoretically eliminates all sources of diffusional band broadening besides longitudinal, giving CE its great potential for high efficiencies. Modifications that favor separation selectivities and/or resolution enhancements can be implemented with wall coatings and the introduction of buffer additives that act as pseudo-stationary phases. The latter is discussed herein as an addition to the μfluidic-SERS platform.

Therefore, μfluidics benefits from the well-established theory and experimental practice of CE. Table 1.1 offers definitions for fundamental parameters governing analyte migration and electroosmotic flow in CE, which also apply in μfluidic

Table 1.1: Definitions of CE Equations Applying to μfluidics

Parameter	Equation	Definition
Velocity of an ion, ν	$\nu = \mu_e E$	μ_e = electrophoretic mobility E = voltage per unit length
Steady state forces due to E field and frictional drag, F, on a spherical ion	$F_E = qE$ $F_F = -6\pi\eta r\nu$ $qE = -6\pi\eta r\nu$	q = ion charge η = solution viscosity r = ion radius
Electrophoretic mobility in terms of physical parameters	$\mu_e = \frac{q}{6\pi\eta r}$	*
Magnitude of electroosmostic flow in terms of velocity, ν_{EOF}	$\nu_{EOF} = \frac{E\,\xi\,\varepsilon}{\eta}$	ξ = zeta potential: electric potential across solid-liquid interface ε = dielectric constant
Magnitude of electroosmostic flow in terms of mobility, μ_{EOF}	$\mu_{EOF} = \frac{\xi\,\varepsilon}{\eta}$	*
Observed solute mobility, μ_{obs}, where EOF is measured with a neutral marker moving at ν_{EOF}	$\mu_{obs} = \frac{l}{tE} = \frac{lL}{tV}$ $\mu_{obs} = \mu_e + \mu_{EOF}$	t = migration time l = capillary length to detector L = total capillary length V = applied voltage
Resolution, Rs (general)	$Rs = \frac{2\,(x_2 - x_1)}{(w_1 + w_2)}$	x_2, x_1 = migration distances of two analyte bands, 1 and 2 w_2, w_1 = baseline peak widths
Experimental determination of plate number, N	$N = 5.54 \left[\frac{t}{w_{1/2}}\right]^2$	$w_{1/2}$ = width of peak at half height in units of time

electrophoretic separations.[24] These parallels lead to the application of similar theoretical treatments for resolution, efficiency, and sources of

band broadening. Also directly applicable to the μfluidic platform are theoretical treatments for specialized versions of CE that include running buffer additives to enhance selectivity when separating neutrals and classes of compounds with nearly identical electrophoretic mobilities. A recent review of such techniques on μfluidics reflects the burgeoning techniques' heavy reliance upon established capillary chromatography theory.[25]

Conventional CE-style separations generally only suffer longitudinal diffusion contributions to band broadening under ideal conditions including no wall interactions, plug-like flow profile (see Figure 1.1a), which negates radial diffusion contribution to band broadening, and Ohmic linearity, i.e., increases in voltage applied result in proportional increases in current. Chromatographic or electrophoretic efficiency is based on the number of theoretical plates (a reflection back to the days of distillation) available in a separation system and determines its power to resolve many components. In CE, efficiency rather than selectivity, as in HPLC, is the most important parameter in attaining maximum resolution; an even greater need exists for good efficiency and attendant high resolution on some of the shortened channels of μfluidic platforms. Efficiency is CE can be related to molecular diffusion in chromatography by the following, wherein only longitudinal diffusion is assumed to impact band broadening, or variance, σ:

$$\sigma^2 = 2Dt = \frac{2Dl\,L}{\mu_e} \qquad \textbf{Equation 1.1}$$

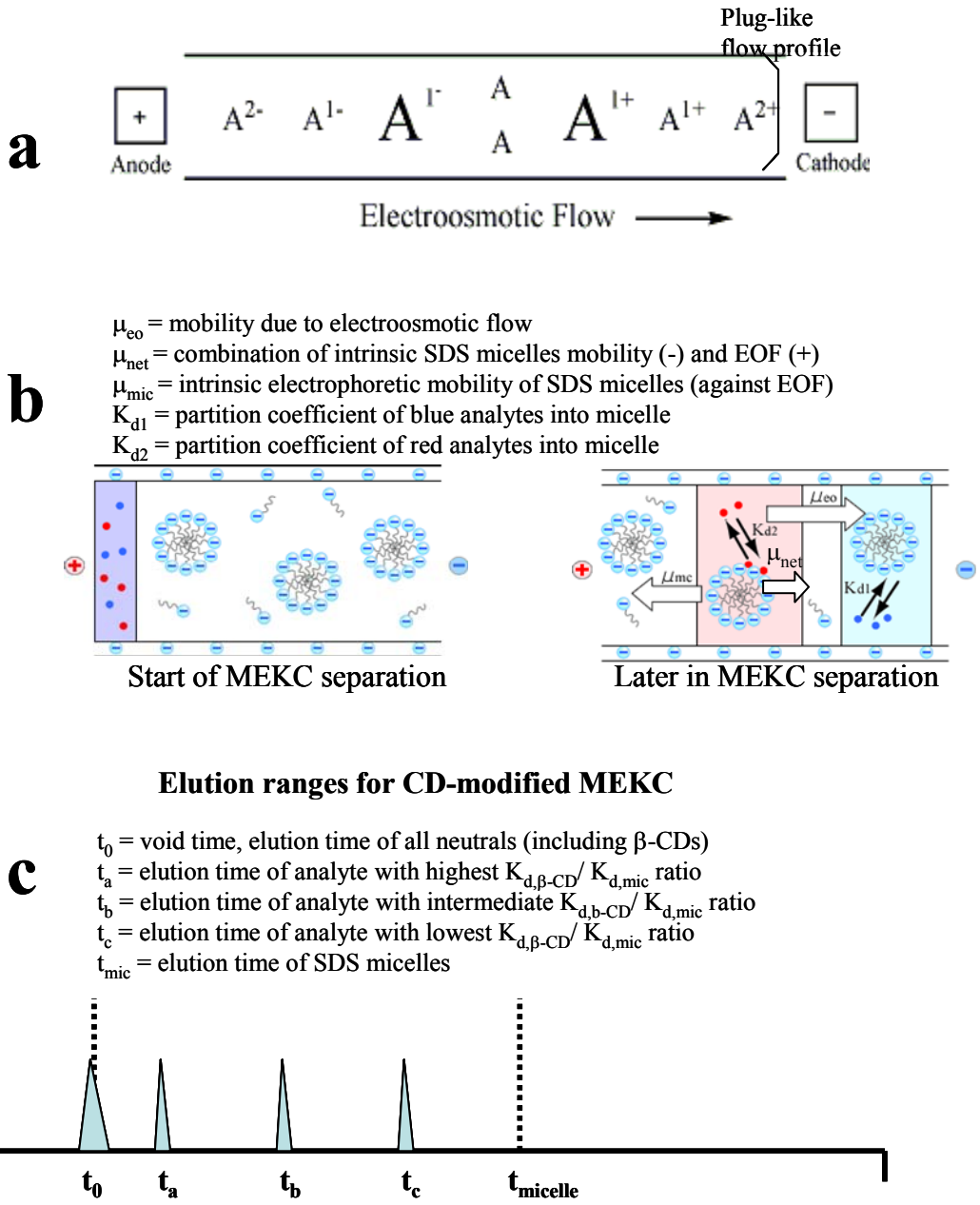

Figure 1.1: Depictions of CE and CD-modified MEKC. (a) Schematic showing plug-like flow profile and separations charged and neutral analytes (A-, A+, etc.) according to their respective electrophoretic mobilities and electroosmotic flow. (b) Separation of neutrals based on differential association with the hydrophobic micelle core. (c) Representative elution ranges of analytes of varying distribution between b-CDs and micelles for enhanced resolution and peak capacity in CD-modified MEKC. Mechanisms and wall chemistrites are similar for capillaries and μfluidics.

Because variance is a measure of band diffusion and is inversely proportional to number of theoretical plates, the theoretical limit for *N* in straight CE or CE-style μfluidics is

$$N = \frac{\mu_e V l}{2DL} = \frac{\mu_e E l}{2D} \qquad \textbf{Equation 1.2}$$

where N is number of theoretical plates, V is applied voltage, l is capillary length to the detector, t is migration time, L is total capillary length, D is diffusion coefficient of the analyte, me is electrophoretic mobility, and E is applied field in voltage per unit length. Resolution can be empirically measured following the general equation in Table 1.1, but the impact of analyte zone width and mobilities on resolution for CE and electrophoresis - style μfluidic separations are best illustrated by Equation 1.3, assuming no instrumental contribution to band broadening, i.e., system achieves an infinitely narrow sample injection,

$$\mathbf{Rs} = \frac{0.177\,\Delta\mu_e\,V^{0.5}}{[D\,(\mu_{e,\,avg} + \mu_{EOF})]^{0.5}} \qquad \textbf{Equation 1.3}$$

where $\Delta\mu_e$ is the difference in mobilities of the two species, $\mu_{e,avg}$ is the average of the two mobilities, μ_{EOF} is the electrophoretic mobility, V is applied voltage, and D is the solute's diffusion coefficient. As an examination of the equation implies, Rs approaches infinity (i.e., best separations are attained) when electrophoretic mobility is perfectly balanced by electroosmostic flow. In real separations, however, practical limitations on analysis time in conventional CE as well as the tedious control over injection of bands onto μfluidic cross channels require that optimal resolution simply based on balancing μ_e and μ_{EOF} is rarely attempted. This control becomes more difficult to maintain with

increasing separation channel lengths because the extreme the value for ratio of separation channel length to load channel length becomes, the more tedious application of even small changes in potentials at each reservoir to attain appropriate field strengths becomes.

Specialized Modes of Electrophoretic Separations

The need to separate neutral compounds from environmental and biological sources via a high efficiency method with low-reagent consumption represented an analytical imperative twenty years ago, just as a current push exists for moving such useful separations onto a robust, integrated portable platform with novel, improved detection modes. Integration of selective phases into CE running buffers accomplished such separation of neutrals, and several examples of the transition from capillary to chip with conventional detection modes such as laser induced fluorescence (LIF) exist.[26]

Micellar electrokinetic chromatography (MEKC), also known as micellar electrokinetic capillary chromatography (MECC), was first employed in the mid-1980s as a separation strategy for neutrals based on the analytes' hydrophobicity and resulting differential association with either the interior of the micelle. Another pseudophase buffer additive category includes a variety of macrocavitand oligosaccaride molecules called cyclodextrins (CDs) in cyclodextrin distribution capillary electrochromatography (CDCE). Combinations of the two, that is MEKC and CDCE, have proven invaluable assets in separations of polychlorinated biphenyls (PCBs),[27] polycyclic aromatic hydrocarbons (PAHs),[28] as well as the neutral hydrophobic toxins used in this work, including the fungal byproduct mycotoxins and endocrine disrupting chemicals (EDCs) from such diverse sources as plasticizers, pesticides, and synthetic reproduction

modulators. In MEKC, depicted in Figure 1.1b, analyte association depends only on hydrophobic association with the core of the micelle, shown in Figure 1.2a. Adding neutrals CDs to an MEKC matrix can significantly enhance the resolution of neutrals because the CDs add a second pseudo-stationary phase into and out of which the analytes can partition. The modes of interaction of CDs with analyte involves not only hydrophobic assocations but also hydrogen-bonding and charge interactions with the polar hydroxyl groups that encircle the rim of the macrocycle, shown in Figure 1.2.b. Thus, each neutral analyte's mobility is defined by the fractional time it spends in one of three, instead of two, matrices: the hydrophobic micelle interior, in association with the hydrophilic rim and hydrophobic cavity of the CD, or the aqueous running buffer. This partitioning among three phases offers an additional level of variation among very similar structurally analytes' migration and that often means resolution otherwise unattainable in conventional MEKC. In MEKC and CD-modified MEKC alike, a retention window is created between the t_0 (migration time of EOF: analogous to column void time, coincides with elution of all neutrals) and $t_{micelle}$ (elution time of micelle). Since β-CDs were the only macrocyclic oligosaccarides used in these studies, and they are themselves neutral, the β-CDs elute with the neutrals.[29] Figure 1.1c depicts the separation of neutrals a, b, and c with high, intermediate, and low ratios of association with CD to association with micelles, respectively. A pertinent expression for the velocities (v_b) of neutral analytes in CD-modified MEKC is noted in Equation 1.4.

$$\mathbf{v_b = E\,(f_{mic}\mu_{mic} + f_{\beta\text{-}CD}\mu_{\beta\text{-}CD} + f_{rb}\mu_{EOF})} \qquad \textbf{Equation 1.4}$$

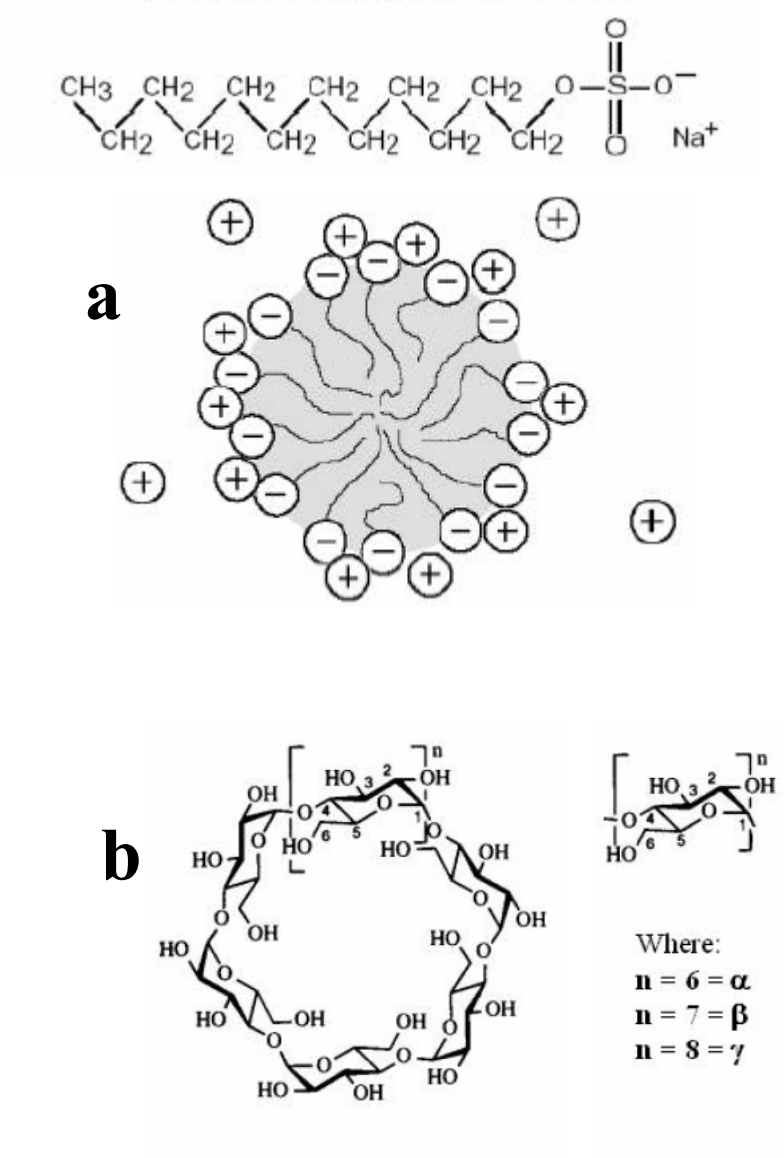

Figure 1.2: Pseudo-stationary phase components. They include (a) SDS (top, individual surfactant molecule; bottom, solution form of micelle) and (b) CDs.

Note that f_{rb}, f_{mic}, and $f_{\beta\text{-CD}}$ refer to the fractional amounts of solute in the running buffer, micellar interior, and each type of CD interior, respectively. E is the electric field applied per unit capillary length, μ_{EOF} represents the electroosmotic flow rate (which would govern the neutrals' elution were they never to complex with the pseudo-stationary phase), and μ_{mic} or μ_{CD} are the net mobilities of the micelle and CD, which define the mobility of the analyte-phase additive complex.

Manipulation of the length of the elution window, and thereby the peak capacity of the system, is achieved by lowering pH or adding organic modifier to slow flow. Conversely, increased resolution is often better attained by changing the proportions of pseudo-stationary phase or adding organic modifier, in this case not to slow the flow, but instead to alter the partitioning coefficient between the mobile (buffer) phase and the pseudo-stationary (micellar and/or CD) phase.[30] Spontaneous aggregation of sodium dodecyl sulfate (SDS) into a spherical micelle creates a statistical distribution of micelle sizes centered around sixty surfactant molecules per micelle. These formation events of course occupy a finite amount of time. From a random configuration at 0 ns, small clusters form within 1 ns and only two larger clusters remain at about 3 ns. It needs about 10-50 ns for the remaining two clusters to merge into the final micelle.[31] This constant formation-dissolution of micelles discussed earlier contributes another layer of dispersion based on statistical location options for each analyte molecule within a moving zone: in the mobile phase (running buffer) or in a micelle of each of a polydispersity of sizes. The inclusion of the intact CDs) removes this element of polydispersity and likely also alleviates some band broadening due to different micelle sizes and formation times.[32] Conventional CE ideally suffers no mass transfer band

broadening as prevalent in GC and HPLC; however, the pseudo-stationary phase capillary chromatographies are subject to mass transfer of a sort. Analyte partitions into and out of the cavity of a CD or hydrophobic core of the micelle, and this movement takes some small amount of time. Although N for MEKC and CDCE techniques can suffer a reduction compared with conventional zone electrophoresis due to this partitioning, the ability to resolve otherwise untenable combinations of neutrals on low-volume platforms is worth some loss in capacity.

Microfluidics

Most cite the original μfluidic as being the GC column created as a model to help describe gas and liquid flow in small channels by studying the transport of gases in silicon micromachined channels by Pfahler, et. al., in 1991.[33] However, the seminal work in modern fluidics as pertains to the research described herein was carried out in the labs of J. Michael Ramsey, particularly by Steven Jacobson and Christopher Culbertson,[34,35] and George Whitesides.[36,37,38] Whereas Ramsey's group led the charge in proving the analytical merit of transferring the principles and chemistries available for capillary electrophoresis onto wholly glass μfluidic devices, Whitesides pioneered the more facile, geometrically more forgiving, and more readily disposable fabrication of devices in the elastomeric polymer polydimethylsiloxane (PDMS). From the semiconductor and microscopy fields, μfluidic workers have inherited photoresist technology for etch resistance during glass device preparation, positive relief creation from which polymer devices can be molded, and precise depth and geometry determination using reactive ion etching and electron beam lithography. The fabrication

of μfluidic devices alone has occupied a staggering number of scholarly journal articles over the past thirteen years.

Microfluidic separation and fluid handling systems have garnered much attention in the past decade as a portable, small footprint means of carrying out chemical and biological processes on a manageable, solvent- and sample-conserving platform.[1] Electrokinetically driven processes where electric fields are used to generate channel flow within a device have received the most attention. Electrically driven separation techniques such as CE,[39-41] open channel electrochromatography (OCEC),[42,43] MEKC,[44] and capillary gel electrophoresis[45,46] have been described by a number of research groups. Microfluidic versions of these techniques (many developed for conventional CE at least in part by the Sepaniak group) have shown performance either equivalent to or better than conventional laboratory devices; in many cases they offer the rare combination of improved analysis, in less time, with less reagent and power consumption, simultaneously. By creating redundancies of sample inputs and operational fluidic channels on the same chip (horizontal integration), and patterning in the footprint of a titer plate, high-throughput can be facilitated. Comprising myriad patterns of channels, reservoirs, and flow directors, μfluidic devices were originally, and are still, widely fabricated from glass.[47] However, the body of literature describing their fabrication from polymers has grown steadily since their emergence as alternatives to the tedium of creating glass devices.[48] The polymer most widely employed is PDMS due to its several advantages over other elastomers. Some of these advantages include: minimal optical absorption in the near UV,[49] physical flexibility and chemical

robustness,[50] propensity to conformal sealing with semi-smooth surfaces including itself, [51] and availability for chemical modification of its surface. [37]

An aspect that is vital to work involving the inclusion of living organisms into μfluidic devices is the high oxygen/carbon dioxide permeability of PDMS,[52] which is necessary for the use of live bioreporters in proposed studies. Several reports detail good viability for various cell lines in PDMS. Cell patterning to probe interaction between two cells lines,[53] cell growth in two-dimensional networks,[54] complete cell lysis and separation apparati,[55] and two- and three-dimensional cell perfusion studies[56,57] have been pursued in PDMS. The cell types include carcinoma, conventional endothelial, and E. coli. Viability is generally limited according to specific experimental test parameters, not cells' incompatibility with their elastomeric homes.[53-57]

Despite being governed by the theories of the CE or other chromatographic incarnations transferred to its platform, μfluidic separations and fluid delivery have individual sets of requirements for successful implementation of established experimental methods. Figure 1.3 shows some examples of μfluidic devices used in this work. Figure 1.3a and 1.3b represent early uses for nanocomposite metal-elastomer SERS substrates, i.e. for fluidic delivery (a) and titer wells for assaying 50 microliter aliquots of sample with SERS (b). Figure 1.3c shows one incarnation of the current μfluidic-SERS device under the microscope objective of the JY Horiba LabRam Raman spectrometer. Figures 1.3d and 1.3e show layouts of the cross channel μfluidic device (d) with either and simple or offset injection intersections. Figure 1.3e at far right is a CCD camera image of one such injection intersection within a device fabricated for this work. The video CCD option on the LabRam was crucial, not only for visualizing clear

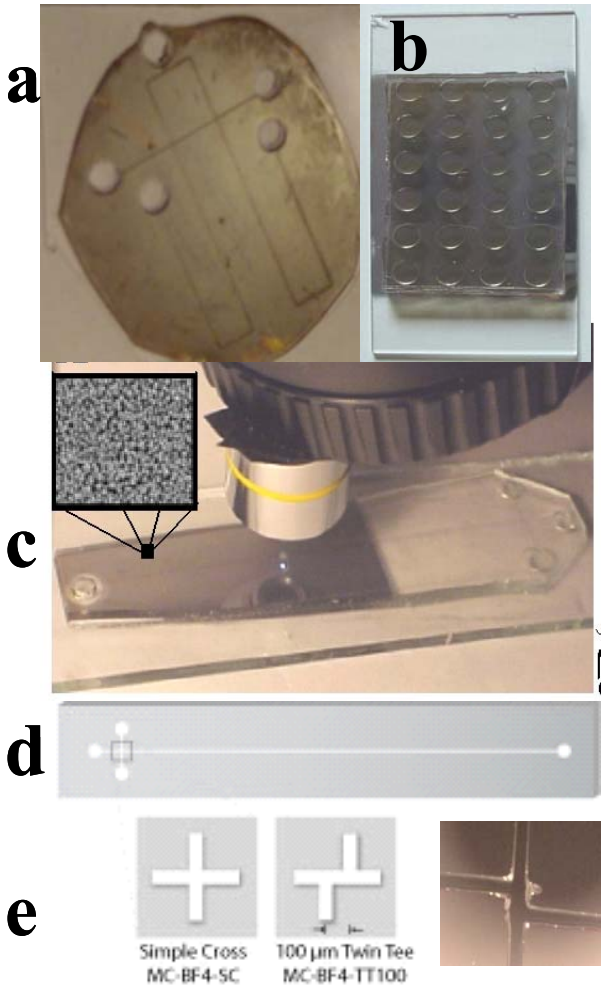

Figure 1.3: Representations of µfluidic devices. These show devices used in this and other work and demonstrate flexibility in function as well as small size. Commercial injection tees and one created in-house are compared along the lowest row.

channels and intersection geometries but, more importantly, for aligning the long dimension of the μfluidic separation channel as perfectly as possible with the movement of the LabRam's XYZ stage. This alignment serves the critical purpose of maintaining the integrity of spectral collection during location and SERS mapping of electrophoretically delivered and separated bands. If the stage and separation channel are out of sync, useless spectra are collected from outside the walls of the μfluidic channel.

Beyond the intricacies of fabrication discussed later in Chapter 2, the central requirement distinctive from older methods for separations on μfluidic chip is introduction of sample. No longer is this task feasible simply from the front end of the separation channel due to its confinement in a quasi-two dimensional plane. Most often, to address sample introduction most efficiently, a μfluidic is constructed with channels for sample loading transecting the main separation channel. Figure 1.4 shows such an intersection with the resulting patterns of flow when "pinched" versus "floating" injection schemes are employed. These names refer to presence ("pinched") or absence ("floating") of potential applied to the buffer inlet and outlet reservoir. In the "pinched" voltage arrangement, potential applied at the buffer inlet and outlet initiate a minimal flow toward the sample waste to restrict sample leaking out into the separation channel during the electrokinetic load step. An indicator of flow directions is imposed upon a photograph of a real integrated μfluidic-SERS device in Figure 1.5, and relative voltages as well as a representation of the switching circuit that selects between resistor arrays. The ability to tune between a small injection, a sample overload, and no injection at all, becomes increasingly more difficult as the ratio of separation channel

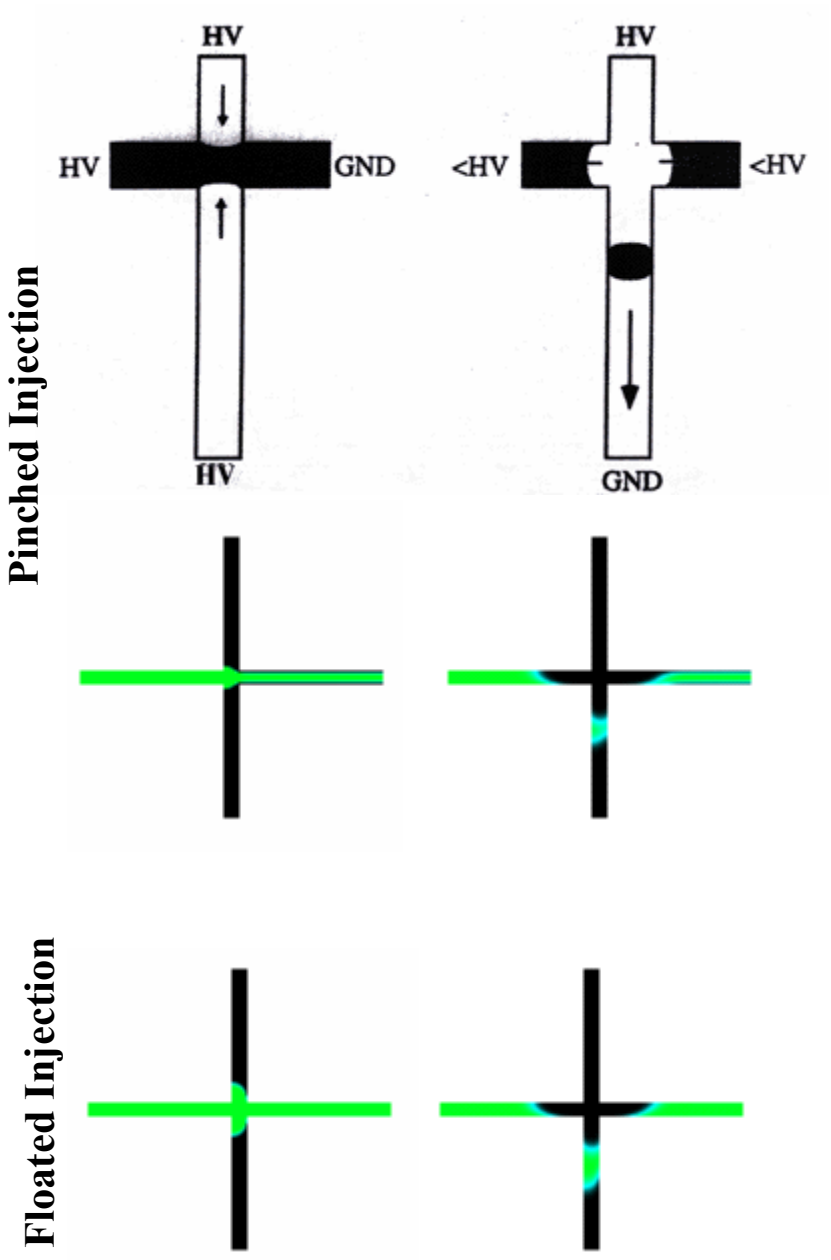

Figure 1.4: Pinched vs. floated injections cross sections. Contrast in injection length between the two cases results from potential being applied at all four reservoirs to control flow into separation channel during load and to prevent diffusion from cross injection channel during separation.

a

4 reservoirs	*% Total Potential: Load*	*% Total Potential: Separation*
Buffer waste (BW)	100%	0%
Buffer inlet (BI)	45%	100%
Sample inlet (SI)	90%	65%
Sample waste (SW)	0%	55%

b

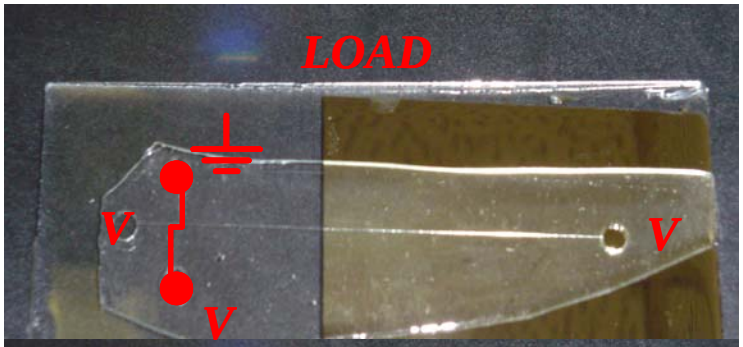

c

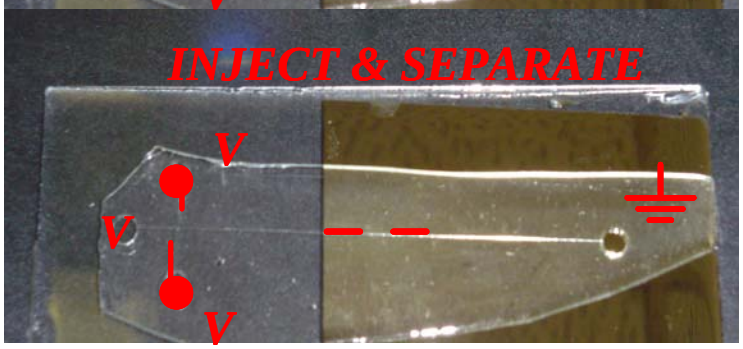

d

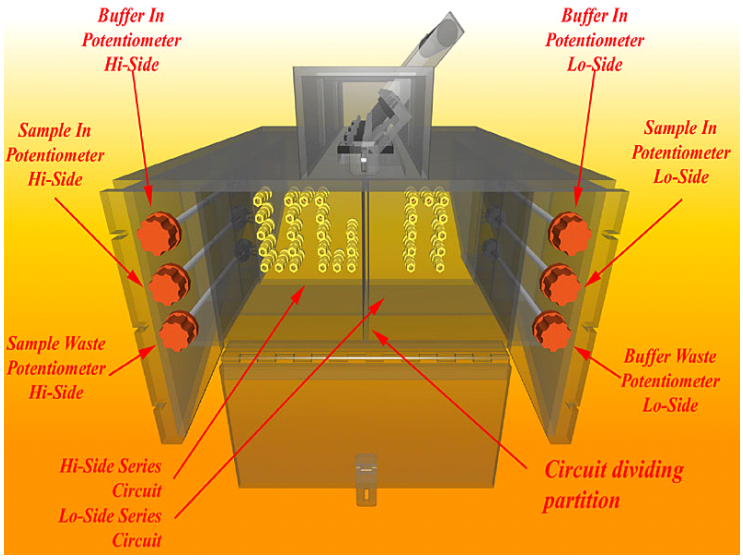

Figure 1.5: Visualizing aspects of electric field application. Shows voltaes schemes (a), resulting sample movement (b,c), and switching circuit with resistor arrays that actuates voltage selection.

length to load channel length increases. However, pinched injection voltage schemes can result in narrow injected bands relative to floating injections, which can improve resolution. Electrokinetic loading across an intersection from the front of the separation channel as in CE removes the electrokinetic bias, so long as the load time is sufficient to allow sample components of all μ_e to cross the intersection. The voltage percentage applied to each reservoir is determined by the connection of that reservoir to a high voltage supply through a resistor array. Many groups have developed sophisticated solenoid switching for their resistor arrays with computer control and sub-millisecond timing.[58] As the focus of this work was to integrate a vibrational spectroscopy onto a μfluidic and ***not*** to fundamentally push the limits of the μfluidic separation technique, a homebuilt switching circuit with manual (~0.3 second) actuation sufficed. Figure 1.5a gives the approximate applied percentages of potential necessary to initiate an injection as shown in Figure 1.4 and subsequently actuate a separation free of extraneous sample leakage into the separation channel. Cartoons of these two steps are shown in Figure 1.5b and 1.5c. Figure 1.5d displays CAD designs of the circuit, comprised of two resistor arrays with variable connectors for each reservoir (buffer inlet, buffer outlet, sample inlet, sample waste) for each high voltage supply (load supply, separation supply). This switching circuit and its resistor arrays were designed and manufactured in-house in order to facilitate complete creative control over the actual switching (knife blade throw switches) and tuning (potentiometers for each electrode lead on each resistor array). These potentiometers give fine adjustment of resistance and hence percentage of total potential applied at each electrode, each electrode lead plugs into the yellow connectors (see Figure 1.5d) on both the load ("lo-side") and separation ("hi-

side") resistor arrays on each side of the protective, insular Plexiglas® partition. Other methods of sample injection involve optical gating, wherein sample is constantly injected and photobleached until the laser pulses off for a split second, defining picoliter sample volumes; although excellent for providing short sample injection, this method can only be employed with certain types of samples and expensive, largely non-portable, high-powered lasers.[59]

Background of Surface Enhanced Raman Spectroscopy

The inelastic scattering, or "secondary radiation" as C.V. Raman termed it in his Nobel Prize-winning work in 1929,[60,61] of light due to the interaction of photons with the vibrations of molecules due to an induced dipole, i.e., the polarizing of the electron cloud within a bond, has developed in spurts since its inception, unable until recently to compete with infrared spectroscopy due to instrumentation deficiencies. However, the past three decades have seen an upsurge in Raman spectroscopy due the several concurrent instrumental improvements. The broad application of laser irradiation sources in the 1960s offered orders of magnitude increased power at a nearly single wavelength and decreased spectral interference of irradiation with scattered light as well as offered longer wavelength (lower energy) more monochromatic irradiation that helped mitigate the pervasive fluorescent interference that plagues the Raman technique. Selection of Raman bands over Rayleigh and other scattered light was also prodded along by employment of triple monochromators, which have since been supplanted by highly efficient holographic filters that increased the throughput of scatter to the transducers. Transducers have also morphed from the single channel photomultiplier tubes, to photodiode arrays (PDAs), to now state-of-the-art charge-

coupled devices (CCDs) which decrease spectral collection time (multichannel, simultaneous spectral collection with no scanning) and suffer far less inherent electronic noise than PDAs. A representation of a modern Raman spectrometer in a confocal configuration, such as the JY Horiba LabRam that was used in all the work described, appears as a block diagram in Figure 1.6. The most critical components not yet mentioned include the spectrograph for efficient spreading and collection of scattered light and a video CCD camera option for aligning μfluidic-SERS devices on the XYZ stage. The confocal geometry of this Raman scattering collection scheme is amenable to μfluidic-SERS platform because the laser beam can be focused down through the μfluidic top plate to the SERS substrate within the channel with negligible loss in signal response. Pelletier's text gives an excellent description of the operation of Raman spectrometers. [61]

A Physical Picture of SERS

Mathematical descriptions of the theoretical aspects of surface enhancement's effect on Raman spectroscopy have been developed.[74,79] However, some controversy over exact mechanisms, as well as the complexity of the mathematics, can blur a practical understanding of the SERS phenomenon. Therefore, a simplified but useful attempt is made here to create a physical picture of the SERS effect.

The basis of the electromagnetic enhancement mechanism of SERS is the amplification of the EM fields associated with both the impinging radiation and the scattered light via interactions with a nanostructured metal surface. Radiation of an appropriate wavelength impinging on a noble metal surface can initiate oscillations, at the radiation wavelength, in the loosely held conduction band electrons of the metal.

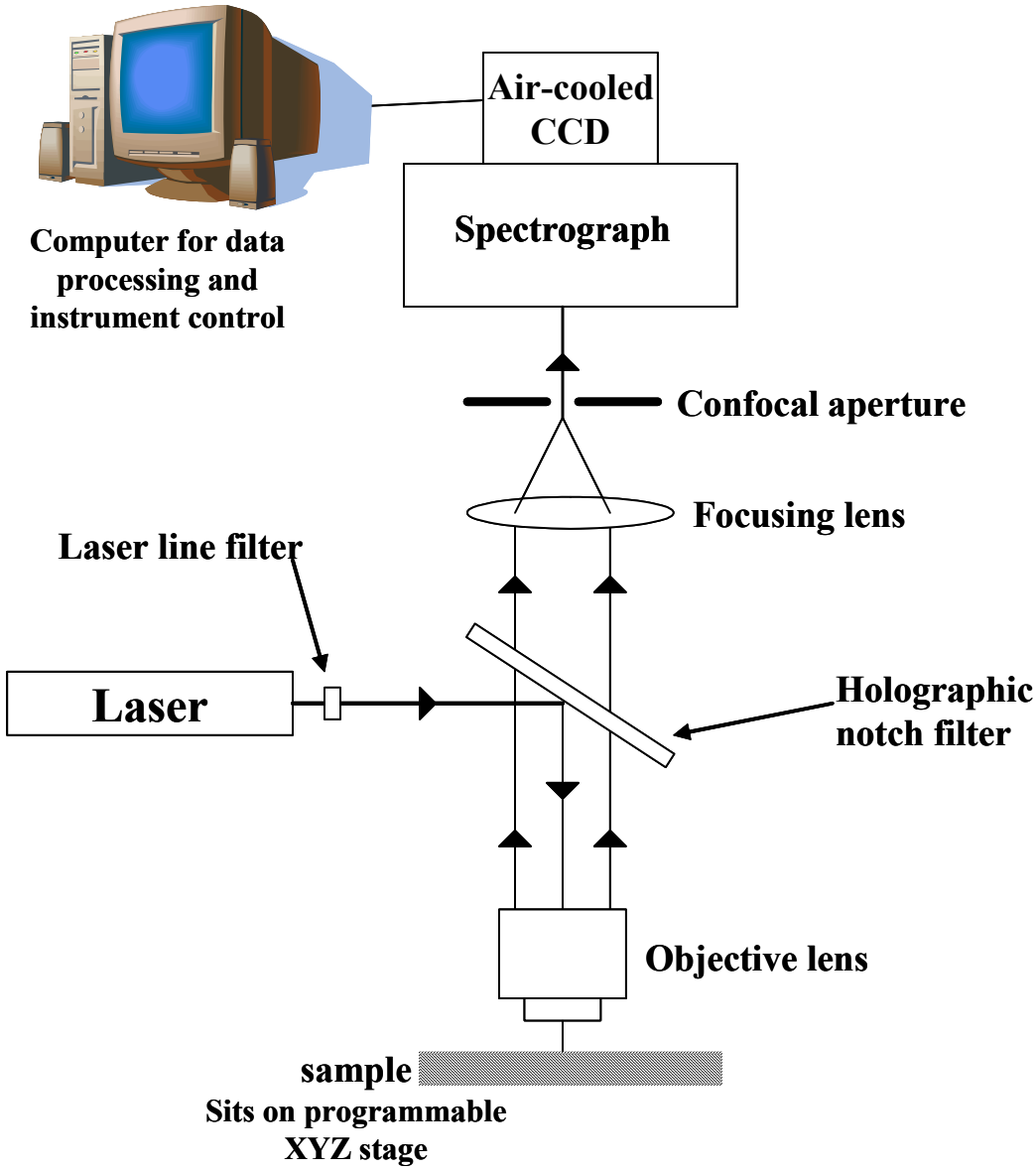

Figure 1.6: Diagram of confocal Raman instrument.

Electrons rush in waves along the metal's surface, propagating parallel to the metal as "surface plasmons." In an extended structure such as a flat metal surface, the surface plasmon is much like a traveling wave. However, the presence of protrusions such as discrete metal nanoparticles or nanometer scale surface roughness can create confinement situations where, if the impinging radiation is resonant with the metal structures, a standing wave is created that can produce areas of intensely enhanced EM fields. These fields amplify both the initial light impinging upon an analyte molecule as well as the inelastically scattered light radiating from the energy interchange between the impinging light and the molecules' vibrating chemical bonds.

In extended arrays of metal protrusions or nanoparticles, the creation of standing electron waves and the concomitant large surface plasmon related fields, bares some analogy to the standing waves generated via lasing action in the laser's cavity. Factors that influence the intensity of a single lasing cavity mode include the dimensions of the cavity as determined by positions and curvatures of the end mirrors, the refractive index of the lasing medium that influences the wavelength and speed of light, and the reflectivity of the mirrors. In a similar fashion, the dimensions of a metal nanoparticle or protrusion and the dielectric properties of both the metal and the surrounding medium govern the magnitude of the resonant effects that gives rise to surface plasmons. From this physical picture it is clear that tuning of these properties, particularly the morphological properties, as they relate to the wavelength of the impinging radiation is essential in designing superior performing SERS substrates.

The SERS substrate's propensity to couple constructively with a particular laser wavelength can be roughly gauged by measuring the optical extinction band(s) of the

substrate via a UV-vis transmittance scan, such as the ones shown in Figure 1.7, a further discussion of which is given later in this section. The attenuation of incident radiation depends on several factors, e.g., absorption and reflection, the most relevant to this discussion being the coupling of the incident radiation to generate a surface plasmon field. In our prior work involving regular periodic arrays of metal nanoparticles formed by nanolithography, there was an expected inverse relationship between SERS performance and the amount of backscattered radiation (i.e., greater extinction yielded better SERS performance).[88]

The physical deposition process and colloidal solution preparations create randomly spaced and sized nanoparticles in a statistically determined wide distribution of sizes and shapes (i.e., regular to high aspect ratio spheroids). Regions of highest enhancement have been found in modeling results for corners and small radius of curvature areas of metal particles or protrusions, lending a lightening rod effect to the shapes, and locations in proximity with around those shapes, that best enhance signal. Figure 1.8 illustrates this point with discrete dipole approximation calculations that model field strengths around a prolate spheroid.[89] Note that the most intense fields are near the tip of the spheroid. The calculation was performed for the case of the laser polarization along the long dimension of the spheroid. Rational design and creation of substrates by computer aided design programs which guide electron beam lithography or reactive ion etching can lead to substrates with more of these focused loci with the added benefit of heightened intra- and inter-substrate homogeneity and thus increases in reproducibility of high SERS activity.

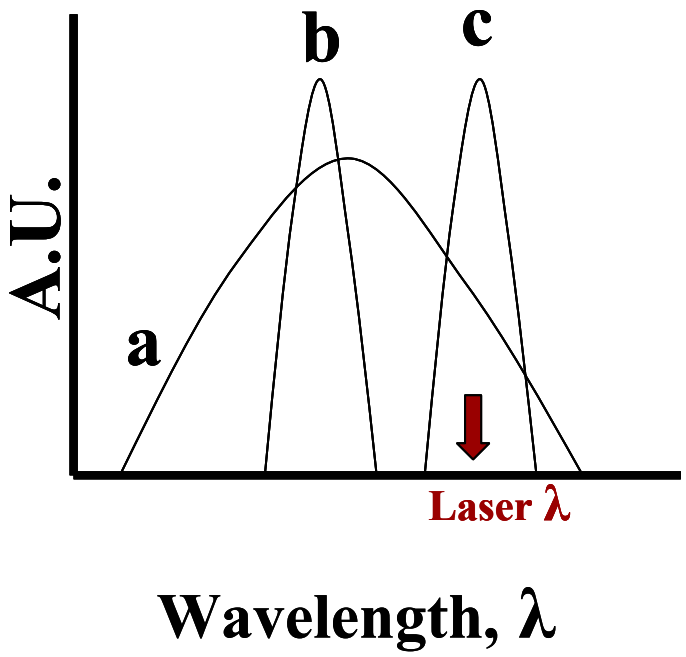

Figure 1.7: Depiction of hypothetical extinction bands for different SERS substrates. (a) Broad extinction for a heterogeneous Ag-PDMS nanocomposite. (b) More narrow extinction for regular periodic arrays created with EBL. (c) Demonstration of a regular periodic array with its size, shape, and arrangement altered to tune the substrate's extinction to overlap with a hypothetical laser wavelength.

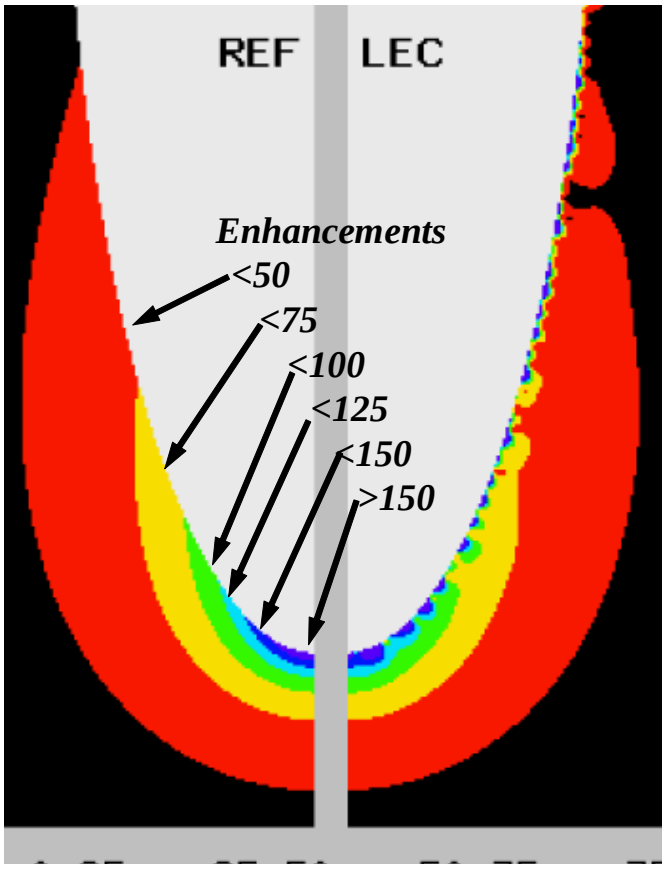

Figure 1.8: DDA calculation that models enhancement around a silver prolate spheroid. Theoretical irradiation is with 633nm laser excitation. "REF" refers to an exact solution of Laplace's Equation, and "LEC" refers to the DDA with a surface correction (see Reference 107 for full explanation). Note that enhancements are most pronounced around the tip of the structure.

Additionally, an increase in homogeneity would narrow and potentially intensify the extinction band (as shown in Figure 1.6b). Increases in SERS enhancement can be achieved by improving the energetic match between impinging source light with the extinction band of the metal-dielectric substance combination comprising the substrate. Although multiple laser lines are available, a more practical approach to getting overlap of the extinction band of a substrate with the laser line involves creating arrays of metal protrusions and/or nanoparticles that have sizes, shapes, and arrangements tailored to best exploit a particular wavelength of laser radiation. For example, the laser light in Figure 1.7 would be a marginally acceptable irradiation source for the randomly sized and arranged nanoparticle substrate whose extinction band is Figure 1.7a. The extinction bands represented by Figures 1.7b and 1.7c demonstrate an example of how tuning size, shape, and arrangement of nanoparticles could bring a substrate into optical overlap with, and thereby increased coupling to and enhancement from, a particular laser's radiation. Additionally, because regular arrays can mitigate some of the spatial irreproducibility among signal enhancement associated with SERS substrates, rational design represents path to making SERS a more analytically relevant tool.

Theoretical predictions indicate that dimer pairs of metal particles can produce exponentially increased fields between them.[89] Thus, the importance of particle spacing is seen. Part of exploiting such long range effects in both the substrates available now and those developed in the future involves finding methods to favorably position analyte molecules within locations of highest enhancement. Nanofabrication of composite materials that not only include high surface plasmon fields but also means to

enhance the sequestering of analyte in special regions of the substrate, such as spatial confinement using molecular recognition phases, is also much needed.

Vibrational spectroscopies offer marked advantages in structural information content when compared to UV-vis techniques that rely on electronic transitions of molecules for spectral readouts. Contrasting the SERS and fluorescence spectra in Figures 1.9a and 1.9b, respectively, demonstrates the significant difference discussed in Chapter 1 between the broad, nondescript fluorescence emission band with the much more distinctive vibrational spectrum is demonstrated for an analyte of international environmental and biomedical import. Aflatoxin B2 is a known carcinogen and suspected teratogen, produced by fungi growing on nuts and grainstuffs, which is monitored at trace levels in human food commodities as well as animal fodders due to its propensity to bioaccumulate in the fatty tissues of livestock, thereby pre-concentrating the toxin in meat products delivered for human consumption. The ability to collect such descriptive spectra from an analyte like Aflatoxin B2, that is to say, analytes which pose threats to human and environmental health as well as national security, foreshadows the discussion of applications of μfluidic-SERS for analysis of EDCs in chapters 4 and 5.[62] In comparing vibrationally informational phenomena, Raman is vastly more amenable to aqueous environments than infrared spectroscopy. It is for this reason, combined with the technological maturity of source radiation, wavelength selection, and efficient transduction, that Raman has gained and continues to gain greater usage within the biological and analytical communities. However, improvements in spectrometer instrumentation alone cannot compensate for the fact that the Raman scattering cross section for most molecules ($\sigma = 10^{-29}$ cm^2) can be up to

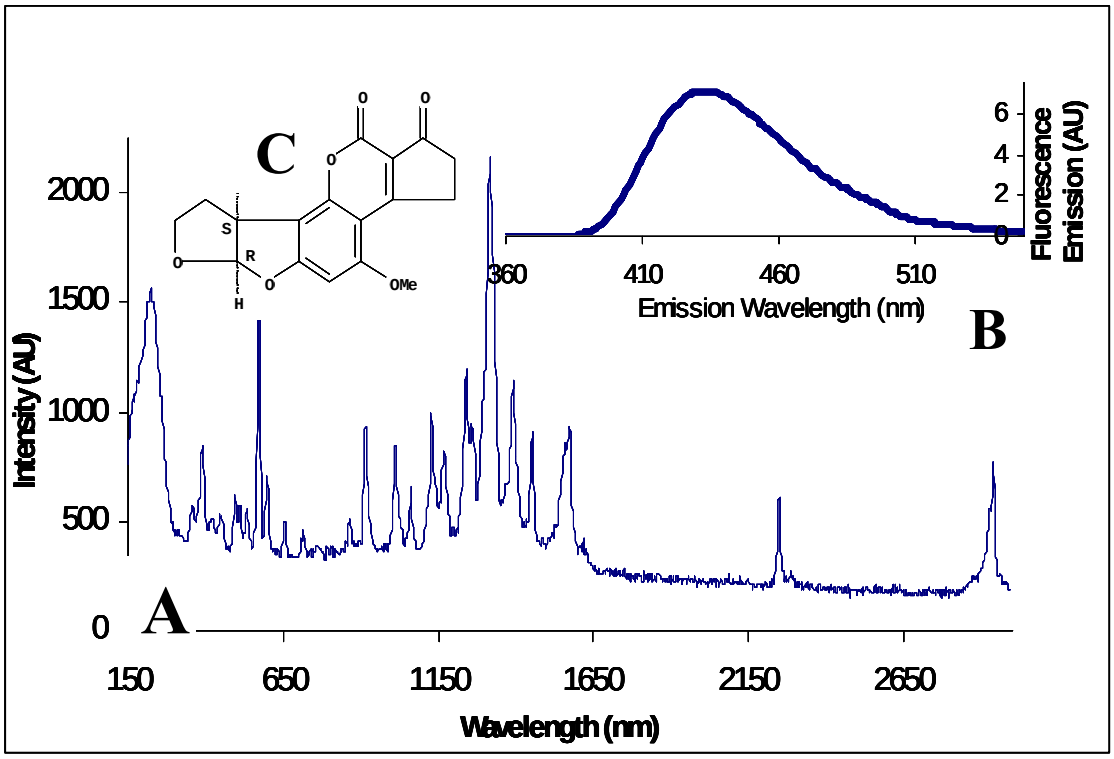

Figure 1.9: Contrast between LIF and SERS spectra for a toxin sample. (a) non-descript fluorescence emission with (b) information-rich SERS vibrational spectrum for (c) alflatoxin B2

eleven orders of magnitude smaller than other typical optical spectroscopies such as UV-visible absorbance ($\sigma = 10^{-18}$ cm^2), fluorescence ($\sigma = 10^{-19}$ cm^2), or IR absorbance ($\sigma = 10^{-20}$ cm^2).[63,64] Scattering or absorption cross section relates the probability of the rate of incident photons' interaction with a molecule to the rate of the scattering in area by that molecule. Raman transition dipoles are a function of analyte polarizability (α) and the magnitude of the electromagnetic field (**E**) according to the following:

$$\mu = \alpha \mathbf{E} \qquad \textbf{Equation 1.X}$$

where μ is the induced dipole moment within the transiently polarized molecule. **E** is the electric field of the incident radiation, whose photons have an electromagnetic field which exerts its oppositely directed forces on the molecule's protons and electrons.[65] This interaction yields the transient polarization that results in either a net energy loss between incident and scattered photon (Stokes Raman Scatter) or, generally less often due to the sparse initial population of vibrational levels above v_0 according to the Boltzman distribution, a net energy gain between incident and scattered photon (Anti-Stokes Raman Scatter). This energy loss or gain of the scattered photons relates to the vibrational energy of the molecule as

$$E_{scattered} = h\nu \pm \Delta E_{vibrational} \qquad \textbf{Equation 1.X}$$

where $E_{scattered}$ and $\Delta E_{vibrational}$ are the energy of the scattered radiation and change in difference in initial and final vibrational energies, respectively; h is Planck's constant;and ν identifies the incident radiation in wavenumbers.[66] The wave model of Raman also tells us that polarizability, α, is the propensity of a molecule's electron cloud to be deformed by an electromagnetic field and does not have a constant value but

varies by molecule, vibrational, and rotational mode. The intensity of scattered radiation is proportional to ν^4 and E_0^2, where ν equals the wavenumber of incident radiation and E_0 equals the maximum amplitude of the incident electromagnetic field, and the intensity of Raman scattering in particular is proportional to the rate of change of the polarizability squared, always accounting for the fact of Boltzman's imperative that the greatest population of molecules lies in the ground state under most conditions. Despite an elegant theoretical basis having been established for Raman in the literature spanning 1930-1970s, the severely limited sensitivity of the technique for most applications restricted its use during that period to glasses, metals, ceramics, and composites containing far more than trace percentages of components of interest. A comparison of the energetic transitions for the two main laser spectroscopies used in the work, Stokes Raman and fluorescence, along with conventional absorbance appears in Figure 1.10. Also shown is anti-Stokes Raman, wherein a molecule begins in a raised vibrational level and scattered radiation is of equal or higher energy than impinging radiation. Resonance Raman results when the virtual level coincides with a real molecular excited state and can yield significant enhancement of SERS signal beyond even the normal chemical and EM enhancement factors.

Crucial work in the 1970s indicated that proximity of molecules to a noble metal surface can significantly enhance both the incident and any resultant fields from said metal surface, sparking a revolution in the use of Raman spectroscopy, not to mention subsequent fundamental studies of plasmons, charge transfer electrochemistry, and metal nanoparticle physics.[67-71] After observing inexplicably high Raman signals from pyridine adsorbed to a roughened silver spectroelectrochemical electrode,

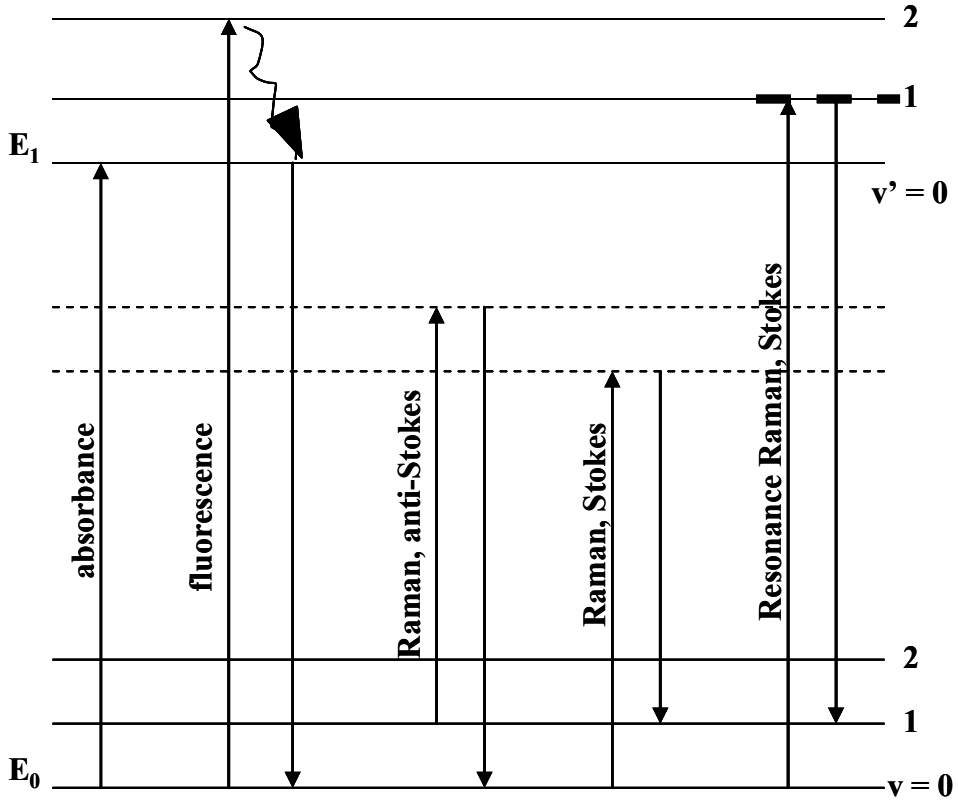

Figure 1.10: Jablonski diagram. Shows energetics of absorbance fluorescence emission, anti-Stokes and Stokes Raman scatter, and resonance Raman scatter (example shown is Stokes Raman). Note that virtual states are donated with dashed lines.

Fleishman asserted that increased surface area allowed more molecules to scatter and have their scattered light be observed within a small field of view/optical interrogation.[72,73] Van Duyne and Creighton, in separate publications released concurrently, reevaluated Fleishman's initial explanation, noting that calculations including pyridine's Raman scattering cross section combined with the number of molecules interrogated could only account for, at most, 0.01% of the signal experimentally observed.[74,75] Even after three decades of research, exact mechanistic details of this enigmatic surface enhancement effect are still being debated, but a central understanding is generally accepted and pertinent to the discussion of μfluidic-SERS as a novel analytical combination. Via two distinct but complementary mechanisms of electromagnetic (EM) and chemical enhancement, surface enhancement effectively increases the otherwise tiny scattering cross-section of most molecules. Hence, intensity of Raman-scattered light can be enhanced up to a reported twelve orders of magnitude good for low-volume studies of single molecules,[76] although normal, non-molecular resonance enhancement factors are usually closer to between four and seven orders of magnitude. This is still a helpful and rather impressive improvement, especially in light of the rich degree of structural information available from the narrow vibrational bands in SERS spectra for molecules with the requisite change in polarizability (a requirement for Raman's inelastic scattering) and orientation and proximity to metal nanoparticles, protrusions, or loci of several nanoparticles.

Electromagnetic theory of SERS, and the widely accepted explanation of its electromagnetic enhancement mechanism, is based on classical optics of colloids and small particles.[76] The enhancing surface plasmons propagating among metal protrusions

or nanoparticles are initiated by impinging radiation (usually from a laser) that is somewhat resonant, i.e has some energetic overlap with, the extinction bands of the SERS substrate, which are determined in large part by the dielectric constant of the substrate medium and the arrangement of particles or protrusions in or on the substrate. In this mechanism, the identity of the analyte molecule does not add to or detract from the degree of enhancement. One generally accepted governance when SERS substrates' extinction is not easily measurable is that noble metal nanoparticles must be smaller than the wavelength of the incident light and that, although molecules of interest do not have to be touching metal, they be within a specific close range, as electromagnetic enhancement decays cubically with distance from the particle.[M9, M10]

The second enhancement mechanism, more hotly debated than EM, is that of chemical enhancement.[79,80] Specifically, in the charge-transfer model, a molecule briefly receives noble metal electrons into its lowest unoccupied orbital, and this overlap of metal and adsorbed analyte electronic wavefunctions leads to increased polarizability (α), or new energy levels, as well as lowering the energy of its excited electronic transitions. This chemical interaction thereby both increases the likelihood of an inelastic scatter event due to changed polarization and also quenches the fluorescence that so perniciously competes with Raman scattering.[81] Although chemical enhancement serves as an excellent supplement to some of the exploratory analytes used for preliminary testing in this work, the more broadly applicable EM enhancement mechanism is relied upon most heavily. Therefore, upon full maturity, the technique of μfluidic-SERS will be more pertinent to real analytical samples.

Some limitations of SERS include its nature as a surface phenomenon, or, more specifically, a phenomenon limited to a finite volume of regions within a substrate where molecules can orient favorably in proximity to the metal and their scattering signal can be enhanced. This limits the linear dynamic range (LDR) of SERS at the high end. The low end of the LDR is limited by the sensitivity of the SERS substrates and proper delivery of analyte to the loci of great enhancement. Historically, creation of reproducible SERS substrates, and hence reproducibility of the analytical scattering signal, has been an obstacle and has curtailed the quantitative and qualitative power of the technique. Methods to address both sensitivity and substrate reproducibility include using regular metallized substrate structures optimized for maximum enhancement created via electron beam lithography (EBL). Extension of the upper limits of the LDR involve rational spatial and temporal interrogation of gradients of analyte within electrophoretic bands. Both of these approaches are discussed in later chapters.

Rationale Behind Integrating μfluidic-SERS

Mating any separation, and especially CE and its related chromatographies, with the most structurally descriptive detection mode possible improves analytical power of the total method by increasing information content of the data output and helping to mitigate practical problems attendant to separations such as changing migration/elution times and coelution. Vibrational optical spectroscopies offer said high structural information content. Of those, Raman scattering is conveniently compatible with aqueous matrices and can yield spectral data for many classes of compounds in imperative need for analysis for environmental, biological, and national security pursuits. The integration of random nanocomposite substrates [comprised of PDMS] for

surface enhanced Raman spectroscopy (SERS) in the earliest part of the research described herein followed as a natural consequence of concurrently proving the nanocomposites as functional SERS substrates along with learning of the fabrication methods required to created μfluidic separation devices in said material. As mentioned earlier in the discussion of efficiency and resolution in CE-style μfluidic separations, abbreviated channel lengths in μfluidic devices mean that efficiency becomes even more imperative to retain acceptable resolution. However, the integration of structurally descriptive detection modes like SERS can address coelution problems by positively identifying components whose zones are mixed based not on migration time or a non-descript broad band absorbance or fluorescence signal, but instead on the spectrum of narrow vibrational bands resulting from the two components as collected in the outer edges of each component's migration zone. Early work with colloids in CE running buffer, electrofilament deposition of CE effluent onto SERS substrates, and counter-current introduction of SERS active colloid at the outlet end of a capillary pursued the CE-SERS combination in order to lessen some of these same disadvantages in conventional CE. However, flow changes and the resulting loss in band resolution, in addition to the extremely tenuous maintenance of the electrofilament, proved inconvenient. Integration of SERS substrate into the walls of a sample vial is also employed, but the ratio of analyte in a two mL cylinder of sample solution to the amount that diffuses to the vial's walls means total mass detection efficiency is low and time of analysis is long. In light of these similar approaches to integrating SERS substrates directly into analytical devices, especially μfluidics rigged for separations,

becomes a promising avenue to almost symbiotically mitigate problems of both the separation and the spectroscopy.

CHAPTER 2

Fabrication, Set-up, and Compatibility Tests of μfluidic-SERS Devices

μfluidic Devices

Although commercial μfluidics suppliers abound, our novel integration of a SERS detection region meant that early testing benefited from the in-house creation of devices tailored to the individual functionality of each analysis task. Eventually, commercial channels were integrated into hybrid PDMS-glass devices, but only after many other chip creation strategies were exhausted of their testing potential. Fabrication of microfluidic devices was approached in various ways, all with inherent advantages and disadvantages. The most prominent methods will be described briefly here with a particular focus on the technology most utilized. Table 2.1 provides a synopsis of the fabrication methods tried in pursuing integration of the μfluidic-SERS devices.

Photoresists and PDMS Casting

A common theme is the employment of photoresist methods to create etchant masks (i.e., barriers that are resistant to the compounds used to chemically remove material) and positive reliefs for defining where channels in glass are etched and creating a mold over which PDMS can be cast, respectively. Because photoresists factor so prominently in the fabrication of devices used in this research, some discussion of photoresist methods is warranted. First pioneered and currently advanced for the manufacture and testing of semiconducting high-end apparati, the application of photosensitive polymeric resists was co-opted by the fledgling arena of micro-total

Table 2.1: Procedures for Fabrication of μfluidic Devices

Channel Fabrication Method	# # positive relief mold for PDMS casting **direct channel creation
SU-8 ##	Spin-coat negative SU-8 photoresist onto transparency; expose (365 nm, 45 sec) through stainless steel mask (fabricated in-house with 0.006" jeweler's slotting saw blade). Develop in PGMEA; hardbake (115ºC, 25min).
Etch copper ##	Spin Shipley 1813 positive photoresist onto glass; softbake (90ºC, 30min). Same exposure as SU-8. Develop in organic base developer from Shipley; water rinse; hardbake (110ºC, 45min). Etch 30 min in stirred, acidified ferric chloride. Water rinse.
Pressure mold PTFE ##**	##Mill negative reliefs out of stainless steel; place PTFE on a heated press to be molded into this negative, creating a positive relief mold. **Alternately, tungsten wire is fashioned into channel pattern and pressed into PTFE to create channels.
Etch glass**	Clean glass in RCA solns; convection bake to remove residual water. Spin Shipley 1813 positive photoresist onto glass; softbake (90ºC, 30min). Same exposure as SU-8. Develop in organic base developer from Shipley; water rinse; hardbake (115ºC, 25min). Etch 90 min in gently stirred buffered HF. Remove residual photoresist with acetone, rinse glass with water.
Construct with mscope slides**	Clean 2"x5"glass base and four 0.17 mm-thick coverslips in RCA solns; convection bake to remove residual water. Spin diluted sodium silicate solns onto glass pieces; adhere in place to create channels, using 75 mm wide spring steel in channel pattern as a spacer. Anneal at 90°C for 1 hr.

analytical systems in the IBM-Zurich labs first and most aggressively.[82] The connection between nanoscale information storage and computational task execution was bridged in the clean rooms there in the early to mid-1990s, and from that point, seasoned chromatography and optical detection veterans in universities and national laboratories procured resists, silicon wafers, and exposure units to create ever-more elaborate and highly functional devices.

About 80% of the science of μfluidics begins with a photosensitive resist, though. To protect glass on a substrate that will eventually contain an etched out microchannel, a phenolic resin matrix, with a photolyzable diazonaphthaquinone-type sensitizer is used.[83] The exposure of this resist to light initiates polymer breakdown that triggers an increase in solubility for exposed areas upon immersion in an aqueous organic base solution. Such systems are known as positive tone photoresists, in contrast to other phenolic polymer resist matrices that are doped with photo-catalyzed cross-linking moieties that solidify an otherwise viscous but mutable media upon exposure to the wavelength of light to which the photosensitive unit responds. During the process of creating a raised geometry, hardened resist design over which elastomer can be poured and cured to create rapid prototypes and disposable μfluidic devices (see injection intersection of one such device in Figure 1.3e, rightmost panel), these negative tone photoresists are developed (that is, the design created via photo- or electron lithography is brought out by dissolving away the non-useful regions) in an appropriate organic solvent, usually that which existed in very low proportions in the original resist matrix; one common developer solvent good for several classes of negative photoresist is propylene glycol methyl ether acetate (PGMEA).

Also crucial to the creation of functional photoresist layers is the precise and controlled application of bake steps throughout the preparation. The bake steps serve to remove excess solvent from the photoresist matrix after spin-coating and before exposure, ensuring the most defined line possible at the interface between resist that is develop away and resist that remains in place on the substrate. For etching glass, this interface determines the prevalence of chipping away of the protective resist during the glass' etching time in buffered hydrofluoric (HF) acid solution. Chipping leads to incomplete conformal sealing with the silver-PDMS nanocomposite top plate and compromised electrophoretic flow characteristics result due to excess shallow edge volume around the more defined channel. Inadequate bake times for positive relief creation with MicroChem's SU-8 negative tone photoresist lead to incomplete development or lift-off of positive relief structures. Both these conditions result in an unusable structure for molding PDMS μfluidic devices, which were made by mixing in a 10:1 bulk copolymer: curing agent ratio, degassing for thirty minutes, pouring over whichever flat glass or positive relief was appropriate, and curing at 70°C for 45-60 minutes. Dow Corning's Sylgard 184 has found wide application beyond it industrial niches in electrical insulation and biomedical devices.[49] A proprietary dimethylsiloxane copolymer bulk with fumed silica and cross-linked via heating with a vinyl ended platinum catalyst, this commercial polymer preparation has become a staple for analytical chemists and many other types of scientist who study disposable, oxygen/carbon dioxide permeable μfluidic devices that support EOF, due largely to the presence of the fumed silica bulking material.[84]

Glass Devices

Preparation of glass-nanocomposite μfluidic devices in-house, although a lack of clean room access meant these devices were never consistent enough in depth or cross sectional area for optimal performance, proved crucial in testing the utility of such a glass-elastomer hybrid device and led to the eventual purchase with confidence of a commercial channel piece which offered more facile filling and flow control than all-PDMS devices. A Micralyne (Edmonton, Alberta, Canada) TT-100 commercial μfluidic channel-containing device, as seen in Figure 1.3d and the left-most and center panels of 1.3e, has been recently purchased and tested pursuant to studies performed on homemade glass channels that revealed good reproducibility of injections created according to the method below. Following a cleaning cycle in boiling RCA-1 and 2, [RCA 1: distilled H_2O: 25% NH_3: 20%H_2O_2 is 5:1:1; RCA 2: distilled H_2O: 37% HCl: 20% H_2O_2 is 6:1:1; Etchant: 85.75% distilled H_2O, 9.25% conc HCl, and 5% buffered HF (40% NH_4F: 50% HF is 7:1] 130mm x 42mm x 4mm pieces of soda-lime glass were blown dry with N_2(g), baked in a convection oven for 20 min., and placed in a closed container to minimize dust accumulation prior to processing. Later, the positive photoresist Microposit S1813 from Shipley (phenolic resin matrix, diazonaphthaquinone-type sensitizer) was spin coated onto the glass at a rate of 3000 rpm with an initial acceleration of 10,000 rpm/sec. After a soft bake step at 90°C for 40 min., an aluminum mask created in-house via milling with a 0.0006" jeweler's slotting saw blade, with the pattern containing a long separation channel (line width: 125 microns) and an offset injection port (total port length: 400 microns) was placed over the photoresist-coated glass, and this apparatus placed under a UV lamp (365nm) for

3min. Following development and rinsing steps, the photoresist-coated glass bears the pattern of the μfluidic channel as the only regions of bare glass. The device is hard–baked at 130°C for 45min. and then placed in buffered, stirred HF etchant solution for 75 min. After rinsing, the glass is conformally self-sealed with light, even pressure to a PDMS cover slab with buffer reservoirs created in it prior to device assembly with a 5mm diameter core bore. Nanocomposite regions for SERS detection are directly integrated into the cover slab, as described in the section of this chapter "SERS Substrates: Nanocomposites". The resulting channels were ~200-350 microns wide and 10-20 microns deep.

Once etched (or procured from a commercial source), sealing of glass containing μfluidic channels was most often accomplished by simple conformal sealing of a PDMS cover plate to the smooth glass surface, especially since this was how SERS nanocomposite regions were integrated into the μfluidic platform. Reservoirs were cut in the PDMS with 4mm diameter cork bores, as they allow for large buffer volumes relative to the channel size. This was an important aspect of functional devices for two reasons. First, electrolysis products were more dilute and the separation could be carried on for longer and more repetitive times. Second, and critical to the collection of SERS data from separated analyte zones after the termination of separation voltage, larger reservoirs experienced less Laplace pressure.[85] This phenomenon is the result of an increased surface stress on a droplet with a high degree of curvature and yield a net flow from the "flat" droplet to the "bulbous" droplet, an effect that is dissipated in droplets with greater in-reservoir volumes, since the pressure is spread over a large underlying cylinder of stagnant buffer. The impact of hydrodynamic flows caused by these uneven

pressures can be devastating to both chromatographic efficiencies and bandshapes as well as SERS signal collection: not only is the flow destroying a separation by re-mixing resolved bands but analyte is being diluted and swept away from SERS detection regions as signal collection proceeds in vain.

SERS Substrates

Nanocomposites

To reiterate, the SERS effect results when electromagnetic radiation impinges on a suitable metal surface, and conduction electrons, termed surface plasmons,[77] produce a secondary electric field at the metal surface which adds to the incident field. When these oscillating electrons become spatially confined, as is the case with isolated metallic features, there is a characteristic frequency (plasmon frequency) at which exists a resonant response of the collective oscillations to the incident field. This condition yields intense localized fields that can interact with analyte molecules in contact with the surface, amplifying their inelastic (Raman) scattering of radiation and quenching their fluorescence.[78] Factors that influence a SERS substrate's effectiveness include noble metal type (Au, Ag, etc.), surrounding dielectric medium, nanoscale configuration of metal structures in dielectric, as well as chemical environment around the substrate.[79-81] Creation and optimization of SERS substrates began before integration into μfluidic devices and continues during and after as well. SERS substrates were created completely in-house for this research via physical vapor deposition (PVD) of noble metals onto the elastomer PDMS to produce random nanocomposites and via a combination of electron beam lithography (EBL) and PVD to create more advanced

preliminary substrates. These novel materials have been characterized in terms of morphology, optical properties, and, in particular, their SERS capabilities.[21,22,51,87,88]

While referred to as a surface effect, in fact, SERS is intimately related to nanostructure phenomena. Modeling work has demonstrated how the EM field created by photon energy being converted into surface plasmon waves is magnified both between particles and can extend away from a paricle pair. A top view and a space-filling representation of this was nicely compiled in Hao and Schatz' work and is shown in Figure 2.1.[78] Due to the range of field enhancement being linked to proximity to metal nanoparticles and moderated by the dielectric of the matrix surrounding the particles, the SERS effect changes with a molecule's distance from the enhancing substrate, as shown in Dr. R.J. Hinde's model is Figure 2.2a.[89] These observations, although based on ideal spherical two-particle systems, do much to elucidate the enhancement effects encountered when using experimental SERS for analytical purposes, and an interesting class of nanostructured materials utilized in this work for such analytical SERS involves the creation of dielectric material-nanometallic composites such as those described above and shown in the inset scanning electron micrograph (SEM) of Figure 2.2b. In these nanocomposites, the metallic nanoparticles are dispersed within the dielectric material during the process of PVD, wherein a vacuum of ~10^{-6} Torr is created around the inverted elastomer slab, and a tungsten boat containing 99.9% pure silver or gold metal is resistively heated to approximately 250°C. The potential applied across the tungsten boat determines the rate of deposition and particle size are determined due to energetics of the metal nanoparticles both in the sublimed plume as well as upon immediate entry into the elastomer surface. Although a

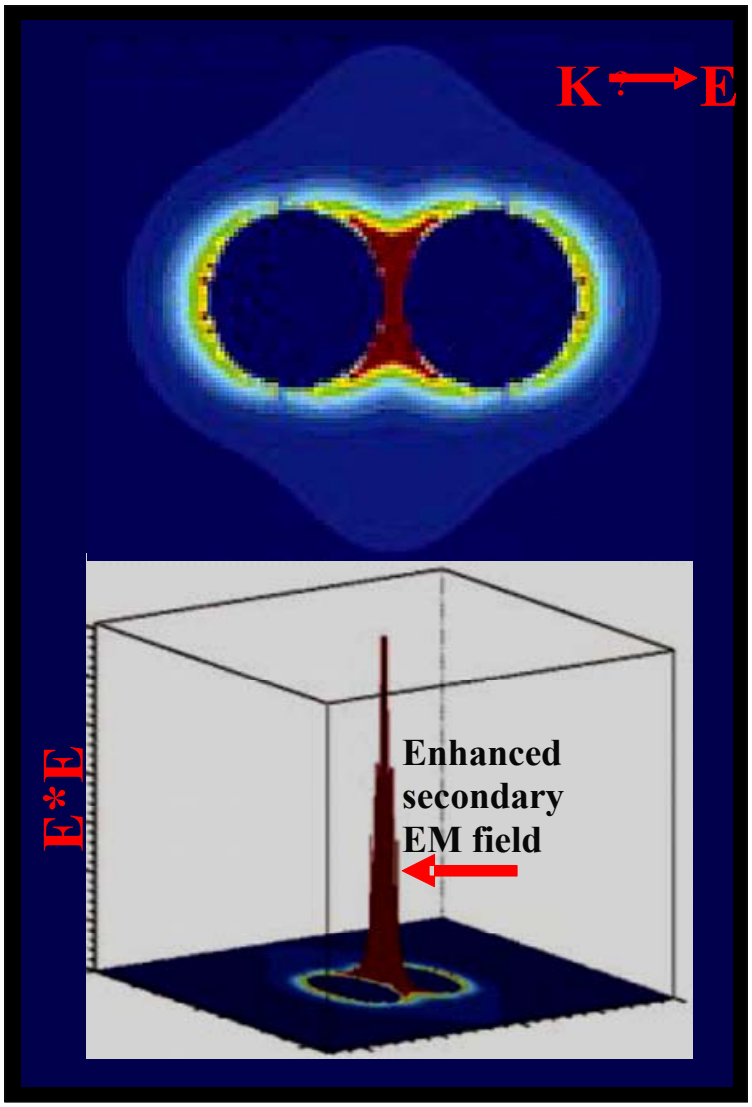

E. Hao, G. C. Schatz, J. Chem. Physics 120, 1, (2004)

Figure 2.1: Enhanced EM field near metal nanoparticles. In the work described herein, a rough metal-PDMS surface eprmits the conversion of photon energy, K, into surface plasmons, whichare a coherent oscillation of electrons at the metal-substrate interface, E. Surface plasmons are confined to the region between metallic nanoparticles and decay with distance for the focus of enhancement.

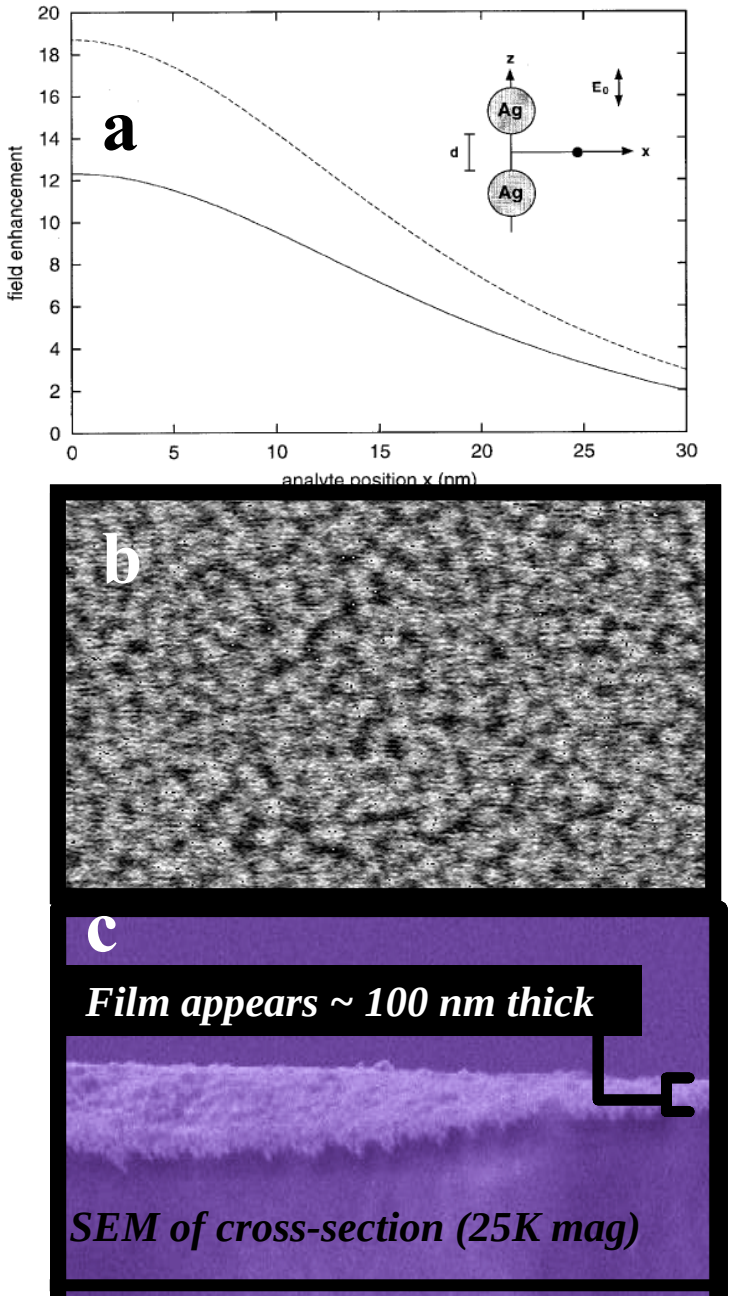

Figure 2.2: Theoretical and SEM analysis of silver nanoparticles within nanocomposite. (a) the importance of proximity of analyte molecule (represented by solid black dot) to the enhanced field between coupled silver nanoparticles; field enhancement factors were modeled for this two sphere system by Dr. R.J. Hinde. (b) top-down at 90K magnification shows quasi-spherical shape of particles and three-dimensionality of arrangement. (c) indicates that nanoparticles are embedded to a depth of ~100nm.

quartz crystal microbalance within the deposition unit reports a nominal silver thickness of 20nm, as seen in the cross-sectional SEM in Figure 2.2c, metal embeds approximately 100 nm into the PDMS. The unique optical responses of these structures are determined to a large degree by their surface plasmon resonances (frequency and intensity), which are strongly dependent on both the morphology and dielectric properties of the composite material.[77,86-88] Surface plasmon resonance can be tailored by controlling the shape, size, and spacing of metallic nanoparticles.

Among numerous advantages that the metal-PDMS nanocomposites exhibit as SERS substrates are the following: (i) Because the particles are suspended in a polymer, the entire effective metal surface is accessible to analyte. (ii) The suspended particles are somewhat protected from the local environment, therefore oxidation and other deleterious effects are reduced. (iii) Optical backgrounds from the polymer are small and easily subtracted. (iv) The polymer can be molded in practical shapes (e.g., titer plates or μfluidic channels) prior to metal deposition. (v) PDMS (and related polymers) are excellent solid phase extractors for organics and can concentrate analyte near the metal surface once μfluidic separation voltage is terminated. (vi) Since the polymer is pliable it can be physically manipulated to alter inter-particle distances to influence optical properties including SERS activity. With these discoveries of Ag-PDMS as a viable, high performing SERS substrate, the next logical step was to move to chip-based μfluidic separations, since PDMS is one of the most common polymer-based chip materials. Considering the ubiquity of μfluidic devices, expanding the detection modes available for miniaturized functional devices to include vibrational spectroscopies such as Raman was certainly warranted. Addressing any separation with a structurally

information-rich spectroscopy provides reliable identification of analyte mixtures. An example of the first combination of these emerging techniques is shown in Figure 2.3,[86] showing both the real-time LIF detection (Figure 2.3a) of a separation of riboflavin (I) and resorufin (II) and the reconstructed electrophoretic peaks detected by tracking SERS intensity of vibrational bands specific to each compound along the nanocomposite region of the channel (Figure 2.3b). Figure 2.3c and Figure 2.3d represent high quality spectra collected by the averaging at electrophoretic band center. The data collection and handling schemes proved non-trivial and are discussed fully both later in this chapter and in chapter 3. The apparent noisiness of the reconstructed electrophoretic bands stems from inhomogeneous enhancement along the nanocomposite region; this issue was addressed by using lateral averaging along each step of the band as well as by implementing a running weighted averaging smoothing regime described in Chapter 3.

EBL-SERS Substrates

Early modeling work showed that both analyte proximity to substrate as well as proper arrangement of nanostructures relative to each other can maximize SERS efficiency.[78,89] The effect of analyte proximity to enhancing couples of particle was demonstrated in collaborative computer modeling work between Dr. R.J. Hinde and Dr. M.J. Sepaniak, among others, with results in Figure 2.1c showing decreasing enhancement with increasing distance from the nanoparticles whose coupling yields field enhancement.[89] However, analyte proximity is only part of the story of increasing SERS enhancement by tailoring physical characteristics of the substrate. The best SERS sensitivity, and hence the extension of the linear dynamic range at the low end, will be

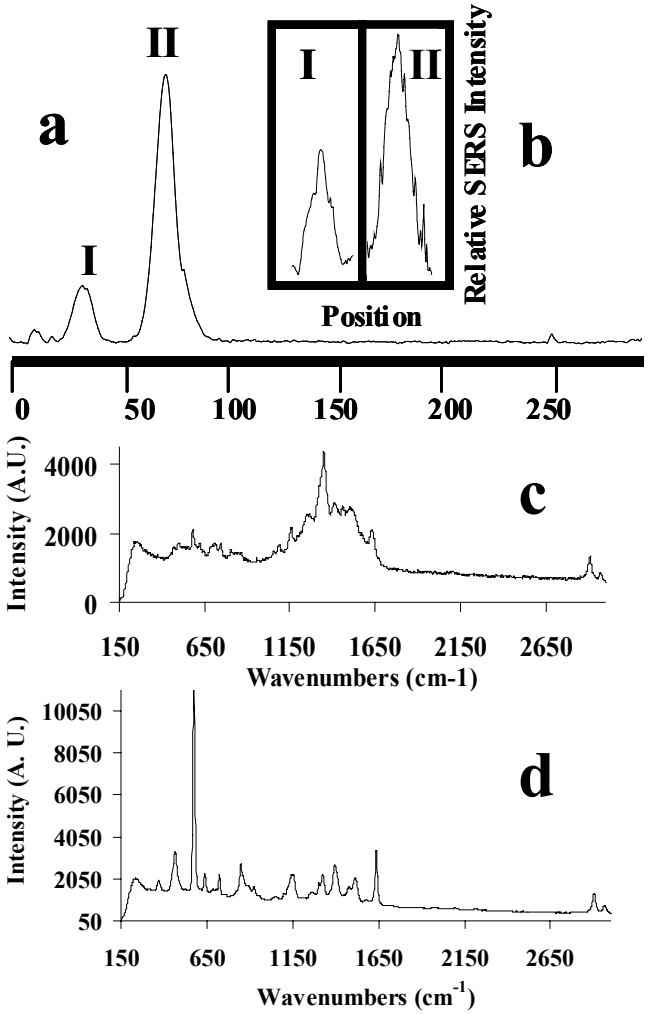

Figure 2.3: Separation with LIF and SERS detection on an integrated mfluidic-SERS device. Separation and detection of (I) riboflavin and (II) resorufin. LIF detection real time (a) is complemented by (b)recreated bands. Panes (c) and (d) show riboflavin and resorufin SERS spectra, respectively.

reached with rationally designed, optimally arranged metal particles created by nanoscale lithography, including EBL and RIE of polymer photoresist structures and patterned silicon, respectively. As these substrates represent the future of SERS, several have been tested on the μfluidic platform. EBL has emerged as the most promising current alternative for the fabrication of new substrates with uniform nanoscale features.[90-93] These techniques also offer the possibility to create new substrates with controlled inter-particle coupling, which can be an important contributor to SERS enhancement.[94,95] EBL has been shown to produce highly ordered surfaces that are very SERS active[t] and promises the relative straightforwardness of creating well-defined nanoparticle geometry and unique spatial arrangements that other techniques cannot similarly achieve. These components can be manipulated to produce uniquely tuned localized surface plasmons, probe particle size, shape, and orientation with respect to laser polarization, and produce homogeneous analyte environments that, in a practical sense, are useful for reproducible very low-level analysis. Size of nanofeatures affects the degree to which an impinging light source at a particular wavelength can initiate the propagation of localized surface plasmons that induce strong electromagnetic fields and significantly enhance Raman scattering signals. Nie's early work gave a guide for nanofeature sizes if interrogation of the substrates were to be done with a 633nm HeNe laser: 200nm diameter colloidal particles worked best for 647nm excitation, so features were created with diameters between 100 and 300 nm.[79,88] Size therefore seemed to have much less impact on SERS signal collected in integrated μfluidic devices than did spacing or shape/arrangement. Inter-particle spacing studies on square pillar nanofeatures of different spacing were shown to give better signal for the smaller, more

closely spaced set, (compare "square 1" and "square 2" responses in Figure 2.4a) likely due to a match of the smaller, more densely nanofeatured array's extinction band to the impinging 633nm HeNe laser used to interrogate this nanofabricated SERS substrate within the μfluidic channel.[88] Computational simulations using the discrete dipole approximation suggest that the strongest signal enhancement arises from molecules' proximity to the nanoparticle's vortices (loci).[96-98] Appropriate alterations in symmetry of individual nanofeatures and geometric assembly of collections of nanofeatures shows that arrangements ("ellipse 1", Figure 2.4a) that maximize proximity and focus EM fields to specific loci offer the more promise to both maximize the efficiency with which analyte molecules occupy enhancement as well as actually increasing the expanse of these regions where greatest enhancement occurs relative to symmetrical shapes and arrangements, i.e., symmetrically spaced squares. As a final reinforcement of how crucial the interplay of impinging radiation with nanofeatures is for these systematically created substrates is, note that the pattern "ellipse 2" is aligned along the direction of laser polarization and yields the highest overall raw signal, a result of maximized field interaction in that orientation. Here, we assay SERS signal intensity (for Rhodamine 6G spectrum, Figure 2.4b) with varied nanostructure type in μfluidic devices. Not only will increased SERS sensitivity of substrates improve the performance of μfluidic-SERS but the μfluidic platform can also serve as an ideal multi-channel, low volume analyte delivery platform for comparing various iterations of nanofeatures in less time and with control of fluid (analyte) delivery. These studies serve as a proof-of-concept for EBL-created substrates in μfluidics, as analyte was

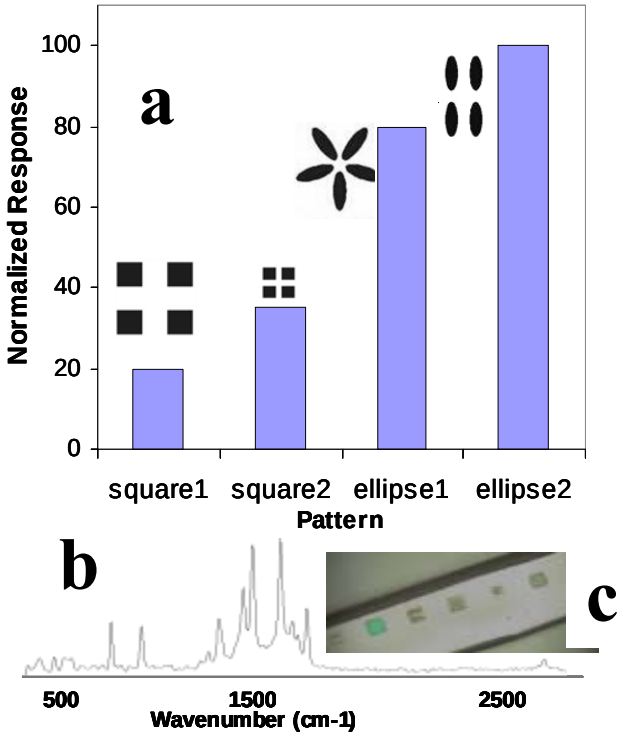

Figure 2.4: Integration of nanostructured SERS substrates created via electron beam lithography onto the μfluidic-SERS platform. Shown is (a) normalized response factor of each type of pattern assayed in the μfluidic; (b) the spectrum of rhodamine 6G delivered μfluidically and followed for intensity comparsions; and (c) a photograph of the nanostructured SERS substrates within the μfluidic device. Each square is an array of identical nanostructures.

introduced to integrated, rationally designed SERS patterns via μfluidic delivery for assay of SERS activity, shown in the photograph in Figure 2.4c.

Experimental Set-up

Once assembled, the hybrid SERS μfluidic device was mounted such that the beam from an Ar+ laser (488nm and 10 mW; Cyonics Uniphase, Inc.; San Jose, CA) was focused at a point in the channel just before the nanocomposite region. Buffer and sample were placed in the four reservoirs and electrodes connected each reservoir to its own blade switch on a manifold that selected between a resistor array rigged for pinched injection loading of the sample across the offset channel and a resistor array rigged for separation. The load array distributed 90% total voltage ($V_{tot,load}$) to sample and buffer inlets, 100% $V_{tot,load}$ to buffer waste, with ground at sample waste (refer back to Figure 1.5d). The load voltage was applied by a Bertan Associates high voltage supply (0-3kV; Franklin Park, IL). The separation resistor array distributed 50% total voltage ($V_{tot,sep}$) to sample inlet, 50% $V_{tot,sep}$ to sample inlet, 100% $V_{tot,load}$ to buffer inlet, with ground at buffer waste. The separation voltage was applied by a Spellman Instruments high voltage supply (0-30kV; Plainview, NY). Sample was loaded across the offset channel for ~30 sec and the switch manifold is then thrown, switching to separation mode. Typical voltages applied for sample loading and separation were 125 V/cm and 160 V/cm, respectively. Fluorescence emission from separated bands passing through the Ar+ beam was collected in a 180˚ geometry and directed back to a RCA-1-P28 photomultiplier tube linked to a Pacific Precision Instruments photometer (Concord, CA). Output voltage from the photometer was converted at 1 Hz by a PMD-

1208LS data acquisition board with TracerDaq® strip chart software (Measurement Computing; Middleboro, MA).

Voltage was terminated after all analyte bands had moved past the LIF detection window, and the μfluidic device was transferred to a JY Horiba LabRam Raman Microscope equipped with a Wright Instruments CCD and an ETRI helium-neon laser (633nm). Interfaced with the LabRam was an x-y-z programmable translation stage (Marzhauser Wetzlar,GmbH; Wetzlar-Steindorff, Germany) that was used to trace out paths of spectra along the channel. At each programmed step, a spectrum was collected with at-sample laser power of 2.2 mW and an accumulation time of 1s. An electrophoretic band was located using spectral identification based on comparison of in-channel spectra to standard spectra previously collected in borate buffer matrix. The stage was then reprogrammed to take smaller steps to recreate the electrophoretic band shape by following the intensity of resorufin's vibrational band at 600 cm^{-1} and riboflavin's at 1200 cm^{-1}. The final programming of the stage created a grid 275μm x 75μm at the electrophoretic band's center to yield 33 averaged spectra for improved signal-to-noise. Raman data was processed with LabSpec software, Version 4.03. A depiction and more complete discussion of this data collection scheme appear in Chapter 3.

Compatibility Testing and Data Collection

Once the components of the μfluidic-SERS device were created and initially tested, certain treatments were employed to modify the surface chemistry of the channel devices; SERS collection efficiency was compared among the various incarnations of treated μfluidic devices. Testing of such parameters as buffer compatibility, channel

depth, and polymer treatment strategies aided in the identification of an optimal device and method.

Compatibility of Separations and SERS Parameters

Although one of the most attractive features of Raman as a detection mode for conventional electrophoretic separations is the negligible background created by aqueous systems, any reaction that compromises the noble metal surface similarly compromises detection. Exposure of the Ag-PDMS substrates to water oxidized the silver over a period of several hours, so this rate of substrate degradation did not interfere with the timescale of most relevant electrically actuated separations. However, certain electrolyte solutions can hasten substrate degradation, so buffer system selection was central to accommodating both substrate viability and electrokinetic separations. The effect of buffer anions on substrate performance may depend on their relative reactivities with silver. The spectra in Figure 2.5 demonstrate the most extreme example of how a buffer system can compromise the silver substrate. In this case, upon immediate introduction of a 10 mM phosphate buffer matrix to the substrate, growth of the silver oxide bands at 250 and 400 cm^{-1} and total disappearance of the PDMS SERS bands at 2500cm^{-1} indicate that the phosphate anion interacts readily with the silver metal and deactivates the surface for SERS enhancement, disallowing use of this buffer system with the metal-polymer nanocomposite that includes silver. Based on tests of substrate lifetime with four common CE buffers (acetate, borate, citrate, and phosphate), a sodium tetraborate system was chosen in which the substrate viability persisted longest and gave the spectra with the clearest vibrational signature over background.

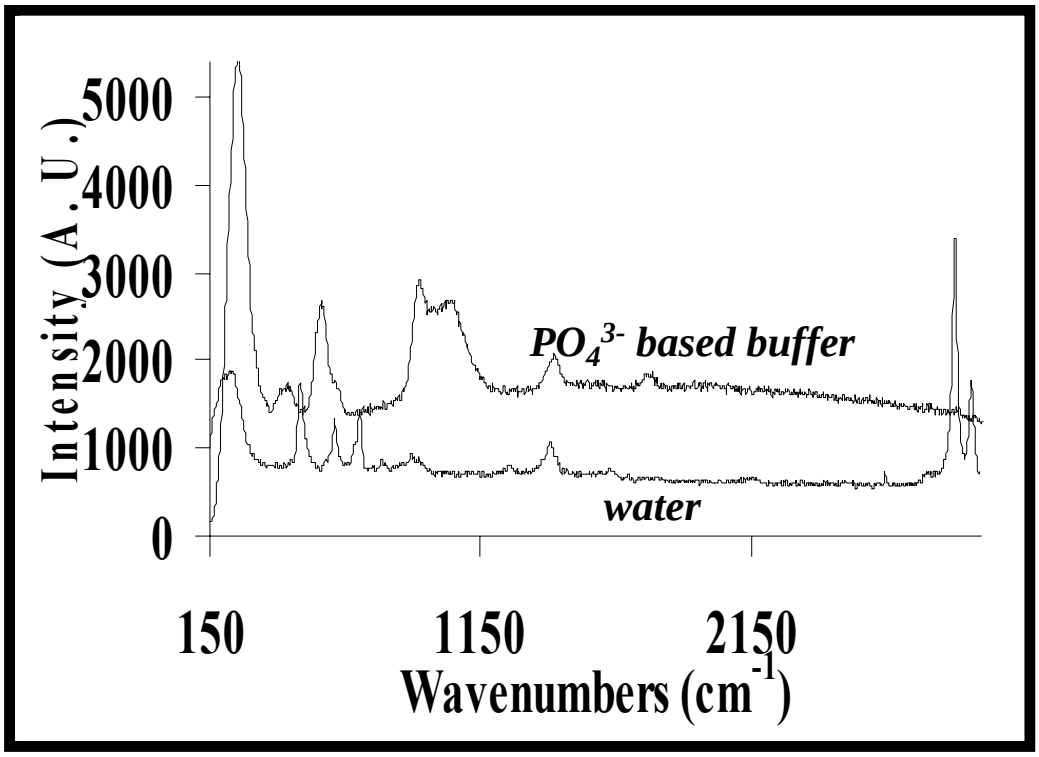

Figure 2.5: Effect of electrophoresis buffer matrices on SERS substrate performance. Note the disappearance of in phosphate buffer of even the SERS bands from PDMS and the extreme growth of the silver-oxide bands (indicators of substrates death).

The application of voltage does not adversely affect the silver component of the nanocomposite substrate region because the particle interspacing and metal film thickness fall below the point of electrical conduction, or percolation threshold. Were the SERS substrate to be conductive, electrophoresis would be impeded because instead of the μfluidic channel carrying a current and the analytes experiencing a field, the sensing wall of the channel would carry the field. An experiment was performed to prove that gold and silver nanocomposite SERS substrates were nonconductive and therefore would neither suffer compromised SERS signals (often conduction shorts out the propagation of scatter-enhancing plasmons) nor display unpredictable Ohm's Law behavior during voltage application and current monitoring over the course of the separation phase of the μfluidic-SERS experiments. During the course of a long PVD for both gold and then silver, a specially prepared piece of PDMS was hooked through a vacuum-sealed connection port in the lid of the high vacuum stainless steel bell jar to a nanoammeter via very ginger contacts to two isolated regions which had already been deposited with a completely conductive layer (100nm) of the respective metal. A 5 mV potential was applied across the plain PDMS void that separated the two metallized connection points, and the nanoammeter read out current during the course of the metal deposition. Prior characterization of nanocomposite substrates indicated that optimal deposition rates and thickness for silver was 1.0 /sec, at at thicknesses of ~20nm. This value falls well under the percolation threshold determined in the deposition conductivity monitoring experiment, the results of which are shown in Figure 2.6. Final notes concerning compatibility between separation and SERS conditions include the fact that deposition of metal onto the PDMS did not interfere with its ability to

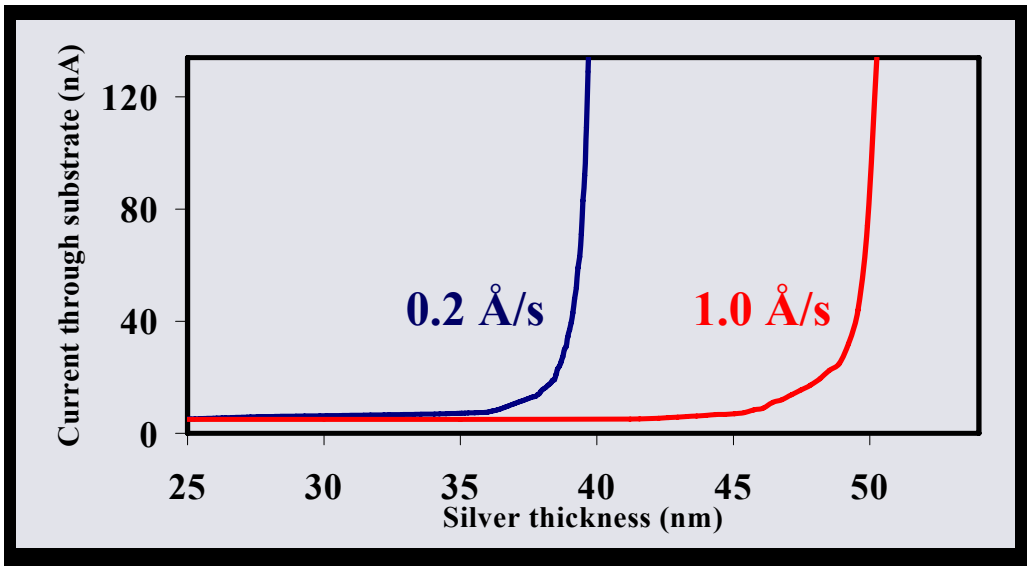

Figure 2.6: Results of percolation threshold measurement. Indicates that silver-PDMS SERS substrates are well below nominal metal thickness required for conductivity.

conformally self-seal, and the material still supported EOF, although it must be noted that, due to an inherent reduced surface silanol content, the EOF of native (i.e., surface not chemically altered) PDMS is roughly fourfold less than that of glass.[99]

Separation Data Collection Regime

In order to initially validate the movement and peak shape of analytes within integrated μfluidic-SERS devices, fluorescent markers were utilized with on-line, real-time laser induced fluorescence (LIF) detection followed by SERS detection upon termination of separation voltage and halting of analyte bands within the substrate region of the channel. Figure 2.7 shows an LIF optical detection set-up for a μfluidic device. A conventional CE capillary could be integrated into such a set-up, although it would not require mounting in the exact flat orientation like the μfluidic. Whereas, the chip must be kept level to avoid spilling the contents of the reservoirs, the capillary can transverse the laser beam in any orientation, so long as the ends of the capillary are level, and the beam waist passes cleanly through the cylindrical capillary without lensing. This note highlights an advantage of optical detection on the planar μfluidic devices: flat surfaces on top and bottom of the separation channel allow considerably more facile focusing than in a capillary. When PDMS μfluidic channels were used, as in was the case for all separations shown in this chapter, the three walls of the channels opposing the nanocomposite SERS cover plate were exposed to ozone to increase their silanol content and improve separation speed and efficiency for model separations. No claim is made to have optimized this system for ideal separation performance. The goal of these experiments was simply to demonstrate the feasibility of using nanocomposite SERS substrates integrated directly into μfluidic devices.

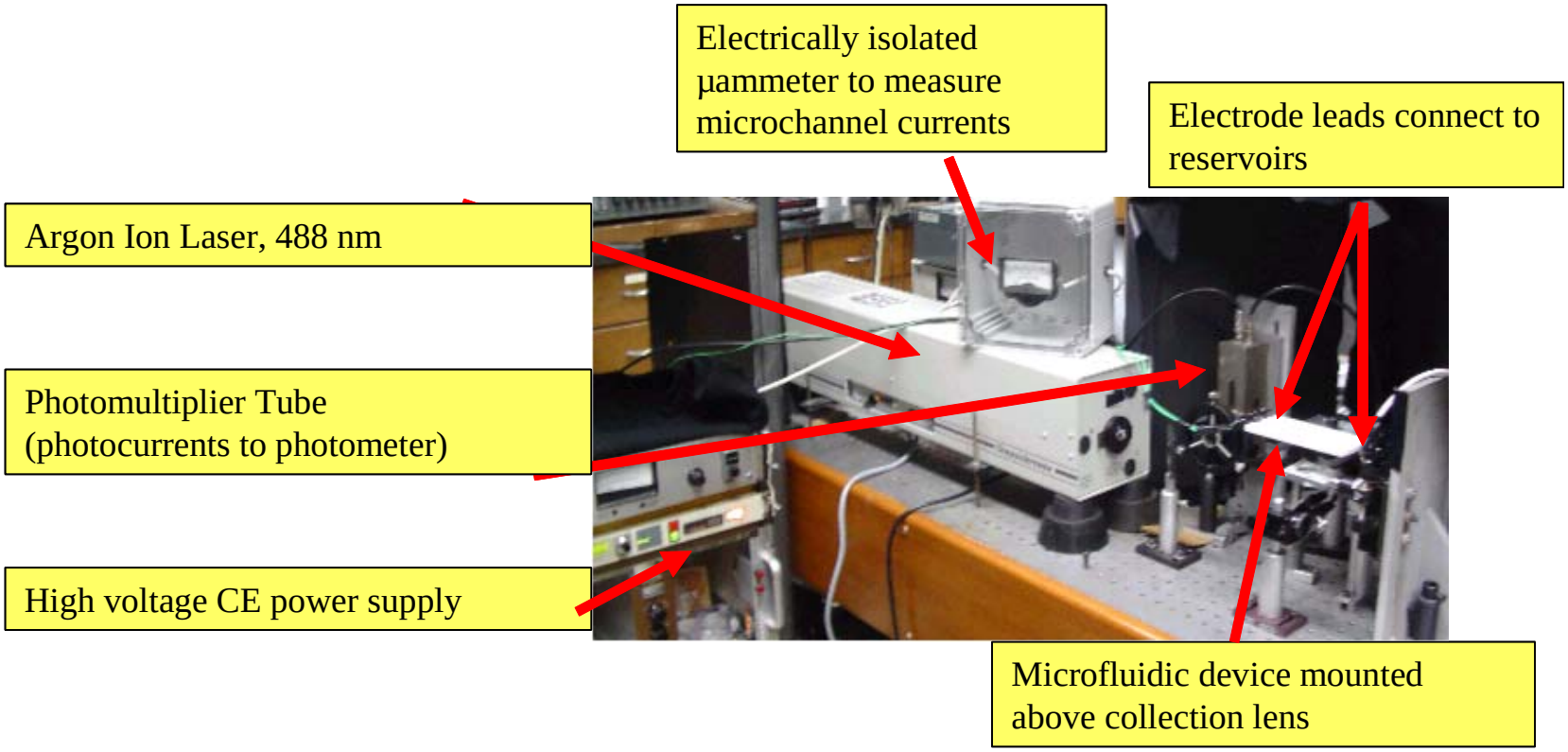

Figure 2.7: Diagram of LIF set-up for µfluidic detection.

After the separation of the model compounds has been detected with LIF, voltage was terminated and the device was moved to a Raman microscope with a programmable x-y-z translation stage. In principle, the Raman spectrometer can accommodate multiple lasers and then be used for fluorescence detection in the non-substrate regions of the μfluidic device. The spectra of Figure 2.8a demonstrate the low contamination caused as analyte bands pass through the nanocomposite region of the device by comparing the background signals from regions of the nanocomposite where analyte had already passed by (upper spectrum) and where analyte had never touched (lower spectrum). The lower spectrum is typical background for these substrates that can be easily subtracted from true SERS spectra. The upper spectrum does show some signal for the strongest resorufin band at 600 cm^{-1}. This low level of contamination offers promise that no artificial tailing will be observed in the SERS reconstructions of electropherograms, and, more importantly, that the vibrational bands from disparate analytes will not clutter and confuse spectral fingerprints for different components. SERS spectra are collected in a three-step process: band location (500μm step length), band recreation (100 μm step length), and optimum spectral collection (grid of 3 rows of 11 steps each, all spaced 25 μm apart). To clarify the magnitude of the distinctly programmed spectral collection regimes, Figure 2.8b depicts the three steps and their relative scope along the physical length of the μfluidic channel and along the resorufin electrophoretic band. In order to maximize signal to noise and gain the most descriptive vibrational spectrum possible, the third step averages 33 spectra from the center of the electrophoretic band, i.e., the location of the greatest amount of analyte on the SERS substrate. This highlights an important nuance of our novel method: as SERS is a surface phenomenon,

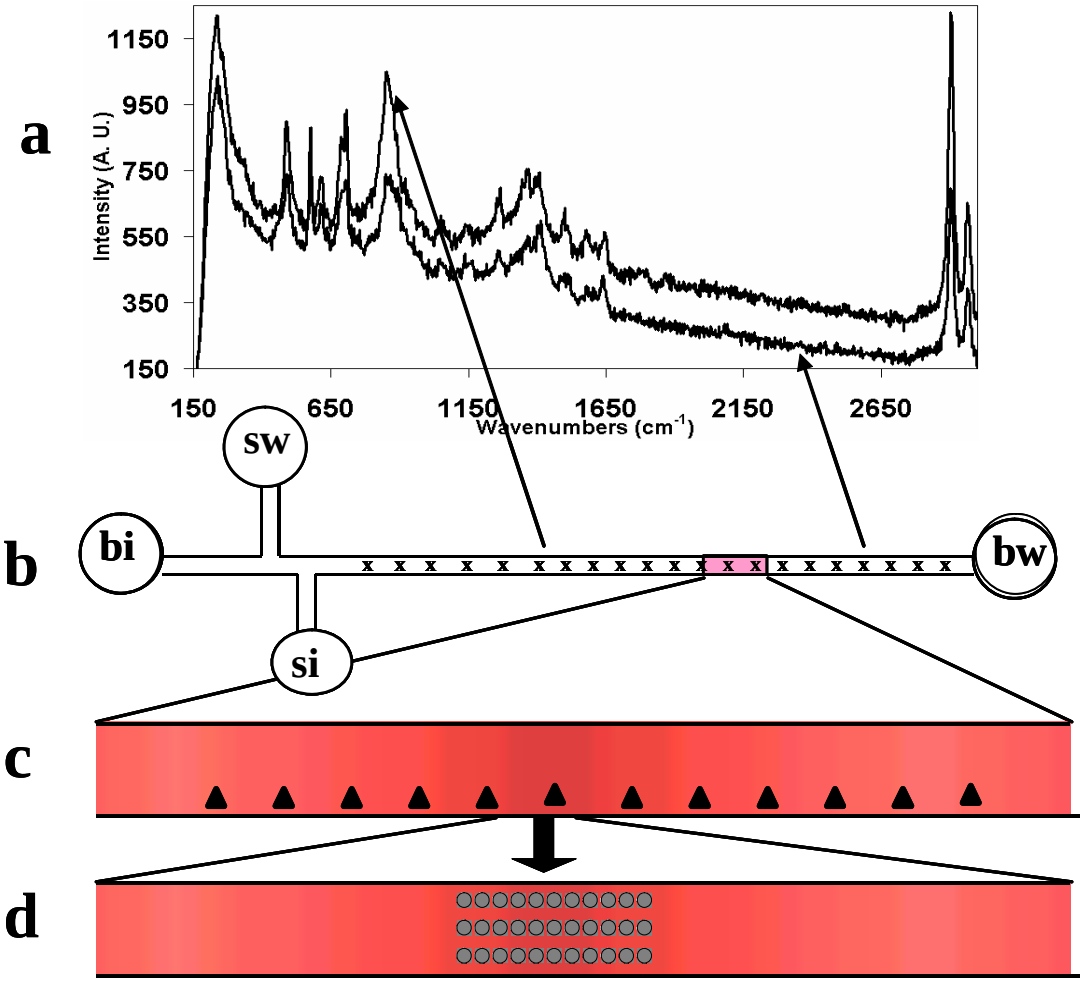

Figure 2.8: Scheme for locating and SERS mapping analyte bands within μfluidic device with deomonstration of minimal contamination by moving band. (a) Demonstration of minimal contanimation during separation step; (b) band location; (c) re-creation of electrophoretic band profile; and (d) collection of high S/N spectra.

the ***amount*** of material (moles) available to the active substrate becomes far more important than actual concentration, although concentration certainly influences amount in situations with identical surface areas. Based on the concentrations, injection port geometry, and degree of dilution by the pinched injection scheme, we calculate that less than 10 femtomoles of each analyte is injected during a typical run.

CHAPTER 3

Improving Analytical Figures of Merit for Integrated μfluidic-SERS

Sensitivity

Temporal Considerations

Although SERS can be employed on-the-fly in μfluidic separations (Figure 3.1), some sensitivity as well as the rich vibrational information available upon carefully interrogating an entire electrophoretic band on the substrate after the termination of separation voltage may be compromised. The apparatus shown in Figure 3.1a includes external electrodes connected on one end to high voltage for separations and interfaced on the other end with the buffer reservoirs of an integrated μfluidic-SERS device secured under the LabRam's confocally arranged microscope for constant signal collection with small spatial displacements for each collection to prevent thermal and photolytic degradation of the SERS substrate with consecutive illuminations on the same spot. These spatial movements are longitudinal in a direction opposite the direction of an electrophoretic band front's movement into the detection region. The results of one of such experiment are shown for p-aminobenzoic acid (p-ABA) in Figure 3.1b.

In order to exploit the nanocomposite SERS substrate region of our hybrid μfluidic devices for on-column structural band determination, however, some analyte must partition from the electroosmotically streaming buffer onto the nanocomposites. Some analyte partitions immediately into the nanocomposite with initial contact between electrophoretic band and SERS detection region. However, as with any

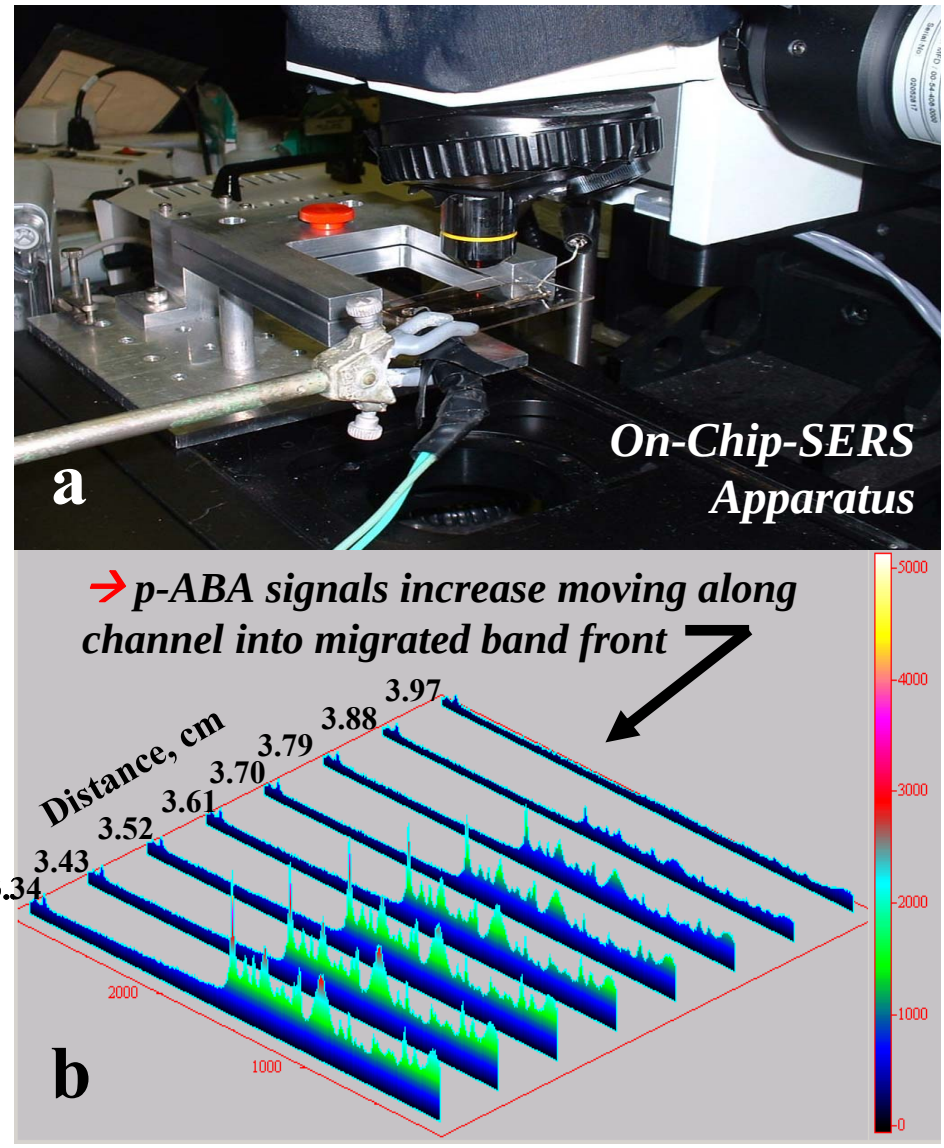

Figure 3.1: Online µfluidic-SERS. During application of separation voltage involves securing the integrated device onto the stage of the LabRam Raman spectrometer, (a) complete with electrodes connected with high voltage supplies (green and grey wires in foreground and at right). An electrophoretic band front for p-aminobenzoic acid (b) is detected with movement into the SERS substrate region of the device concurrent with signal collection.

kinetically controlled phenomenon, a short time delay before detection can improve association and thereby signal intensity and this represents an advantage in terms of minimizing contamination issues. Besides some degree of buffer-analyte ionic association in solution, partitioning involves a minor element of competition between buffer and analyte ions moving partially into the polymer surface to associate with the silver particles. Due to this process, optimum spectra develop temporally. As shown in Figure 3.2, SERS signals quadruple within 30 seconds of stopping separation voltage. The fully developed signals show a six-fold increase two minutes after initial termination of separation voltage. The two culprits for loss of signal are substrate degradation and electrophoretic band dilution. Just as in conventional CE, but magnified by abbreviated channel lengths, hydrostatic flows in the integrated μfluidic-SERS devices significantly augment the slower, relatively less problematic analyte dilution caused by diffusion. Such external flows imposed by pressure and surface stress differences along fluid-air interfaces initiate at the buffer reservoirs and must be closely controlled with reservoir size, levelness of device, and maintenance of equal liquid volumes in reservoirs to mitigate the always deleterious and occasionally debilitating blurring of electrophoretic bands caused by such flows. Figure 3.2a plots the average of two distinctive resorufin band intensities; in complement, Figure 3.2b shows a full spectral profile of temporal growth for the resorufin signal. Signal intensity would diminish due to substrate destruction by laser irradiation and extended exposure to buffer solutions.

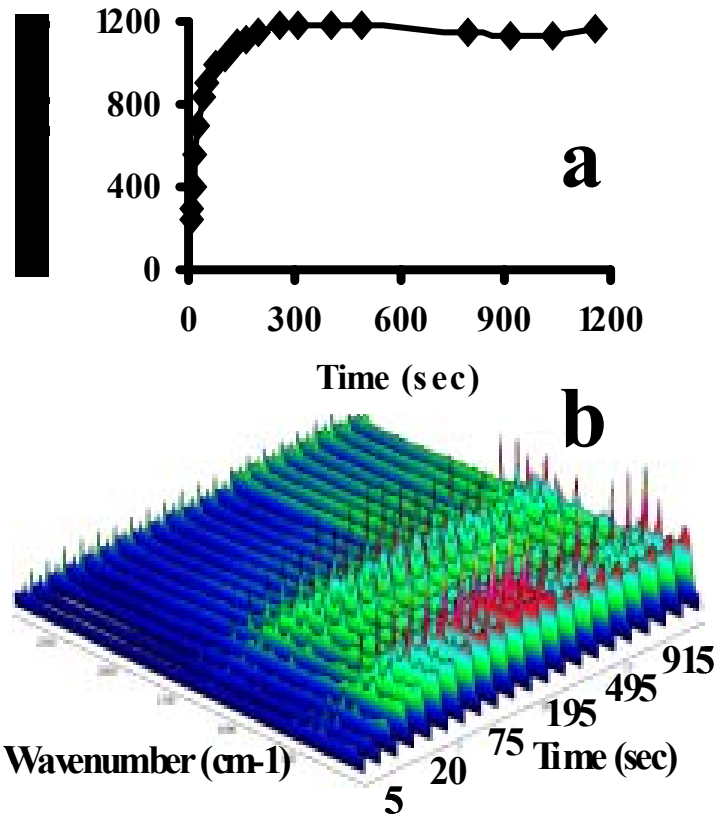

Figure 3.2: Temporal development of SERS signal on μfluidic platform after termination of separation voltage.

SERS Signal Collection Refinements

Proper testing for sensitivity begins with fabrication. More detailed and intense vibrational spectra are attainable if most or all of the analyte within an electrophoretic band reaches the SERS substrate surface. To encourage this, tetraethyl orthosilicate soaks followed by dilute ethylamine treatments were carried out on the non-substrate, channel-containing portions of the devices to decrease the absorption of analyte into the non-substrate walls by creating an increased amount of silicon dioxide nanoparticles within the PDMS matrix using sol gel chemistry. The TEOS swells the μfluidic device and immersion in basic ethylamine reduces the silicate to silicon dioxide particles. This ingenious method renders the PDMS much more hydrophilic and considerably less able to absorb hydrophobic analyte and contaminants.[99] The table inset in Figure 3.3 provides quantitative evidence that both treatment and depth can lend advantages in detecting low concentration or minimally spectroscopically responsive analytes in integrated μfluidic-SERS devices. In order to create deeper channels to study the effect of concentrating more analyte mass over a reduced substrate area, a second, more novel mode of channel fabrication involved casting PDMS over a smooth metal positive relief created by compressing 50 micron wide spring steel between two polished steel bars at a height of ~200 microns. This made for a high aspect ratio channel with depth ideal for demonstrating the sensitivity advantage of focusing the same concentration of analyte in a band over a smaller substrate surface area and thereby increasing the total mass available for detection, that is, by making the channel over the substrate deeper and more narrow. Four different combinations of device treatment and depth illustrate how focusing an analyte band that has suffered minimal loss of its molecules by non-sensing

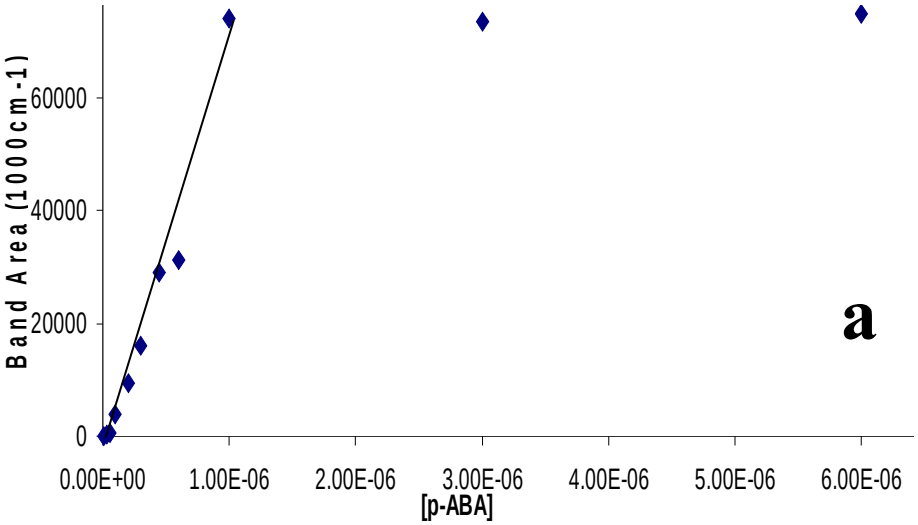

	Deep, 200μm	Shallow, 40μm
Treated	22,000 cts.	2100 cts.
Untreated	5000 cts.	540 cts.

b

Figure 3.3: Calibration curve and evaluation of channel depth and surface treatment. To address LOD on the low end, deeper channels were fabricated and polymer treatment rendered non-sensing regions of the mfluidic-SERS devices less absorptive of analyte via swelling in TEOS followed with reduction in ethylamine. (a) shows a LOD of 7x10-8 M, defined based on concentration which gave a 2 to 1 SERS signal intensity over background vibrational signals and baseline fluorescence hump for p-ABA's vibrational band at 1000cm-1. Differences in signal intensity for resorufin's vibrational band at 573 cm-1 when injected into the variously fabricated and treated channels were compared (b).

walls' absorption yields the greatest signal among the four treatments. The non-linearity of signal improvement with depth, that is, a channel five times deeper gives ten times the signal, may have resulted from the fact that increased depth channels are also decreased width channels and focus the same amount of material over a smaller sensing area, thereby driving the multiple equilibria involved in attaining an analyte's SERS signal. A loose description of these equilibria entails movement of analyte in aqueous buffer phase versus the analyte's being sequestered in PDMS versus being in adequate proximity to silver to be signal enhanced and detected. The situation that most favors increased SERS signal output is one wherein the more readily available silver-analyte associations are created and maintained. As separations cannot utilize analytes that absorb or adsorb all along the μfluidic channel to the SERS substrates (i.e., via thiol linkages), these silver-analyte association events were favored with depth as well as treating or using materials that were relatively unattractive to analytes for association. Glass channels and PDMS channels treated to be more glass-like proved to increase SERS signal collection success, showing a four-fold increase in signal over both shallow and deep untreated channels.

A calibration study such as that shown in Figure 3.3a demonstrates an LOD of $7x10^{-8}$ M for injected bands of p-ABA; this level of detection does not approach the sensitivity necessary for many analytical applications. Each point represents the average of three spectra collected from the same spot on the sample substrate, none of which showed intra-substrate deviation greater than 8%. At low concentrations, the LDR is truncated due to two main, interconnected issues, including the insufficient distribution of analyte into regions of highest enhancement as well as distribution of inadequate

amounts of analyte into regions of mid- to low enhancement to create a scattering signal detectable over the background (defined as 2:1 vibrational signal intensity for a band representative for a particular analyte over graphitic band intensity). The incidence of analyte molecules oriented appropriately within volume regions of enhancement may also be too haphazard for reliable detection, and surface area of interrogated substrate (the volume is nanometer scale in depth if substrates' sensing areas are correctly accounted for) can only be increased so much until laser power density drops enough to take over as the major contributor to reduced sensitivity.

An optimum length of time for spectral accumulation and number of acquisitions for averaging to acquire a signal helps increase S/N as well as maximizing vibrational information content of spectra. However, laser induced sample and substrate destruction begin to both alter and degrade signals, as revealed in Figure 3.4a by following the decreasing ratio of a prominent, descriptive resorufin band at 573cm^{-1} to the graphitic carbonaceous band, a harbinger of polymer and resorufin degradation, at 740-950cm^{-1}. Long acquisition and accumulation times also create prevalent, transient background bands as well as increasing the non-specific background "hump" that leads to obscured fine detail of vibrational spectra, as shown in the spectral insets of Figure 3.4b. This broad baseline has not been concretely explained, but the genesis of its growth is likely in heating and simply the accumulation of broadband radiation collected inadvertently by the CCD during an extended accumulation with no averaging out of statistically irrelevant optical signal.

Also related to thermal and photolytic sample and substrate degradation resulting from laser irradiation, the laser power study shown in Figure 3.5 reveals a

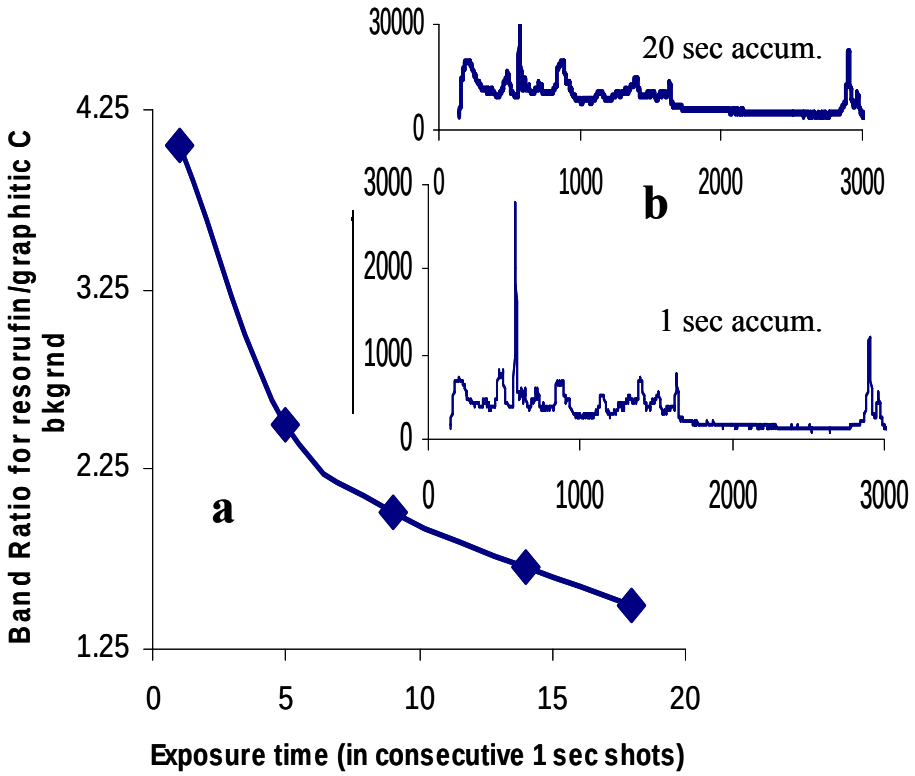

Figure 3.4: Demonstrates growth of non-specific background and loss of vibrational signal with increased acquisition and accumulation times. Consecutive exposures leads to a decrease in relevant signal to background graphitic carbon vibrational bands, (a), and long accumulation times also lead to increased non-specific baseline magnitude, which compromises detail of vibrational spectra relative to shorter accumulation times (b).

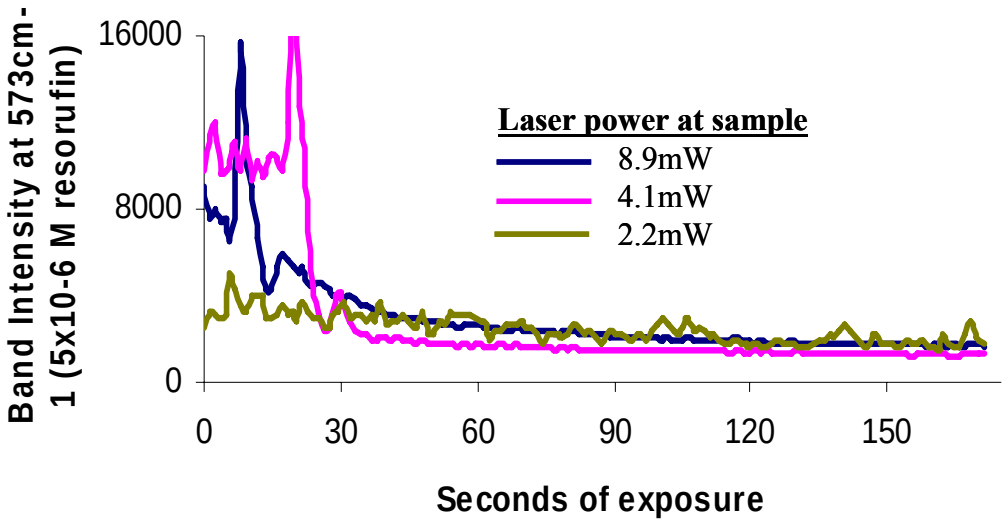

Figure 3.5: Temporal stability and deterioration of signal with different laser powers monitored for the resorufin band at 573cm^{-1}.

fleeting increased signal followed by rapid signal degradation for the resorufin band at 573cm^{-1} with increased laser power at the sample (moderated with neutral density filters). The higher laser power, 8.9 mW, yields the earliest spike in signal before signal intensity drops off, whereas the medium laser power shows a potentially misleading, somewhat stable signal with 4.4 mW laser power, but still a spike and then drop-off of signal. As a result of this study, the lower laser power parameter of 2.2mW was chosen for integrated μfluidic-SERS devices based on this power study of signal collection stability and ensuing time to sample-substrate degradation. This suite of studies represented in Figures 3.3, 3.4, and 3.5 was aimed at probing the limits of advantage to increasing irradiative magnitude to increase sensitivity yields valuable information and ultimately reveals inherent restrictions on improvement for the current SERS substrate. Therefore, weaker SERS responders and/or analytes injected at concentrations low enough to place a quantitative signal in the low concentration nonlinear range for such analytes with our nanocomposite substrate must be addressed with more sensitive substrates altogether.

Selectivity of our nanocomposites is moderately tunable based on selection of noble metal (Figure 3.6a). Regions of various nanocomposite can be directly integrated into a single device with the same facility as creating a device with a single metal (Figure 3.6b), and creating dual region devices for unknown samples can offer immediately broader chemical enhancements. These gold-PDMS nanocomposite substrate regions were created on the same PDMS cover slabs as the silver-PDMS nanocomposite substrate regions via PVD as well. Masking with aluminum foil protected each substrate area while its complementary metal was being deposited. One

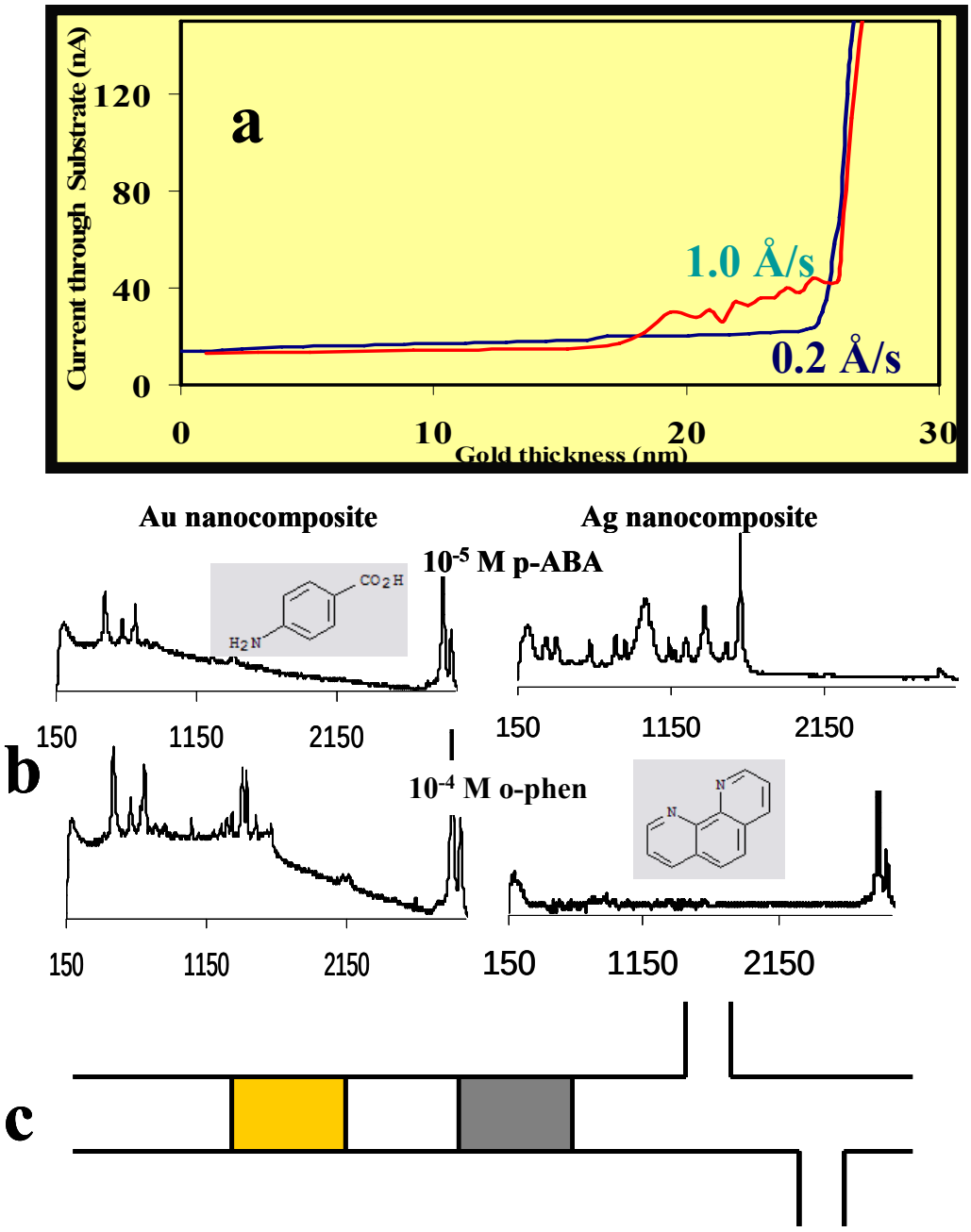

Figure 3.6:Integratin gold nanocomposite for selectivity. Results of percolation threshold measurement at two different deposition rates (a). Selectivity of silver versus gold nanocomposite substrate regions for different analytes (b) integrated onto a common µfluidic-SERS device (c).

interesting difference in the morphology of the gold nanocomposite was the slightly smaller particle diameters of the gold nanoparticles (~50-100nm for silver, ~25-50nm for gold) and increased nominal thickness of metal necessary for optimal signal (20nm for silver, 25 nm for gold; both deposited at 1 Å/second). Both these subtle morphology differences spring from the higher melting and sublimation temperatures of gold during the vacuum physical deposition process, which lead to higher energies within the metal plume and less self-aggregation before embedding into the PDMS. As discussed in Chapter 2, DC conductivity is one way to observe gross changes in metal nanoparticle proximity and determine at what thickness the percolation threshold, i.e. the creation of macroscopic electrical pathways, occurs during the PVD process for gold nanocomposites. These studies (Figure 3.6a) yielded the similar result to silver in that the nanocomposite is nonconductive at the nominal thickness that yields the best SERS activity (22-25nm), although a unique pattern of temporary conductivity is exhibited, whereby conductive paths are formed but the nanoparticles may not fully coalesce into a continuous film. Generally, silver nanocomposites show more overall activity with especially good results with analytes containing carbonyl and hydroxyl moieties (note the selective enhancement of p-aminobenzoic acid, p-ABA), whereas gold nanocomposites respond best to nitro and amine groups (note selective enhancement of o-phenanthroline, o-phen). The interaction of non-thiolated groups with gold is recognized as a relatively weak non-covalent bond that is suggested to be dominated by electrostatic and hydrophobic interactions, especially in the case of biological matrices such as serum, cytoplasm, or complex environmental waters. With this interaction of gold with such nitrogenous functional groups as aromatic amines, imines, and nitro,

biologically-based SERS with gold substrates dominates as the main Raman use for gold. Biochemical analytes as diverse as penicillin, amphetamines, cocaine, heroin, and 3,4-methylenedioxymethamphetamine (the active ingredient in the designer street drug Ecstasy, or "X"), other personal care products in water matrices (a significant area of environmental health risk), studies of activity and uptake in cells, organs, and organisms all benefit from the amenable chemical characteristics of gold as a SERS substrates, despite its lower enhancement factors relative to silver. Due to the inertness of gold, a smaller number of molecules of interest can exploit the full chemical and EM enhancement mechanisms of SERS. Nonetheless, gold substrate regions were utilized in this μfluidic-SERS device development both to demonstrate tunable or complementary selectivity with dual metal detection regions and because, in future work, the environmentally robust nature of gold substrates relative to silver will benefit μfluidic-SERS for some potential field applications where more easily oxidized silver might lose its enhancement advantage to substrate reactivity and subsequent inutility. What's more, the reduced chemical catalysis behavior of gold substrates relative to silver combines with a more limited overlap of gold-PDMS nanocomposites' extinction bands with the wavelength of laser interrogation most often used in this work, 633nm. Although less of such overlap can mean reduced signal enhancement, it can also mitigate problems with thermal and photolytic degradation of sample and substrate, so the analytical response to these gold-PDMS SERS substrate detection regions is a weaker and less informative, but more persistent, signal.

Reproducibility

Mitigating Substrate Inhomogeneity

SERS substrates demonstrate notorious inhomogeneity in nanoscale features on a single substrate as well as among discrete substrates and batches of substrates. A simple mapping experiment of the silver nanocomposite substrate demonstrates just that, including the occasionally "extra-hot" SERS spots (Figure 3.7). regions. This piece of nanocomposite was treated with p-aminothiophenol (p-ATP) to form a monolayer on its silver. A thiolated compound was used to created a self-assembled monolayer of the surface in order that the only thing probed during this mapping was the inhomogeneity of enhancement regions across the substrate, and not additional complicating factors such as the equilibria between solution/PDMS/detectable association with silver. Spectra were collected every 25 μm, and the intensity of the p-ATP band at 1050 cm^{-1} was followed to form the grid shown. The circled regions each highlight a single 25 μm by 25 μm region with a vibrational band intensity more than five times the mean. Visual inspection of the "hot spots" with the CCD camera reveals no distinguishing characteristics, implying the logical conclusion that the best enhancements happen on the nanoscale. The expansion from the dashed box reinforces the vast and sporadic differences between a "hot spot" and its neighboring regions. The two-dimensional traces follow the intensities shown on the grid for seven lateral slices from the total grid. The high spike in the pink trace corresponds with the white square in the grid, denoting the "hot spot" in that region. The reproducibility of the vibrational spectral bands enhanced across a discrete region of substrate suffers accordingly, and the reproducibility of the nanocomposite technique is comprised as a reliable spectroscopic

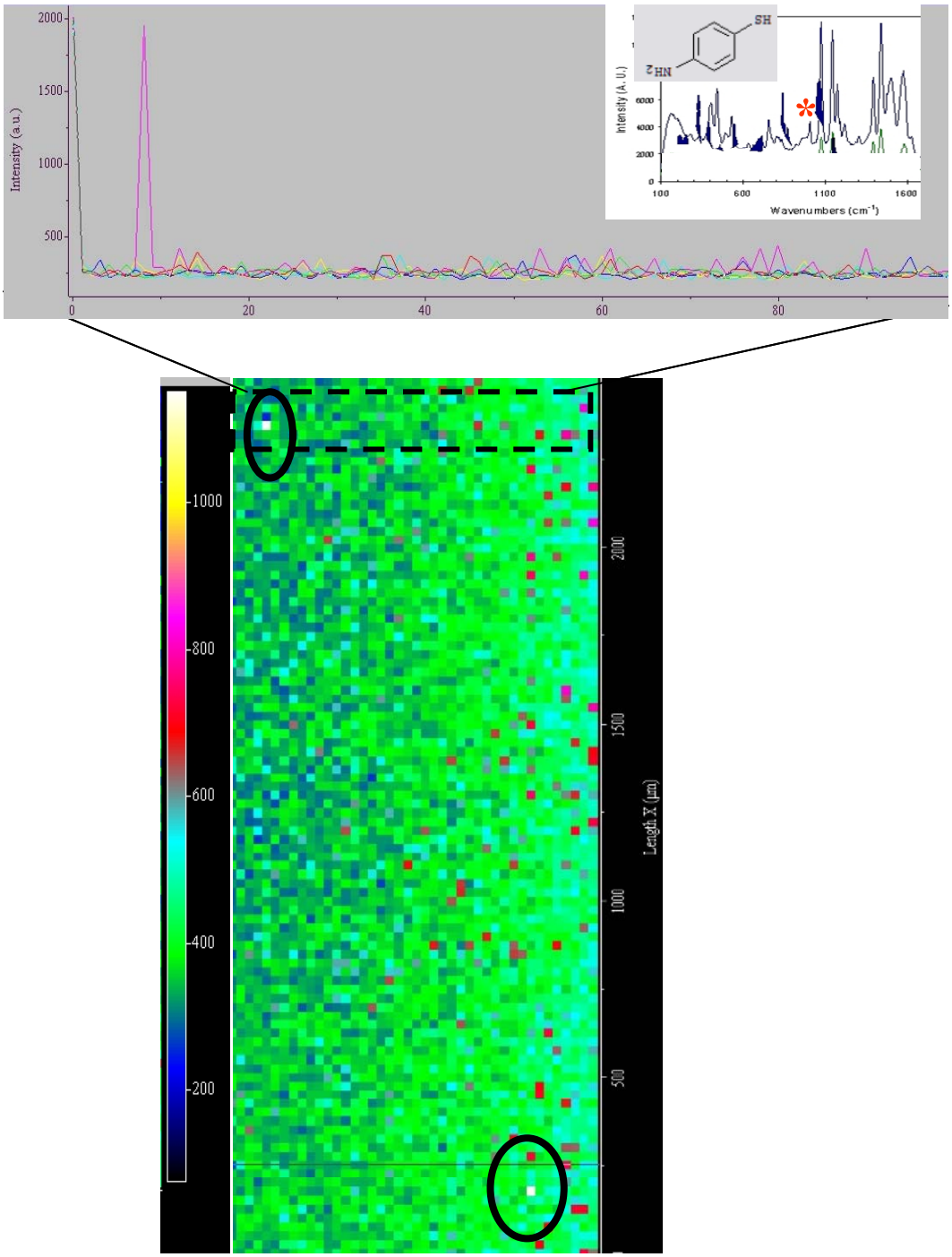

Figure 3.7: Mapping shows occasional occurrence of "very hot" SERS enhancement. Dashed rectangle and its projection show intensity vs position graph for 10 lines of collection, illustrating the dramatic, sporadic intensity differences among 25 μm steps.The inset shows a full vibrational spectrum for para-ATP. The band whose intensity is mapped marked with an asterisk.

transduction mode for separations because non-chromatographic noise is artificially imparted to the reconstructed electropherograms. To mitigate this problem, work has been done to translate the substrate and sample simultaneously (sample translation technique, STT) in order to spatially and temporally spread the illumination and collection of vibrational data over much nanocomposite substrate area at high speeds (1000 rpm).[22,87] This approach also helps prevent photolytic and thermal degradation of both analyte molecules and the substrates themselves, as laser radiation which does not couple to a surface plasmon most often radiates away as heat through the substrates.[22] A helpful conceptual explanation involves thinking of the substrate area in discrete unit, with each one as being subject to a certain time under laser irradiation, regardless of whether that irradiation results in scattering signal collection or not. By translating the substrate, a duty cycle of substrate use is created that extends the life of each segment of substrate by exposing a single unit of substrate area to laser for much shorter time span with periods of non-irradiation in between. Since part of substrate degradation involves thermal rearrangement of the metal nanoparticles within the elastomer, these rests significantly extend the life of a substrate. The μfluidic-SERS platform cannot, at present, be spun around or laterally translated, although a wiggle mirror (for Raman line scanning) installed within the LabRam might accomplish the creation of a similar "duty cycle" of substrate for inside the channel. Thermal and photolytic degradation is controlled by keeping acquisition times low enough that simply passing the laser beam through the upper thickness of the μfluidic channel before reaching the sensing surface within has been sufficient to prevent damage to substrate or analyte thus far. Averaging

out of nanoscale inhomogeneity and differences in intra-substrate activity was a somewhat more nuanced process.

In order to acquire said spectra from across a substrate in a separation channel configuration, but at the same lateral position within the distribution of analyte in an electrophoretic zone, can be averaged to remove some of the deleterious effects of nanostructure depth, change of Raman instrument focus from spot to spot, and extreme spikes and valleys in vibrational intensity caused by locations with very high or very low activity due to specific arrangement or metal chemistry changes. The lateral steps are averaged to minimize the effect of substrate inhomogeneity, which can create artificial noise, in the final reconstructed electropherogram. Figure 3.8 shows a reconstructed electrophoretic band overlaid upon the three spectral intensity values that were actually averaged to comprise each data point along the band. The resorufin vibrational band at 573cm^{-1} was selected from an entire spectrum, and its intensity was followed through the electrophoretic band and is shown as an intensity grid. In addition, apparent chromatographic noise that is actually caused by variations in SERS activity of the nanocomposite in going from one spot to the next can be smoothed by using a regime of running weighted average (n=13) available within the LabSpec version 4.03 software used to collect the raw band data on the JY Horiba LabRam.[V]. This essentially accomplishes *post*-spectral collection what STT accomplishes during spectral collection: an averaging of depth and aggregation anomalies over the course of some finite amount of irradiation and accumulation time and space.

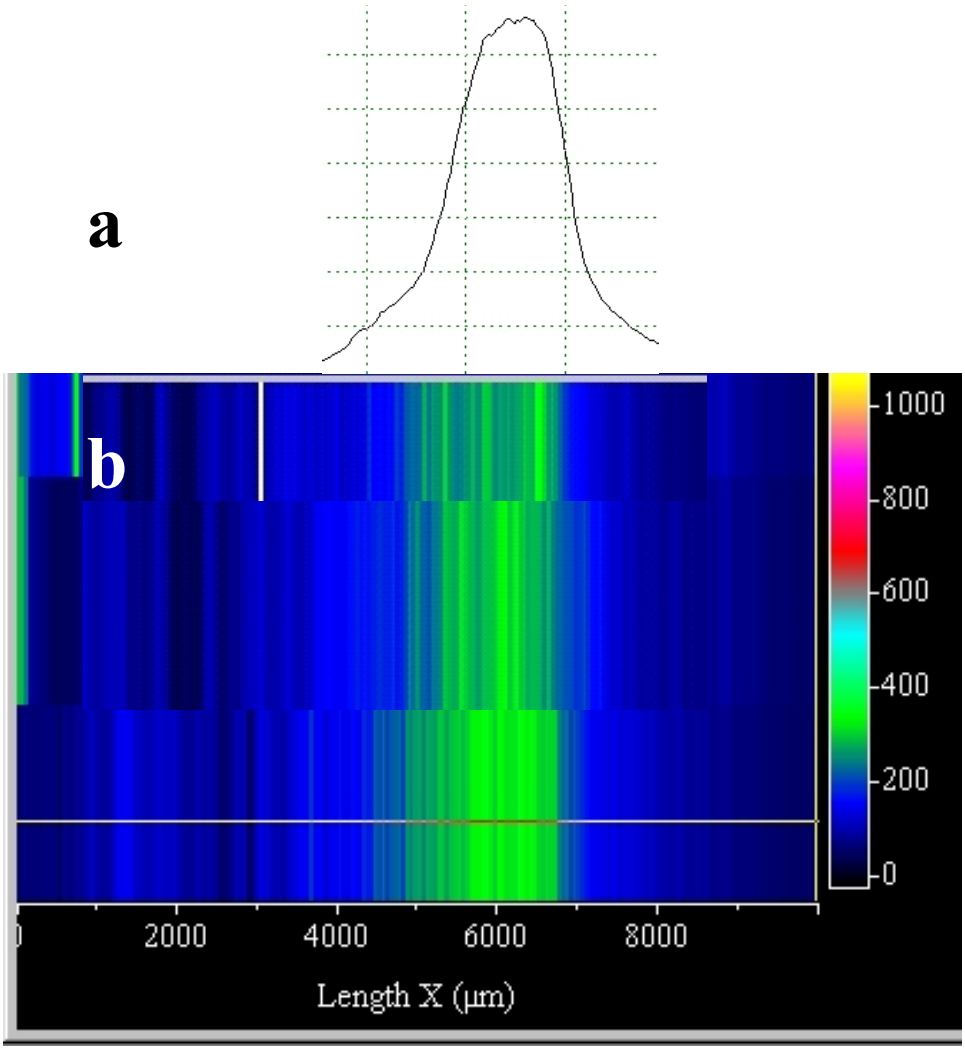

Figure 3.8: Demonstration of lateral averaging result. (a) Compare relative smoothness of the laterally averaged, slightly smoothed band with the unaveraged, single trace inhomogeneity in SERS response that leads to an appearance of artificial noise in the electrophoretic band profile. The grid (b) is simply a map of SERS intensity for the vibrational band followed for resorufin at 573cm-1 and hence a multidimensional representation of the lateral steps averaged for the electrophoretic band profile. Note: the grid has been shifted slightly to prevent flow-related band asymmetry from marring discussion of spectroscopic averaging.

Linear Dynamic Range

Exploiting the Electrophoretic Band Shape to Extend the High End

One special advantage of μfluidic-SERS arises from the fact this integrated technique yields an electrophoretic band, i.e., a Gaussian distribution of analyte mass, over a space that can be interrogated with a spectroscopy that is mass sensitive due to its surface-associated nature. The three dimensionality of metal nanoparticles within the PDMS dielectric is undeniable (recall Figures 2.1 and 2.2), but the locations available with maximum SERS field enhancement are limited nonetheless. As previously mentioned, surface enhancement effects increase the Raman cross-section sufficiently to lend orders of magnitude of sensitivity to the spectroscopy, meaning that more molecules become detectable at analytically relevant concentrations (or total mass amounts) with SERS. As the EM enhancement decays as $1/r^3$ (where r = distance from the center of the enhancing particle or locus), only a certain proportion of analyte molecules in a very concentrated electrophoretic band will be favorably oriented to yield SERS spectra, with the remainder of the analyte mass in excess, residing in non-SERS-active regions, especially at the area of the band containing the maximum mass within distribution. What's more, with analytes that experience both EM and chemical enhancement, not only limited availability of loci for enhancement but also concerns about detector saturation arise. To address this upper limit on linear dynamic range, a novel data collection and processing scheme has been devised that renders μfluidic-SERS more robust for samples containing analytes of varying concentrations as well as wide-ranging SERS response factors, from those that are both EM and chemically enhanced down to those with no chemical enhancement that even compromise the EM

enhancement mechanism by partially oxidizing the metal within the substrate. The inherent analyte mass distribution due to diffusion in electrophoretic bands can be exploited to turn this "mass sensitive" attribute into a quasi-advantage. By having the choice of the entire Gaussian distribution of analyte mass within the electrophoretic band to collect a SERS spectrum, the entire band is sampled for spectra, and the true shape can be interpolated. Careful computational interpolation of electrophoretic peaks truncated due to saturation of the SERS substrate creates a more quantitative representation of the peak for height or area calculation. Two criteria must be satisfied for this approach to work. First, the injection of analyte must be controlled and short enough that no truncation due to sample overloading, and thus non-diffusion controlled band dispersion, of any component's electrophoretic band exists and approximate Gaussian mass distribution can be assumed. Second, SERS spectra must collected after the termination of separation voltage in order to allow for temporal improvement of signal as analyte fully partitions onto substrate as well as the ability to fully exploit the Gaussian distribution by collecting a full grid pattern of spectra within the electrophoretic bands themselves while they are stagnant.

Exploiting this combination insofar as to collect SERS spectra for high concentration or strongly responding analytes in the wings of the Gaussian mass distribution can help extend the linear dynamic range of SERS on the high end of the calibration curve. The process by which this interpolation is implemented begins by actuating separation voltage on the integrated μfluidic-SERS device. Separation voltage is terminated with the analyte component bands halted within the SERS nanocomposite detection region after an appropriate amount of time. Termination of separation is

determined either by simple time counting based on prior experiments with similar analyte and buffer systems or by monitoring analytes by-passing on-line LIF detection in a region of the integrated device prior to the nanocomposite SERS detection region. Upon separation termination, the SERS nanocomposite region is mapped as described earlier to locate the band and subsequently map it fully in a gridded collection of small steps, to which the spectral averaging of laterally across the band and weighted smoothing described earlier are applied.

The interpolation of a full Gaussian from a band truncated by substrate saturation required a more subtle mathematical treatment for which the help of Dr. R.J. Harrison and his student, Malcolm Cochran, computational chemists, were recruited for their more expert assistance in applying mathematical algorithms to quantification of vibrational signals from electrophoretic data. In order discern a value for full peak height and area, the "tails" of SERS-saturation truncated peaks were fitted in a least squares fitting of both tails to a complete Gaussian function by setting limits on the outer edges of those "tails", that is where the mapped band stopped giving SERS signals for the analyte discernable from background SERS signals.[100] Once the Gaussian function was defined, a least squares fitting was carried out to find the interpolated peak maximum according to the equation

$$\textbf{Interpolated peak maximum} = \min((be^{-a(t-t_0)^2}) \qquad \textbf{Equation 3.1}$$

where b is the true height of the peak, a is the truncated height, t_0 is the mass center of the bands as defined by a Gaussian bounded on two outer sides, and t is the distance, in time units, of each modeled point away from mass center. The "min" command indicates that a minimization is computed in order to find b where $t = t_0$, or the peak

height at the interpolated maximum. A schematic definition of these variables appears in Figure 3.9. The calibration curve in Figure 3.10 for resorufin was created using both raw intensity values at electrophoretic band center (blue diamonds) and substituting in an interpolated value for the intensity point for a $5x10^{-5}$ M injected band, which was spectroscopically truncated due to mass-saturation of the SERS sensing surface. The experiment was performed on a hybrid glass-PDMS device because control of flow, and thereby control of precise, narrow injected analyte bands, is increased on this platform. This data was then re-plotted, substituting in the peak SERS intensity value interpolated from the fitting of the saturated $5x10^{-5}$ M resorufin electrophoretic peak's Gaussian tails.

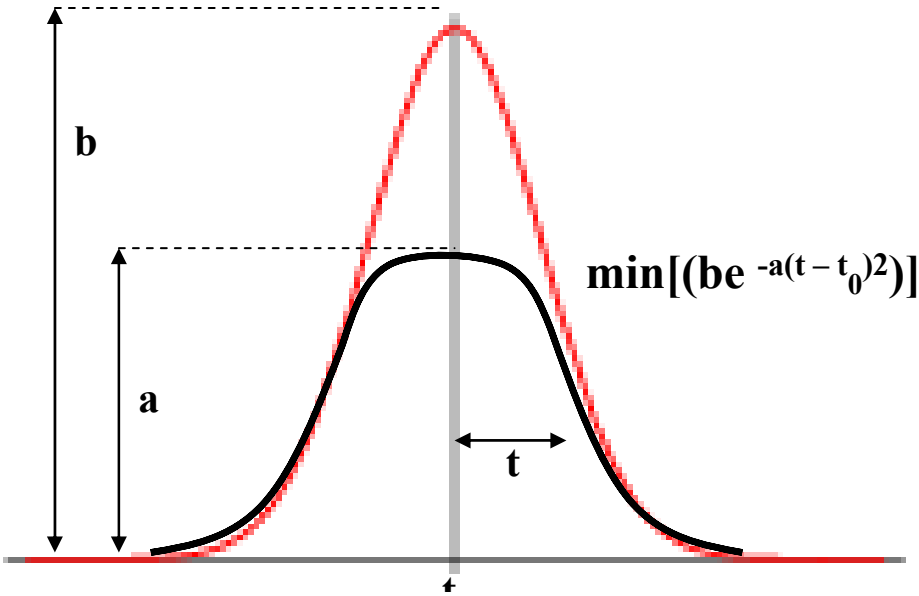

Figure 3.9: Diagram of peak height interpolation variables. Shows result if intensity of SERS response values followed the true Gaussian electrophoretic bandshape (red line) instead of being truncated due to substrate saturation (black line). Variables are fully described in text, but the expression essentially states that the interpolation is based on finding peak height (b) when the distance from peak center (t – t0) is at a minimum ("min" function) with a center of peak mass defined by inputting values from the two Gaussian tails.

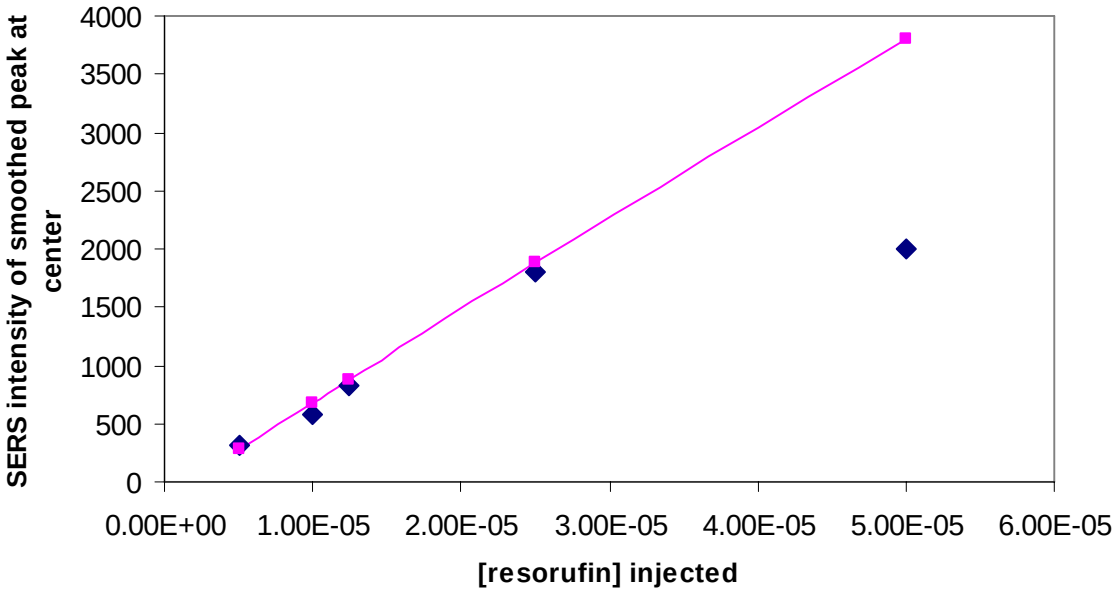

Figure 3.10: Calibration curve from raw and interpolated data. Raw magnitudes of SERS signal at peak of electrophoretic band (blue diamonds) and substitution of interpolated value for peak SERS signal of truncated Gaussian band for the $5x10^{-5}$M resorufin injection (pink squares).

CHAPTER 4

Application of Integrated μfluidic-SERS to Analytical Samples

General Statement of Applicability

Perhaps the most compelling arena for application of a portable μfluidic separation platform with integrated vibrational detection is analysis of environmental toxins and carcinogens. Greater threats to the human population by biochemical warfare agents coalesce in the current scientific zeitgeist with the need for faster, portable analytical tools to assay a food supply that feeds an exponentially growing world population, creating an imperative for development of more functional μfluidic devices with reliable, informative detection modes. A broad range of analytes relevant to environmental health including mycotoxins and endocrine disruptors, among others, were screened for Raman response, and model separations of these analytes were optimized on a shortened capillary with the speed and automation of an Agilent $HP^{3D}CE$® commercial, automated capillary electrophoresis instrument with UV-vis detection. This chapter represents preliminary studies aimed at laying a foundation for future research to strengthen the analytical toolset for toxin assays that include efficient separations and information-rich detection on a portable platform.

Toxin Assays

Mycotoxins are metabolic waste products of fungal growths on grain stuffs and legumes. Bioaccumulation in animal tissues is also a serious concern, as regulations governing amount and type of mycotoxin contamination allowable in animal feeds has

historically been more lax and even those looser requirements were not rigorously enforced until the 1990s. A selection of some mycotoxins for which multiple separation conditions have been reported is shown in Figure 4.1.[101] Acute exposure to these compounds leads to headaches, nausea, abdominal pain, fatigue, and jaundice. Mycotoxins are hepatotoxic, carcinogenic, and teratogenic, which makes them ideal analytes to study in concert with the other, similarly dangerous family of compounds being assayed in preparation for use with μfluidic-SERS, the EDCs. In order to lay groundwork for on-chip separations with SERS detection of toxins routinely tested for in the food supply, mycotoxins were modeled for separation conditions on a shortened capillary (effective length = 7.5 cm; E = 200 V/cm) with 325nm excitation LIF detection (Figure 4.2a) in 10 mM borate anion buffer with 50 mM SDS as the pseudo-stationary phase. Several mycotoxins also screened positive for SERS activity (Figure 4.2b). The shortened capillary and low field strength more honestly mimics the abbreviated separation length in our integrated μfluidic devices, as well as compensates for the necessarily lower field strength in PDMS-glass hybrid chip devices. This is especially important with higher viscosity running buffer, since PDMS is eight-fold less thermally conductive than glass. For this reason, dissipation of heating due to high currents is slower and smaller in magnitude in the hybrid device relative to an all-glass device, so field strengths are kept low to avert excessive Joule heating with its deleterious band broadening and bubble generating effects.

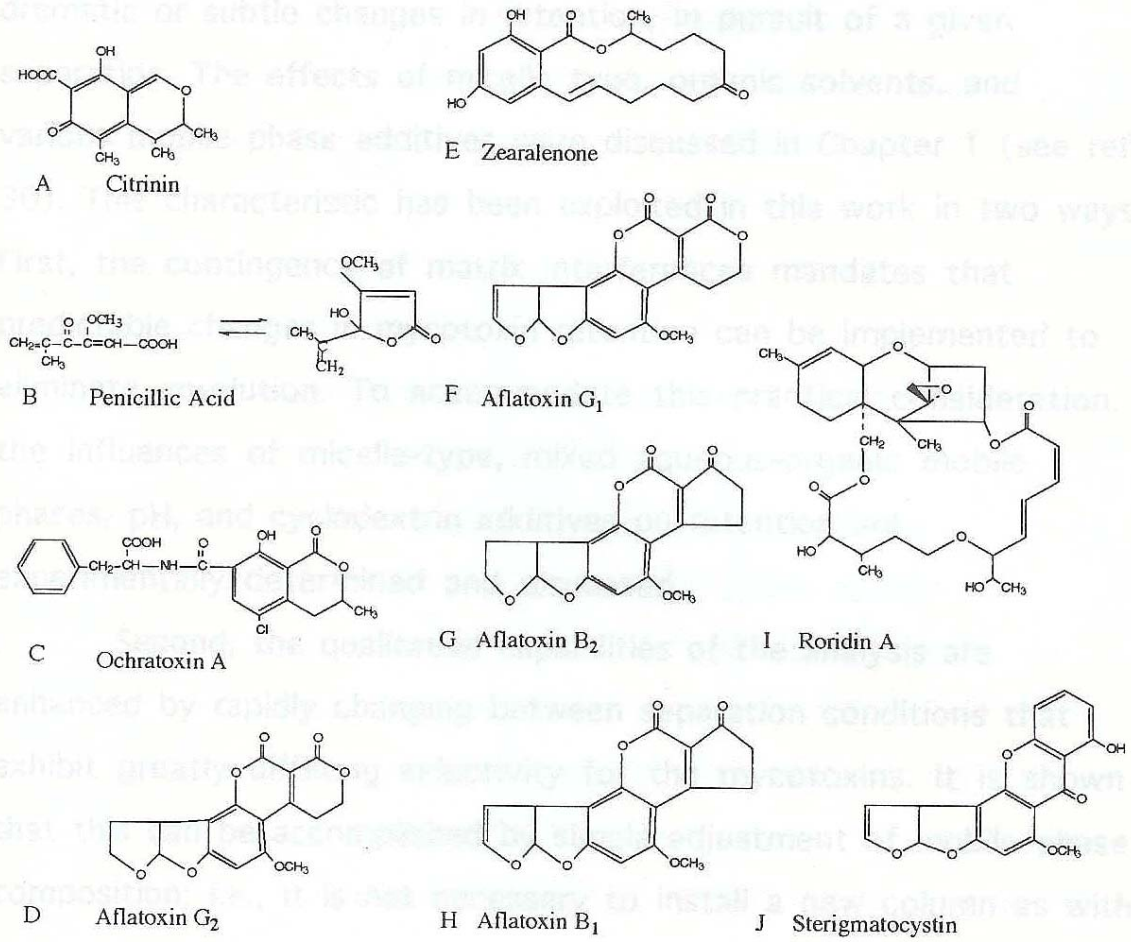

Figure 4.1: Structures of mycotoxins pertinent to integrated μfluidic-SERS studies.

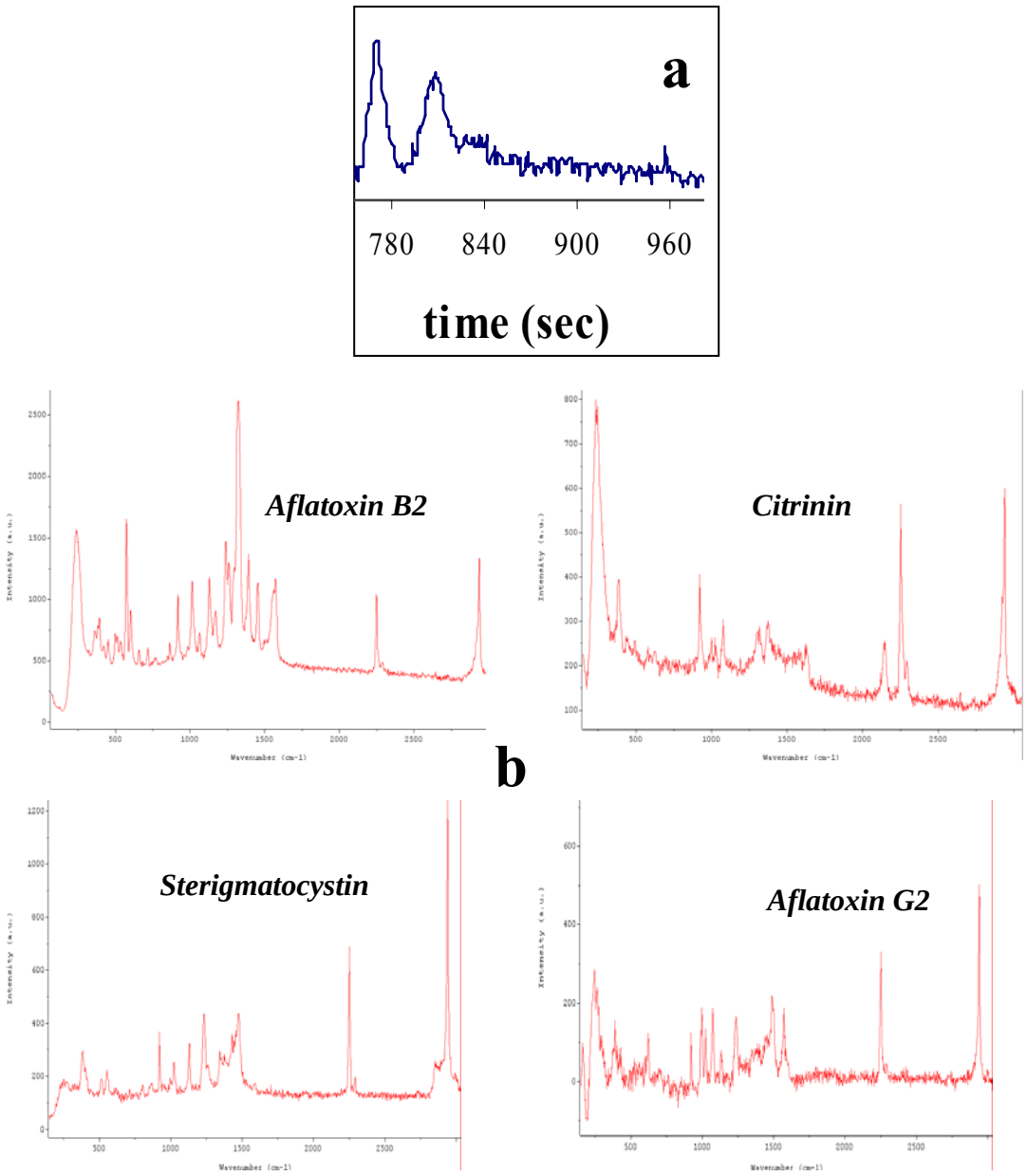

Figure 4.2: Separation on a shortened capillary with LIF detection and SERS spectra of several mycotoxins. (a) LIF Electropherogram of separation of aflatoxin G2 and B2 and (b) SERS responses of μfluidically delivered samples of aflatoxin B2, citrinin, sterigmatrocystin, and aflatoxin G2.

Endocrine Disrupting Chemicals

The label "EDCs" indicates one of any of the many chemicals that can interact with the human or animal signaling system of hormones and receptors by blocking receptors, mimicking hormones to activate or deactivate signaling by actuating the receptor to which they bind, or modulating the production of endogenous signaling hormones by interfering with a receptor pathway. EDCs have caused testicular cancer in the male offspring of women exposed during pregnancy and are suspected to have also led to reproductive hindrance in female offspring.[102] What's more, EDCs have been proven to prevent the maturation of genitalia in lower organisms such as frogs and fish, even at modest environmental concentrations.[103] The long list of suspected EDCs includes steroids and artificial hormones, pesticides (both herbicides and insecticides), plasticizers, concentrated plant extracts, and polycyclic aromatic hydrocarbons. Through its Science to Achieve Results (STAR) program, the Environmental Protection Agency (EPA) has issued a call for extramural research proposals that offer, "innovative approaches for measuring the concentrations and activities of endocrine disrupting chemicals in environmental and biological media."[104] The integrated μfluidic-SERS work described provides fundamental analytical development to buttress a larger project which will fulfill this EPA request and, in so doing, generate tools to address Goals 1 and 2 of the EPA-Office of Research and Development (ORD) Multi-Year Plan for Endocrine Disruptors: Long-Term Goals.[104] The development of novel, field-portable, highly versatile yet selective technologies to meet these chemical analysis needs is quite challenging and ongoing. The integrated μfluidic-SERS approach will eventually offer optical vibrational transduction as a field-appropriate,

quantitative, structurally informative method to investigate EDCs and their breakdown products in realistic samples.

To begin this work, a subset of the 78 priority EDCs (as defined by EPA based on an international advisory conference)[104] were chosen for three reasons: one group had been previously tested with the bioreporters of collaborators in the University of Tennessee, Knoxville, Center for Environmental Biotechnology; group B had been previously assayed by the Dr. M.J. Sepaniak research group; and group C showed some promise for SERS activity due to flavinoid character or extended conjugation. A chart of some of these structures can be found in Figure 4.3. The preliminary analyses of the separation behavior and spectroscopic response of several EDCs was pursued in parallel. Based on the neutral and relatively hydrophobic nature of the samples, separations modeled on the Agilent HP^{3D}CE commercial CE instrument were carried out with under CD-modified MEKC conditions, specifically with pseudo-stationary phases of 25 mM SDS and 5 mM β-CD, in the 12.5 mM borate anion running buffer. Addition of 10% methanol to the cocktail altered association with the phases, slowed flow, and also decreased changed the number of intact micelles present at any one time. These conditions yielded the best resolution attainable for two different samples, as shown in Figure 4.4. Figure 4.4a shows separation of a mix containing more steroidal, purely estrogenic compounds, including an anti-miscarriage drug banned for its extreme teratogenicity (diethylstilbestrol, DES), natural human estrogen (17β-estradiol), a component of modern birth control pills (17α-ethynylestradiol), and a common plasticizer (bisphenol A). The mixture in Figure 4.4b contained mostly phytoestrogens, or EDCs derived from plant products, with DES also included as a marker from the first

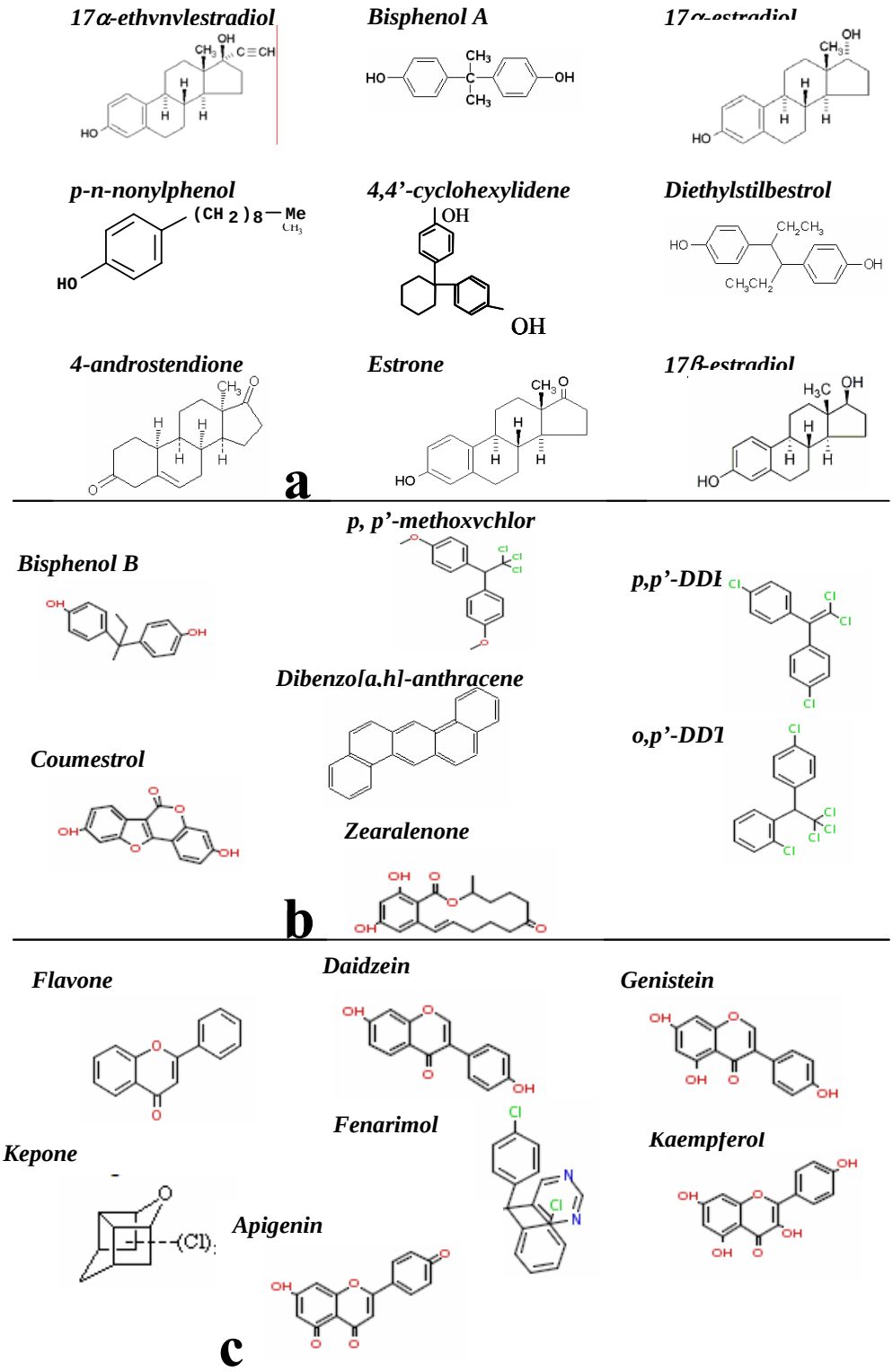

Figure 4.3: Selected EDCs. (a) previously screened against bioreporter yeast. (b) prior research in Sepaniak group. (c) promising for SERS.

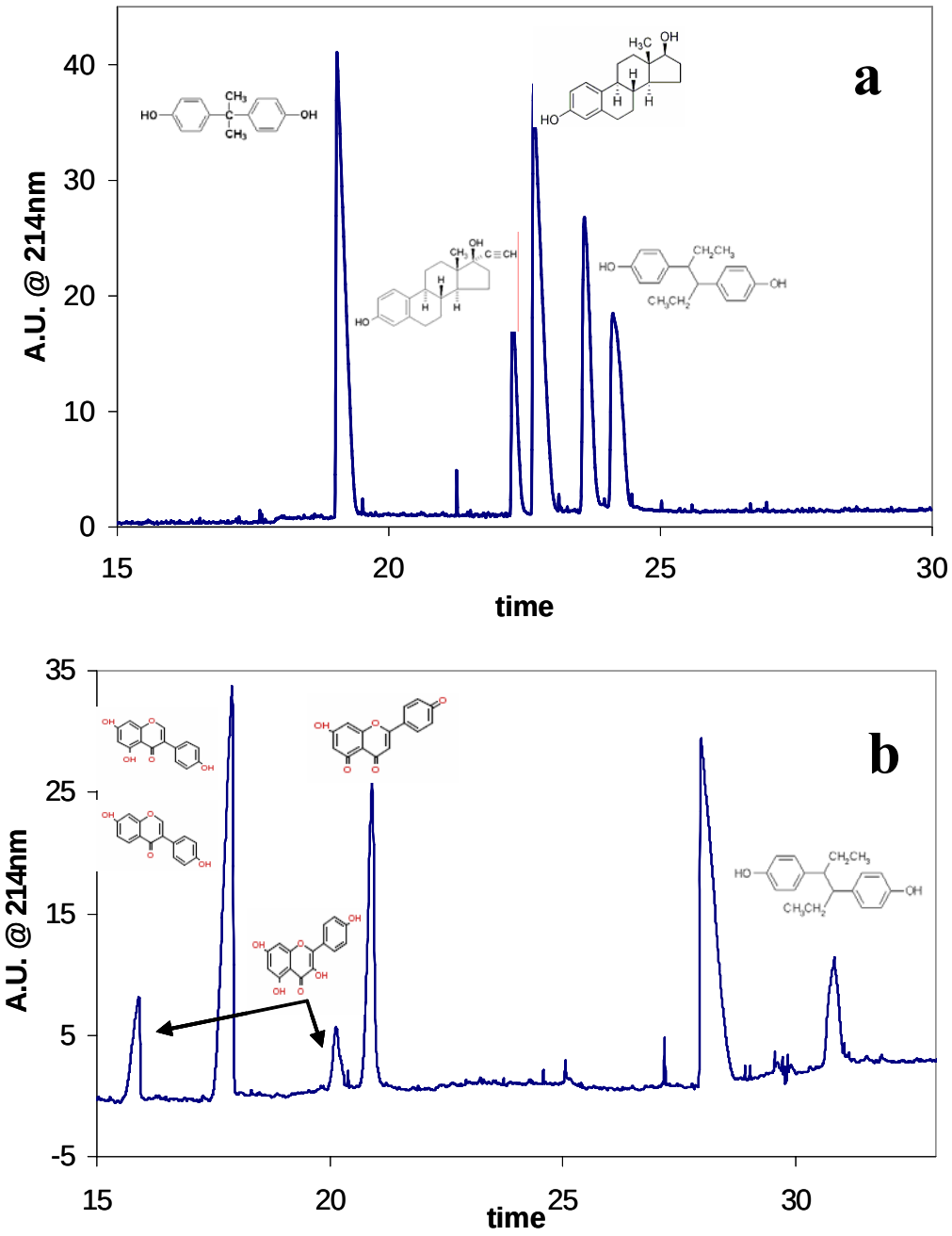

Figure 4.4: Separations of two groups of EDCs. (a) Separation of bisphenol A, 17b-estradiol, 17a-ethynylestradiol, and DES (2) and (b) separation of genistein and daidzein (coelute), kaempferol (2), apigenin, and DES (2). The same conditions were used in both separation and are reported in the text.

separation. The phytoestrogens as well as DES are more susceptible to photodegradation than the other separated EDCs, and this could explain why kaempferol and DES both give split peaks: their breakdown products migrate at different velocities. Individual injections were performed with each analyte under identical conditions to positively ascertain the migration order.

As mentioned, SERS surveys of EDCs have run in parallel with separations. The spectral results are not as ubiquitous among EDCs tested as might have been expected. The probable reason lies as much in the format of SERS testing as in the actual SERS activity of the analytes. Careful study of storage and preparation conditions for the PDMS that would become the nanocomposite substrates showed that PDMS inevitably yields a background spectrum due to accumulation of organic contaminants in the uncured bulk polymer during storage, the cured polymer during heat curing process, and the complete nanocomposite due to hydrocarbon residues co-deposited with noble metals during the PVD process. These interferences can be minimized with proper storage and handling of nanocomposite substrates. Another, more fundamentally instructive opportunity arises from EDC SERS spectral collection on simple nanocomposites; the low water solubility of most EDCs leads to competition from other components (including water contamination) and poor information content and signal to noise ratio for the SERS spectra of these water solutions. Hence, the first spectra collected for EDCs were collected from partial methanol solutions at concentrations higher than would be tested in the integrated μfluidic-SERS assays. However, the proof-of-concept was achieved by showing, as in Figure 4.5, that several of the selected EDCs analyte have descriptive, distinctive SERS spectra. SERS spectra were collected

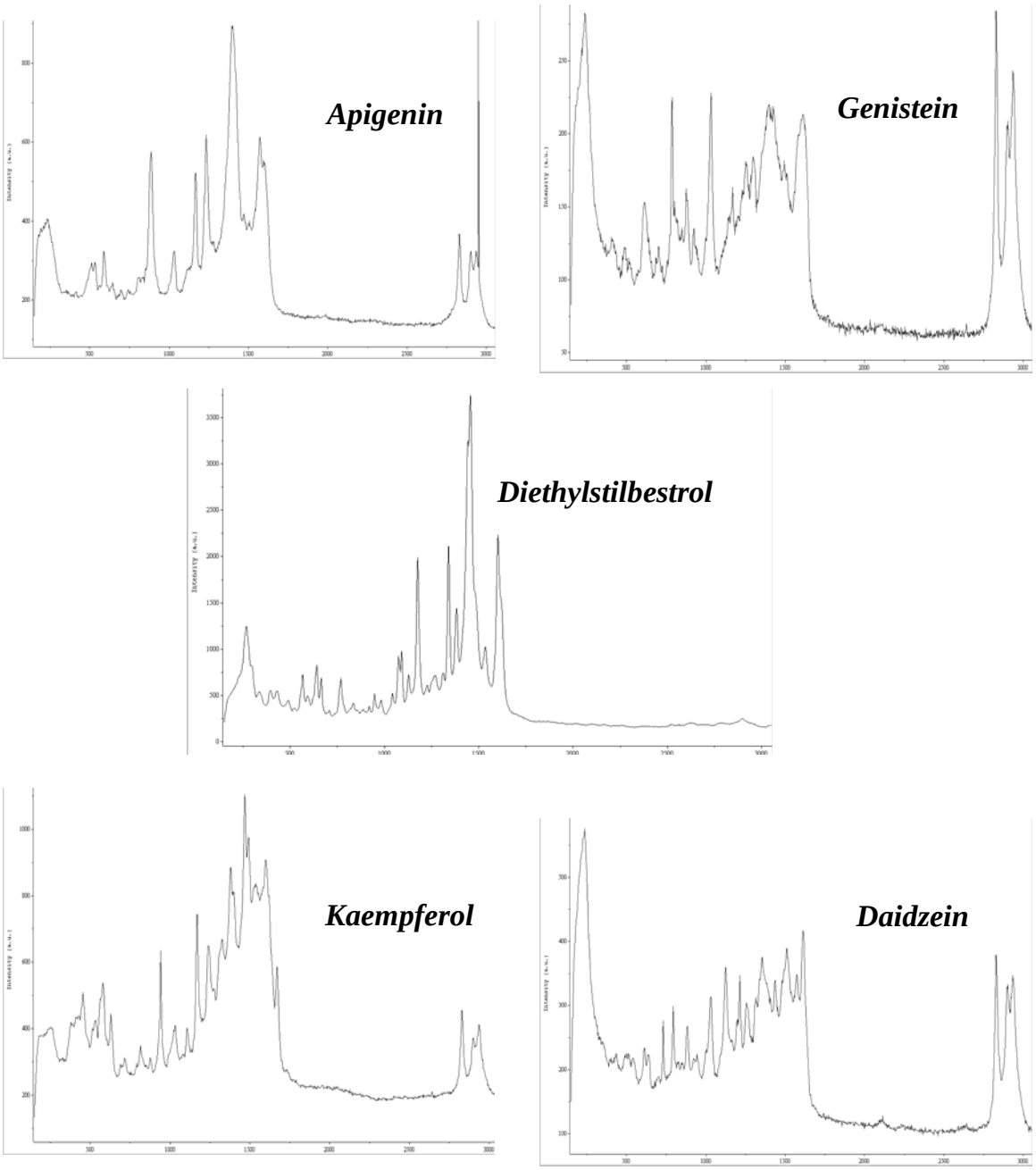

Figure 4.5: SERS activity of some EDCs.

in nanocomposite titer wells with STT from 2mM solutions containing 15% methanol, except in the case of DES, which was 1mM.

The most exciting part of this application work has been the opportunity to interface the integrated μfluidic-SERS devices with early tests of compatibility with the living conditions of live bioreporter organism in preparation for sophisticated synergistic screening and sample analysis of EDC-contaminated samples. If the ultimate integrated EDC testing platform is to be completed to include separation of contaminated samples upon BLYES luminescence with SERS detection of the separated EDC samples, the compatibility of the yeasts' living conditions with the integrated SERS substrates must be examined. Tests were conducted to determine whether SERS substrates would continue to enhance the scattering signal of a model analyte, resorufin at 10^{-5} M, in the presence of the rather complex (see Figure 4.6) nutritive media in which the bioreporting yeasts must live. When substrate is exposed to analyte alone first, no attenuation in SERS signal is noted, although some would be expected for analytes that demonstrate no chemical enhancement whatsoever, as they cannot rigorously compete in the kinetic contest for enhancement sites among the noble metal nanoparticles, particularly in the presence of abundant anions. This mechanism seems to be at work as well when SERS substrate is exposed first to pure media, as the SERS signal from resorufin upon addition to such a pre-existing matrix is weak and crowded with background bands. However, in promising development from these experiments, it appears that when analyte and media are mixed together prior to encountering the SERS substrate, a decent signal results because not all of the enhancement regions have been scavenged by strictly media components. Since the design of the μfluidic-SERS devices

To prepare final YMM:	For 1L add:
21.4ml YMM	855ml
0.250ml vitamin solution	10ml
2.5ml glucose solution	100ml
0.625ml L-aspartic acid solution	25ml
0.200 ml L-threonine solution	8ml
0.0625ml copper (II) sulphate solution	2.5ml

Yeast Minimal Media:

13.61g KH_2PO_4
1.98g $(NH_4)_2SO_4$
4.2g KOH Pellets
0.2g $MgSO_4$
1ml $FeSO_4$ solution (40mg/50ml water)

(50mg leucine	5ml @ 1g/100ml)
50mg L-histidine	5ml @ 1g/100ml
50mg adenine	**10ml @ 0.5g/100ml**
20mg L-arginine-HCl	2ml @ 1g/100ml
20mg L-methionine	2ml @ 1g/100ml
30mg L-tyrosine	**15ml @ 0.2g/100ml**
30mg L-isoleucine	3ml @ 1g/100ml
30mg L-lysine-HCl	3ml @ 1g/100ml
25mg L-phenylalanine	2.5ml @ 1g/100ml
100mg L-glutamic acid	2ml @ **5g/100ml**
150mg L-valine	5ml @ **3g/100ml**
375mg L-serine	10ml @ **3.75g/100ml**
20mg tryptophan	2ml @ 1g/100ml
(50mg uracil	25ml @ **0.2g/100ml**)

Bring to 1L with water. Place on heated stir plate to dissolve. Divide in two and autoclave. Store at RT.

Vitamin solution:	in 500ml add:
8mg thiamine	20mg
8mg pyridoxine	20mg
8mg pantothenic acid	20mg
40mg inositol	100mg
20ml biotin soln (2mg/100ml)	50ml

Sterilize by filtering through 0.2um filter into a sterile bottle. Store at 4°C.

Figure 4.6: Composition for yeast nutritive maintenance media.

which integrate bioreporters will only sample media when is contains EDC (as signaled by the luminescent yeasts), this condition of needing to pre-mix media and analyte in order for the analyte to compete to give a SERS signal will fit into the experimental scheme. One other aspect of these studies revealed that, although the physical presence of yeast cell does not create much vibrational spectra, their micron-scale bulk does change the refractive index of the area immediately over the substrate, dampening SERS scattering signal in a small magnitude by their very presence. Hence, the development of EDC methods with the ultimate aim of integration on a microorganism-friendly chip continues without fear of a halting obstacle such as yeast and SERS being mutually exclusive in conditions required for function. Results of the tests with media and resorufin appear in Figure 4.7. The following chapter expounds further on future EDC work and gives a clearer perspective on the final goal.

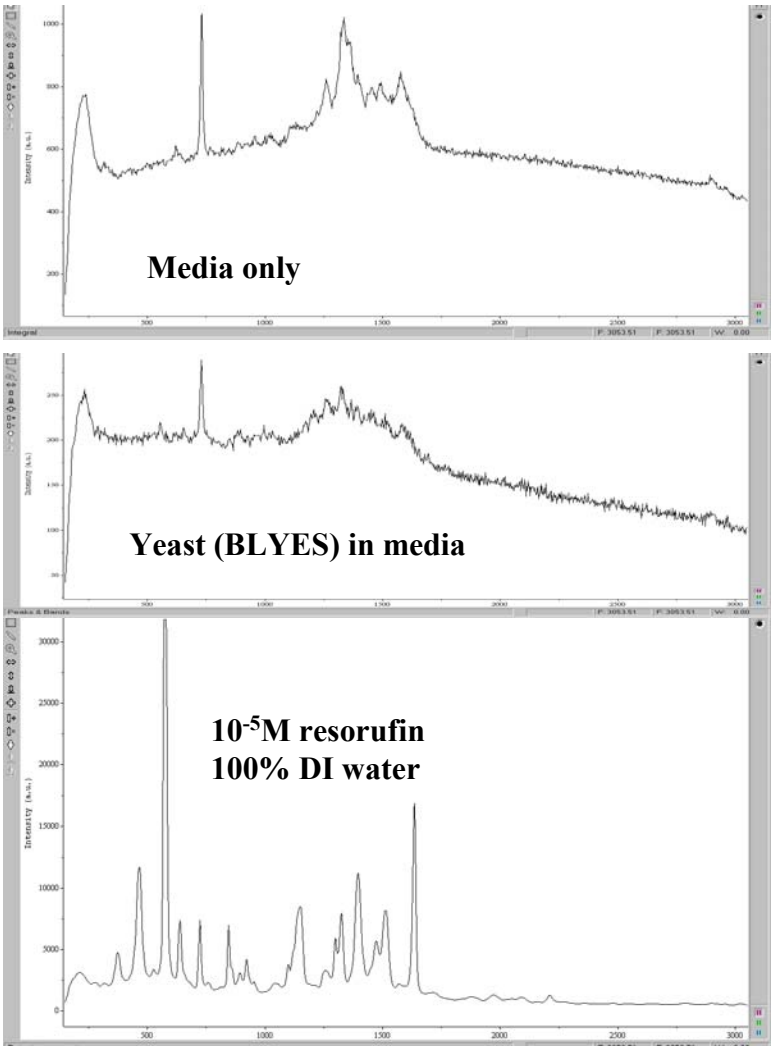

Matrix, analyte order of introduction	Intensity (at 573 cm^{-1})
10^{-5}M resorufin alone (no change with later addition of media)	30,000 counts
Media and resorufin premixed (x2 dilution)	5500 counts
Yeast whole organisms added to premix (x4 total dilution factor of original resorufin)	2400 counts
Media applied before resorufin	<400 counts

Figure 4.7: SERS assays of resorufin standard in yeast maintenance media and in the presence of yeast. Different orders of exposure were used including media premixed, media exposed to substrate and then analyte spotted, and media and analyte premixed in the presence of yeast organism bodies themselves with representative spectra shown.

CHAPTER 5

Concluding Remarks

The widespread development of μfluidics has allowed the extension of efficient separations, fluid handling, and hyphenation with many detection modes to a small, portable, highly controllable physico-chemical platform. SERS offers the powerful advantage of obtaining vibrational spectroscopic information about analytes in an aqueous matrix with negligible background. The mating of electrophoretic separations with vibrational spectroscopy on a μfluidic device will allow the chromatographic efficiency of CE with the unequivocal analyte "fingerprinting" capability of detailed structural information. Utilizing SERS as a means of detection yields redress for the hindrances of electrophoretic separations, including uncertainty in analyte band identification due to changing migration times as well as compromised detection sensitivity for non-fluorescent analytes. This work represents the first steps toward developing a CE-SERS hyphenation on a μfluidic platform with a region of novel metal-pliable polymer nanocomposite SERS substrate fabricated directly into the device. The device fabrication material has been extensively employed by the μfluidics community for over five years. SERS detection can be achieved in real time or after the separations, with on-column laser-induced fluorescence employed as a secondary detection mode used for confirmation of efficiencies and band locations. These integrated μfluidic-SERS platforms have been screened and were proven functional for

for separation conditions and SERS activity of two classes of environmentally and biomedically threatening compounds, mycotoxins and EDCs.

Future Studies for Integrated μfluidic-SERS

Although progress has been made in collection of SERS data from separated bands, the control of experiments on the integrated platform still begs significant improvement. More rationally-designed, optimized EBL and reactive ion etched SERS substrates will extend the linear dynamic range at the low end, allowing for detection of separated bands beyond the part per billion range. Thus far, educated speculation has guided the choice of patterns created by EBL, and empirical results of assays for these patterns' SERS activity dictated modifications to the computer-aided designs that govern the path of the electron beam in creating nanofeatures. Modifications in the practical process of spin coating and developing electron resist added variables to the empirical process as well. Once the most favorable patterns and fabrication conditions are settled upon, the ultimate in sensitive μfluidic-SERS can be pursued with either directly created or stamp-relief molded rational, periodic nanopatterned SERS substrates within μfluidic separation channels. Lower detection limits will benefit both separation efficiency as well as information content, especially helpful advantages is analyzing toxins within contaminated sample of limited supply. Secondary to achieving the goal of lower LODs for μfluidic-SERS, μfluidic delivery offers the ability to individually address multiple nanopatterns (ten of these patterns can be created in a small footprint 3mm x 0.5mm), each with its own μfluidic channel, on a single small-footprint silicon substrate, should multi-analyte testing without cross-exposure among sequential nanopattern grids become necessary or attractive.

Also vital is an increase in careful control of injection and flow within the μfluidic device itself to improve reproducibility and separation capabilities of the total technique. Such improvements will come with solenoid switching circuits, permanent video CCD rigged with appropriate filters to function as a home-built fluorescence microscope for visualization of the injection port to facilitate real-time voltage tuning, and constant use channels with three sides of unblemished glass or treated polymer. Implementation of a wiggle mirror just prior to the microscope objective lens within the confocal Raman spectrometer will accomplish line averaging during spectral collection to simplify both band location within the SERS substrate region as well as the detailed reconstruction of electrophoretic bands based on intensity of vibrational spectral features. Other options for mitigating photo- and thermal degradation as well as averaging out nanoscale inhomogeneities in the nanocomposite involve using a piezo-resistively or magnetically actuated lateral fast transition to accomplish the same spatial and temporal physical translation, in contrast with the mathematical averaging now utilized, to approximate the STT spinning method for the μfluidic-SERS platform. A final interesting opportunity for advancement of SERS as a μfluidic detection mode exists in the further refinement and validation of the extension of the high end of the LDR via computational interpolation of peak heights and areas by fitting to the Gaussian nature of the electrophoretic (or chromatographic) analyte zone. Modifications to account for tailing, fronting, and non-Gaussian peaks would also expand this approach, which could benefit the spectral interpretation of any μfluidic-SERS sample which contains both low and high concentration components and/or a mix of strong and weak SERS responders. Since a goal in analytical technique development is wide LDR

to accommodate unknown samples with diverse components and concentrations of those components, this avenue for investigation looks promising.

Next Steps for EDC Analysis with μfluidic-SERS

To increase the quality and sensitivity of SERS data collected for EDCs, current surveys of nonpolar coatings, such as squalane, polyethyleneimine, and fluorinated hydrocarbons, for nanocomposite and EBL substrates are under way. Modifications of SERS substrates with hydrophobic overlayers for extraction or selective delivery of the most nonpolar EDCs will require a reevaluation of the temporal development of SERS signal. This added effort will be well worth the advantages of increased EDC detection due to preconcentration as well as the screening out of substrate-degrading contaminants and oxidants.

SERS is a sensitive technique selective for those EDC molecules which have a change in polarizability within their vibrating bonds. However, this requirement does make SERS unable to detect many molecules of interest; conversely, cantilevers sensors lack selectivity, as they are simply mass or surface stress sensors whose responses are dictated by their surrounding environment and whatever surface treatment they may have. Future work for the EPA will combine four analysis tools for measurement of environmental EDCs, eventually at concentrations relevant to exposure assessment.[105] Two techniques utilized will be the bioactivity-based bioluminescent yeast reporting (BLYES discussed in chapter 4) and chemical separations, both of which have already shown EDC analysis, mated with two powerful, informative sensing modes that employ novel nanomaterials and are relatively new to EDC detection, SERS and microcantilever array (μCA) sensing. This combination will provide EPA with a

μfluidic device capable of qualitative indication of endocrine activity of a mixture followed by efficient separations and quantitative vibrational information and/or nanomechanical transduction of the various chemicals in the mixture with μCAs. The plentiful chemical information resulting from EDC mixture analysis according to the proposed scheme will elucidate the nature of unknown mixtures before and after they have interacted with the bioluminescent yeast bioreporter. This synergy of structural, kinetic, and separation information will enhance understanding of EDC behaviors regardless of whether the components in the mixture trigger yeast bioluminescence or not. Our work directly addresses two of EPA's three areas of interest ("development of analytical methods for the measurement of mixtures of EDCs in environmental media at relevant concentrations" and "development of rapid chemical or biological detection methods or technologies for environmental exposure monitoring").[106] By incorporating a bioreporter as a yes/no test for endocrine activity on the front end of the integrated μfluidic device, this work also builds on a biotechnology that addresses the third area of interest, "development of activity-based biological indicators for assessing EDC exposure in environmental media".[104-106] The final focus of integrated μfluidic-SERS with respect to EDC analysis is not an end in itself, but instead a component of a more complete system, envisioned in simple form in Figure 5.1. Generally speaking, the system will benefit from all advances in the μfluidic-SERS integrated device as well as utilizing μfluidic delivery of reagents to maintain bioreporter viability and to actuate microcantilever array sensing of separated EDC components. Although this project may seem overly ambitious or complex, prior research has laid the foundation for all of this work. Testing and development of this complete device simply seeks to move these

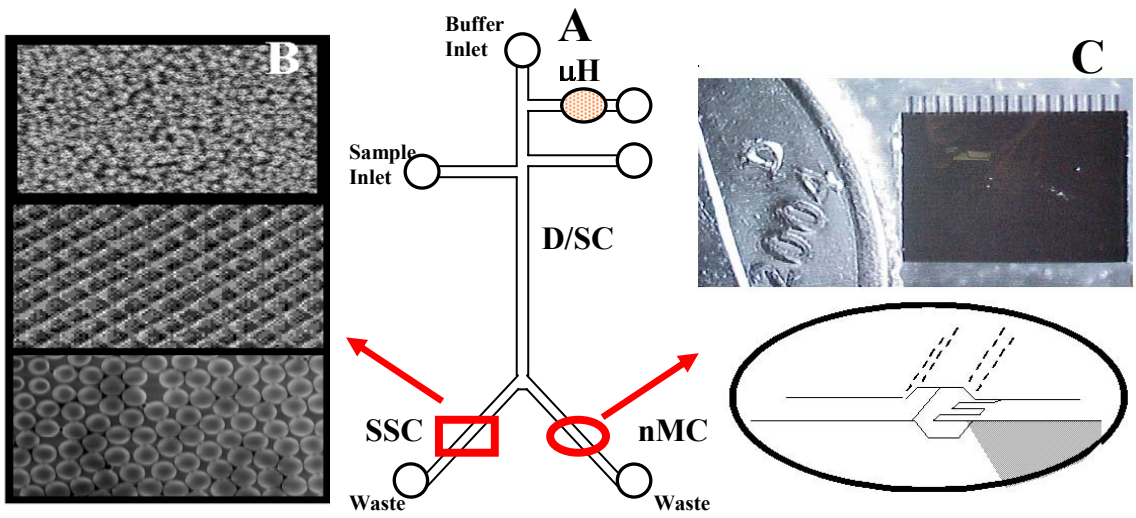

Figure 5.1: μfluidic separation and delivery device to contain SERS, microcantilever, and live bioreporter detection of EDCs. (a) possible mfluidic configuration with EDC mixture laoding either via a biosensing microorganism holding zone or directly to the delivery/separation channel which splits into a surface spectroscopy channel and a nanomechanics channel for detection. (b) SEMs of 3 types of SERS substrate: randomly generated metal-polymer nanocomposite, top; nanowells formed by EBL, center; and nanosphere lithography, bottom. (c) depicts the scale of an actual 16-lever array shown, top, and a microcantilever array, bottom.

techniques forward on a common platform with a clear, applied goal: EDC monitoring. The different types of information gleaned from each component of the device (SERS, microcantilevers, separations) come together to yield a fuller picture of the identity and activity of components of EDC mixtures.

Other crucial improvements to making μfluidic-SERS a robust and reliable analytical tool include methods to increase both the sample volume originally available to the SERS substrate within the μfluidic channels and separation electrophoretic bands as well as strategies to increase the active volume of the substrate that is interrogated. Tangent projects in development concurrent with and for use in integrated μfluidic-SERS devices involve testing near-infrared illumination for gold substrate so these more chemically inert, robust substrates can be employed with increased enhancement factors due to greater overlap of their extinction bands with the longer wavelength lasers. Another related avenue for analyte delivery to the SERS sensing surface entails derivatizing magnetic beads with sequestering reagents and using an external field to draw the sequestered sample molecules selectively to be vibrationally interrogated, thereby minimizing some matrix interference by creating a layer of rationally chosen molecules at the SERS surface. All of these approaches seek to improve the μfluidic-SERS technique by methodically targeting current limitations to help place SERS higher up on the list of trace analysis, since Figure 5.2 shows how rarely used this structurally information-rich tool is according to a SciFinder search of "SERS" and "trace analysis". Adding a component of separation will contribute to both the qualitative and quantitative dimensions of SERS for robust analytical evaluation that will also help increase its utility, especially if rigorously validated in future work.

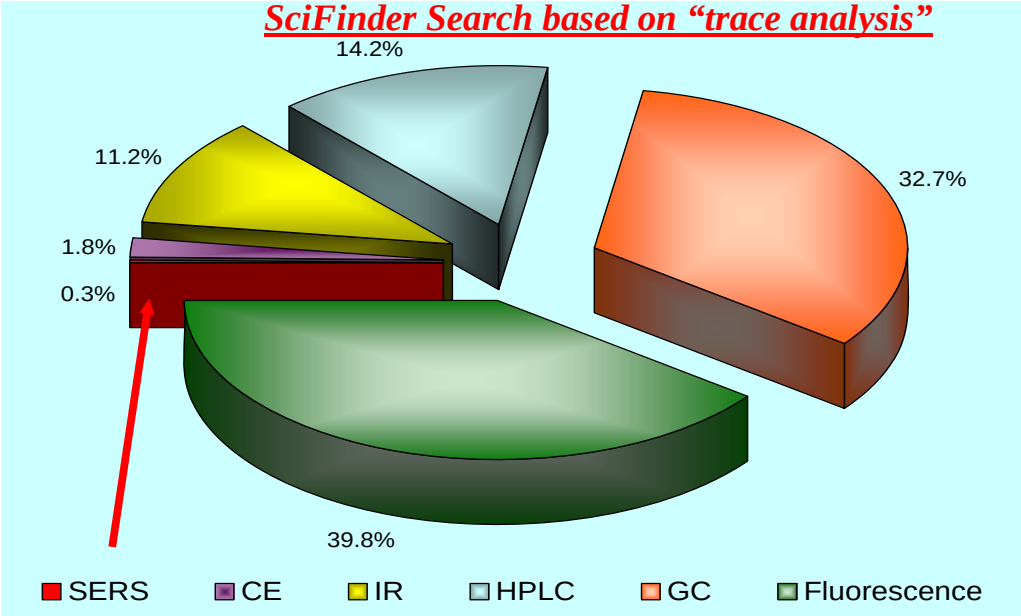

Figure 5.2: Percentage of trace analysis done with SERS according to SciFinder Scholar. Pie chart illustrates the small current percentage of trace analysis done with SERS despite potential for great chemical information conten and sensitivity.

List of References

1 Dolnik, V.; Liu, S.; Jovanovich, S. *Electrop horesis*. **2000**, *21*, 41-54.
2 Szekely, Laszlo; Guttman, Andras. *Electrophoresis.* **2005** *26(24)*, 4590-4604.
3 Li, Dongqing. *NATO Science Series, II: Mathematics, Physics and Chemistry*. **2005**, *193*, 157-174.
4 Yi, C.; Zhang, Qi; Li, Cheuk-Wing; Yang, Jun; Zhao, Jianlong; Yang, Mengsu. *Analytical and Bioanalytical Chemistry.* **2006**, *384(6)*, 1259-1268.
5 Jacobsen, S.C.; Hergenroder, R.; Koutney, L.B.; Warmack, R.J.; Ramsey, J.M. *Analytical Chemistry*. **1994**, *66*, 1107.
6 Anderson, J.R.; Chiu, D.T.; Jackman, R.J.; Cherniavskaya, O.; McDonald, J.C.; Wu, H.; Whitesides, S.H.; Whitesides, G.M. *Anal.Chem.* **2000**, *72*, 3158.
7 De Mello, A. *Lab On a Chip*. **2002**, *2,* 48N-54N.
8 Campion, A;.Kambhampati*, P. Chem. Soc. Rev*. **1998**, *27*, 241.
9 Li, H.; Walker, P.A.; Morris, M.D. *Journal of Microcolumn Separations*. **1998**, *10*, 449.
10 Walker, P.A; Morris. M.D. *J. Chromatogr*. **1998**, *805*, 269.
11 Walker, P.A.; Burns, M. A.; Johnson, B.N.; Morris, M.D. *Anal. Chem*. **1998**, *70*, 3766.
12 He, L.; Natan, M.J.; Keating, C.D. *Anal. Chem*. **2000**, *72*, 5348.
13 Keir, R.; Igata, E.; Arudell, M.; Smith, W.E.; Graham, D.; McHugh, C.; Cooper. J.M. *Anal. Chem***. 2002**, *74*, 596.
14 Nirode, W.F.; Devault, G.L.; Cole, R.O.; Sepaniak. M.J. *Anal. Chem*. **2000,** *72,* 1866.
15 DeVault, G.L.; Sepaniak. M.J. *Electrophoresis*. **2000**, *21*, 1320.
16 DeVault, G.L.; Sepaniak. M.J. *Electrophoresis*. **2001**, *22*, 2303.
17 Huang, X. and Zare, R.N. *J. Chrom. A.* **1990**, *22*, 555.
18 Page, J.S.; Rubakhin, S.S.; Sweedler, J.S. *Anal. Chem*. **2002**, *74*, 497.
19 Giesfeldt, K.S.;. Connatser, R.M; De Jesus, M.A.; Lavrik, N.V.; Dutta,P.; Sepaniak, M.J. *Appl. Spectrosc*. **2003,** *57*, 1346.
20 De Jesus, M. A.; Giesfeldt, K.S.; Sepaniak, M.J. *Amer. Pharm. Rev.* **2004**, *7*, 90.
21 De Jesus, M. A.; Giesfeldt, K.S.; Sepaniak. M.J. *J. Raman Spec.* **2004**, *35(10)*, 895-904.
22 De Jesus, M. A.; Giesfeldt, K.S.; Sepaniak, M.J. *Appl. Spectrosc*. **2004**, *58(10)*, 1157-1164.
23 Stebbins, M. *Development of Strategies for Biochemical Analysis Using Capillary Electrophoresis*. **1997**, *Dissertation, UTKnoxville*, p.2.
24 Heiger, D. *High Performance Capillary Electrophoresis: An Introduction*. Agilent, Inc., Germany: **2000**.
25 Szekely, L.; Guttman, A. *Electrophoresis.* **2005**, *26(24)*, 4590-4604.
26 Ramsey, J.; Culbertson, C.; Jacobson, S.; Ramsey, J.M. *Analytical Chemistry*. **2003**, *75*, 3758-3764.
27 Aguilar, M.; Farran, A.; Serra, C.; Sepaniak, M.J.; Whitaker, K.W. *J. Chrom., A*. **1997**, *778*, 201-205.

28 Copper, C.; Staller T.; Sepaniak M.J. "Characterization of Polyaromatic Mixtures by Micellar Electrokinetic Capillary Chromatography." *Poly. Arom. Compds*. **1993**, *3*,121-135.PAHs
29 Fox, S.; Culha, M.; Sepaniak, M.J. "Development of a Grid Search Molecular Mechanics Modeling Strategy to Study Elution Behavior in Cyclodextrin Modified Capillary Electrophoresis." *J. Liq. Chrom*. **2001**, *24*, 1209-1228.
30 Fox, S. *Design of Molecular Modeling Techniques for Exploring Molecular Recognition Using Cyclodextrins*. Ph.D. Dissertation. UTKnoxville: **2003**.
31 Ma, J. and Smalley, R. *Journal of Physical Chemistry B*, **2006**, .
32 Holland, R.D.; Sepaniak, M.J. "Qualitative Analysis of Mycotoxins Using Micellar Electrokinetic Capillary Chromatography." *Anal. Chem*. **1993**, *65*, 1140-1146.
33 Pfahler, J.; Harley, J.; Bau, H.; and Zemel, J. *Micromechanical Sensors, Actuators, and Systems (ASME, 1991)*. **1991**, pp. 49-60.
34 Jacobson, S.; Hergenroder, R.; Moore, A.; Ramsey, J.Ml. *Analytical Chemistry.* **1994**, *66(23)*, 4127-4132.
35 Tsouris, C.; Depaoli, D.; Culbertson, C; Jacobson, S.; Ramsey, J. M. U.S. Pat. Appl. Publ. [US 2003086333] **2003**.
36 Duffy, D.; McDonald, J.C.; Schueller, O.; Whitesides, G. *Analytical Chemistry*. **1998**, *70*, 4974-4984.
37 Duffy, D.C.; Schueller, O.J.A.; Brittain, S.T.; Whitesides, G.M. *J. Micromech. Microeng*. **1999**, *9(3)*, 211-217.
38 Linder, V.; Sia, S.; Whitesides, G. Analytical Chemistry. 2005, 77, 64-71.
39 Harrison, D. J.; Fluri, K.; Seiler, K.; Fan, Z.; Effenhauser, C. S.; Manz, A. *Science*. **1993**, *261*, 895-7.
40 Harrison, D.J.; Manz, A.; Fan, Z.; Luedi,H.; Widmer, H.M. *Analyical Chemistry*, **1992**, *64*, 1926-32 .
41 Jacobson, S.C.; Hergenröder, R.; Koutny, L.B.; Warmack, R.J.; Ramsey, J.M. *Analytical Chemistry*, **1994**, *66*, 1107-13.
42 Jacobson, S.C.; Hergenröder, R.; Koutny, L.B.; Warmack, R.J.; Ramsey, J.M. *Analytical Chemistry*, **1994**, *66*, 2369-73 .
43 He, B.; Tait, N.; Regnier, F.*Analytical Chemistry*, **1998**, *70*, 3790-3797.
44 Kutter, J.P.; Jacobson, S.C.; Ramsey, J. M. *Analytical Chemistry*. **1997**, *69*, 5165-5171
45 Effenhauser, C.S.; Paulus, A.; Manz, A.; Widmer, H.M. "High-Speed Separation of Antisense Oligonucleotides on a Micromachined Capillary Electrophoresis Device." *Analytical Chemistry*, **1994**, *66*, 2949-53
46 Woolley, A. T. and Mathies, R. A. "Ultra-high-speed DNA fragment separations using microfabricated capillary array electrophoresis chips." *Proceedings of. National Academy of Science U. S. A.*, **1994**, *91*, 11348-52.
47 Bettieri, G-L.; Dodge, A.; Goer, G.; de Rooij, N.F.; Verpoorte, E. "A Novel Microfluidic Concept for Bioanalysis Using Freely Moving Beads Trapped in Recirculating Flows." *Lab On a Chip*. **2003**, *3*, 34-39.
48 Rossier, J.; Reymond, F.; Michel, P.E *Electrophoresis.* **2002**, 23(6), 858-867.

49 Dow Corning Corp. Sylgard 184 Silicone Elastomer Product Information. *Form No. 10-898C-01* **2000**.
50 Linder V; Verpoorte E; Thormann W; de Rooij N F; Sigrist H *Anal. Chem*. **2001**, *73(17),* 4181-4189.
51 Giesfeldt, K.S.; Connatser R.M.; Lavrik, N.V.; Dutta, P.; and Sepaniak, M.J. *Applied Spectroscopy*, **2003**, *57***,** 1346-1352.
52 De Bo, I.; Van Langenhove, H.; Pruuost, P.; De Neve, J.; Pieters, J.; Vankelecom, I.F.J.; Dick, E. *J. Membrane Sci*. **2003**, *215(1-2),* 303-319.
53 Bhatia, S.N.; Balis, U.J.; Toner, M. *Biotech. Prog.* **1998,** *14*, 378-387.
54 Folch, A.; Toner, M. *Annu. Rev. Biomed. Eng*. **2000**, *02*, 227-256.
55 McClain, M.A.; Culbertson, C.T.; Jacomson, S.C.; Allbritton, N.L.; Sims, C.E.; Ramsey, J.M. "Microfluidic Devices for the High-Throughput Chemical Analysis of Cells." *Anal. Chem*. **2003**, *75*, 5646-5655.
56 Borenstein, J.T.; Terai, H.; King, K.; Weinberg, E.J.; Kaazempur-Mofrad, M.R.; Vacanti, J.P. "Microfabrication Technology for Vascularized Tissue Engineering." *Biomed. Microdev*. **2002**, *4(3),* 167-175.
57 Leclerc, E.; Sakai, Y.; Fujii, T. "Cell Culture in 3-Dimensional Microfluidic Structure of PDMS (polydimethylsiloxane)." *Biomed. Microdev*. **2003**, *5(2)*, 109-114.
58 Thomas, C.; Jacobson, S.; Ramsey, J. M. *Analytical Chemistry*. **2004**, *76(20)*, 6053-6057.
59 Xu, H.; Roddy, T.; Lapos, J.; Ewing, A. *Analytical Chemistry.* **2002**, *74(21)*, 5517-5522.
60 Raman, C.V. *Nature.* **1928**, *121*, 619. and Raman, C.V. *Transactions of the Faraday Society.* **1929**, *25*, 781-792.
61 RAMAN OPERATION TEXT
62 Smith, J.E.; Moss, M.O. *Mycotoxin Formation, Analysis, and Significance.* John Wiley and Sons, New York. **1985**.
63 Kneipp, K. *Single Molecules*. **2001**, *2*, 291-292.
64 Stevenson, D.; Vo-Dinh, T. *Modern Techniques in Raman Spectroscopy*. Laserna, J., Ed. John Wiley and Sons, Chichester, UK: **1996**. p. 22.
65 Delhaye, M. and Merlin, J. *Biochimie*. **1975**, *57*, 401-415.
66 Levine. *Physical Chemistry, 2nd Edition*. Wiley Science. New York: **2001**.
67 Novotny, L.; Hecht, B.; Pohl, D. *Journal of Applied Physics*. **1997**, *81*, 1798-1806.
68 Arenas, J.; Tocon, I.; Woolley, M.; Otero, J.; Marcos, J. *Journal of Raman Spectroscopy*. **1998**, *29*, 673-679.
69 Moskovits, M.; Suh, J. *Journal of the American Chemical Society*. **1985**, *107*, 6826-6829.
70 Genov, D.; Sarychev, A; Shalaev, V.; Wei, A. *Nano Letters*. **2004**, *4*, 153-158.
71 Sutherland, W.; Laserna, J.; Angebranndt, M.; Winefordner, J. *Analytical Chemistry*. **1990**, *62*, 689-693.
72 Fleischmann, M.; Sundholm, G.; Tian, Z. *Electrochimica Acta*. **1986**, 907-916.
73 Vo-Dinh, T. *Trends in Analytical Chemistry*. **1998**, *17*, 557.
74 Van Duyne, R. *Journal de Physique, Colloque*. **1977**, 239-252.

75 Creighton, J. *Surface Science*. **1986**, *173*, 665-672.
76 Bjerneld, E.; Johnasson, P.; Kall, M. *Single Molecules*. **2000**, *1*, 239-248.
77 Moskovits, M. "Vibrational spectroscopy of molecules adsorbed on vapor-deposited metals." In *Surface Enhanced Raman Scattering*, Chang, R.K. (ed). Plenum Press: New York, **1982**.
78 Hao, E.; Li, S.; Bailey, R. Zou, S.; Schatz, G.; Hupp, J. *Journal of Physical Chemistry B*. **2004**, *108*, 1224-1229.
79 Doering, W.; Nie, S. *Journal of Physical Chemistry B*. **2002**, *106*, 311-317.
80 Ueba, H. *Surface Science*. **1983**, *131*, 347-366.
81 Lippitsch, M.; *Physical Review B: Condensed Matter and Materials Physics*. **1984**, *29*, 3101-3110.
82 http://www.zurich.ibm.com/st/mems/
83 Mishra, R. *Photoresist Development on SIC and Its Use As An Etch Mask for SIC Plasma Etch*. Master's Thesis. Mississippi State University Press: **2002**.
84 Ocvirk, G.; Munroe, M.; Tang, T.; Oleschuk, R.; Westra, K.; Harrison, D. J. *Electrophoresis*. **2000**, *21(1)*, 107-115.
85 Crabtree, H. J.; Cheong, E.; Tilroe, D.; Backhouse, C. *Analytical Chemistry*. **2001**, *73(17)*, 4079-4086.
86 Connatser, R.M.; Riddle, L.A.; Sepaniak, M.J. *J. Separation Science*. **2004**, *27*, 1545-1550.
87 Giesfeldt, K.; Connatser, R.M.; De Jesus, M.; Dutta, P.; Sepaniak, M. *Journal of Raman Spectroscopy.* **2005**, *36(12)*, 1134-1142.
88 DeJesus, M.; Giesfeldt, K.; Oran, J.; Abuhatab, N.; Lavrik, N; Sepaniak, M. *Applied Spectroscopy*. **2005**, *59(12)*, 1501-1508.
89 Hinde, R.; Sepaniak, M.; Compton, R.; Nordling, J.; Lavrik, N. *Chem. Phys. Lett.* **2001**, *339*, 167-173.
90 Osawa, M.; Suetaka, W. *Surface Science*. **1987**, *186*, 583.
91 Vo-Dinh, T.; Hiromoto, Y.; Begun, G.; Moody, R. *Analytical Chemistry*. **1984**, *56*, 1677.
92 Hill, W.; Wehling, B.; Klockkow, D. *Sens. Actuators, B*. **1994**, *18*, 188.
93 Vo-Dinh, T. *Sens. Actuators, B*. **1995**, *29*, 183.
94 Zou, S; Schatz, G. *Chem. Phys. Lett*. **2005**, *403*, 62.
95 Aroca, R; Martin, F *J. Raman Spectroscopy*. **1985**, *16*, 156.
96 Yang, W.; Schatz, G.; Van Duyne, R. *J. Chem. Phys*. **1995**, *103*, 869.
97 Jensen, Y.; Kelly, L.; Lazarides, A.; Schatz, G. *J. Cluster Science*. **1999**, *10*, 295.
98 Wei, Q.; Su, K.; Zhang, X-X.; Zhang, X. *Proc. SPIE-Int. Soc. Opt. Eng.* **2003**, *5221*, 92.
99 Roman, G.; Hlaus, T.; Bass, K.; Seelhammer, T.; Culbertson, C. *Analytical Chemistry*. **2005,** *77*, 1414-1422.
100 Press, William H.; Flannery, Brian P.; Teukolsky, Saul A.; Vetterling, William T. *Numerical Recipes in C++ : The Art of Scientific Computing* Cambridge, New York : Cambridge University Press, **2002**.
101 Cole, R.O.; Holland, R.D.; Sepaniak, M.J. *Talanta*. **1992**, *39(9),* 1139-1147.
102 Labour Environmental Alliance Society. "*EDCs In Our Lives*." London, England: **1999**.

103 de Fur, P.; Raffensperger, C. "Endocrine Disruptors" in *Taking Action: Strategy Recommendations from the 3rd Citizens' Conference on Dioxin and Other Synthetic Hormone Disruptors*, Baton Rouge, Louisiana, March 15-17 **1996**.
104 http://fedgrants.gov/Applicants/EPA/OGD/GAD/2005-STAR-H1/Grant.html
105 http://www.epa.gov/endocrine/table6.html
106 http://www.epa.gov/endocrine/edrifact.html
107 Hinde, R.J.; Deprince, A.E. *Nanoletters.* In press.

Vita

Maggie grew up and learned the value of work and the beauty of science embodied in helping raise produce and beef cattle on a farm in Solway, Tennessee, with her parents, Ed and Raynella Dossett, her brother Eddie, and her sister Katie. She still spends much of her free time there with Raynella, Katie, and Nathan Butler. Maggie is a proud product of Knox County Public Schools, and with said public education, a little ambition, and a candid interview including the necessity of vocational training in high schools and one unfortunate, over-indulging raccoon, was able to secure herself a full tuition, room, and board scholarship to Furman University in Greenville, SC. At Furman, Maggie earned a B.A. in History and a B.S. in Chemistry, Magna Cum Laude, completing internships in chemistry under Dr. John Wheeler and products liability law during a semester at the Michelin North America corporate headquarters. In December, 2006, Maggie will graduate with a Ph.D. in chemistry from the University of Tennessee, Knoxville, after having been very aptly managed and mentored by Dr. M. J. Sepaniak. During her time at UT, Maggie worked as a National Science Foundation pre-doctoral fellow and a graduate research associate with Linda Lewis, Ph.D., Chemical Sciences Division, ORNL. Maggie plans to keep employment in the Knoxville area in order to maintain proximity to her life-long friends and family as well as the family of her best friend and husband Scott.